UNIVERSITÀ
DEGLI STUDI
FIRENZE

DOTTORATO DI RICERCA IN
INGEGNERIA INDUSTRIALE

CICLO XXVIII

Analytical plunge milling model and machining sound analysis for chatter forecast and detection

Settore Scientifico Disciplinare ING/IND-16

Candidato

Dott. Francesco Rafanelli

Tutori

Dr. Gianni Campatelli
Dr. Antonio Scippa

Controrelatore

Dr. Giovanni Totis

Coordinatore del Dottorato

Prof. Maurizio De Lucia

Anni 2012/2015

ISBN XXX–XX–XXXX–XXX–X
D/XXXX/XXXX/XX

For my family
And friend

You all have my deepest gratitude

This Thesis is the fruit of your support and presence

Thank you

Summary

The main aim of the PhD activity here presented is to develop models and methods for chatter avoidance and control. It is important to remind how auto-regenerative mechanism that lead to chatter is one of the today machining main limit to productivity and the solution of this problem is a typical modern challenge of this industry. Chatter is an auto-regenerative vibration that lead to instability by changing continuously the chip thickness. The physic nature of the problem is well known since sixties, but a unique, always applicable and scientific recognized solution hasn't been found jet. Research activities on this topic has been increased in the last years, since the industrial interest on the topic is high. A lot of different approaches and solutions have been presented, mainly limited to turning and flank milling processes. In this thesis, plunge milling has been investigated. Plunging is a subcase of milling and it is a arising machining process, because of its capability of working deep pocket or other difficult-to-access geometrical features maintaining a good productivity and accuracy also with slender tools. The advantage of the plunging operation is that the cutting forces are more oriented along the axis of the tool, where the tool has its highest stiffness. For these reasons, modeling this operation will be interesting not only for academic researches but also for automotive sectors and for the products for the medical and aerospace industries.

In this thesis, an analytical plunge milling model will be presented and described, starting from the few literature existing papers. New method for cutting coefficients measurement is introduced, as well together with a more accurate configuration description and the solution algorithm in order to achieve the Stability Lobes Diagrams. This is the most used tool for choosing cutting parameters in order to maximize the productivity and avoid instability. This is a graphical characterization of the dynamic behavior of a specific mixture of machine, tool holder, tool and workpiece.

On other hand, the second part of this thesis is focused on developing an active control logic, to be used in a general milling application and able to recognize the milling phase (example air cutting, stable or unstable cut) based on acoustical analysis. A lot of literature exists about active control and suppression technique. However, the most famous indices are built in a way that they can recognize chatter but only in pre-determined conditions. They lack the capability to recognize chatter from air cutting and transitions phase (example engaging, disengaging), causing a full automated control to change parameters or stop the milling task. Within this thesis, new indices will be presented in order to achieve the milling phase recognition goal. The microphone was chosen above others sensors for its high frequency linear behavior, its lower cost and because it doesn't reduce the working area.

Table of contents

List of figures

List of tables

Acronyms List

MRR	Material Removal Rate
HSM	High Speed Machining (High Speed Manufacturing)
SLD	Stability Lobe Diagram
CAM	Computer Aided Manufacturing
TDS	Time Domain Simulation
LDA	Laplace Domain Approach
ZOA	Zeroth Order Approximation
SDM	Semi Discretization Method
DDE	Delayed Differential Equation
ODE	Ordinary Differential Equation
TVA	Tunable Vibration Absorber
TMD	Tunable Mass Damper
AWH	Active workpiece Holder
SSS	Spindle Speed Selection
SSV	Spindle Speed Variation
SSR	Spindle Speed Regulation
FRF	Frequency Response Function
DOF	Degree Of Freedom
FE	Finite Element
RCSA	Receptance Coupling Structure Analysis
DIEF	Department of Industrial Engineering of Florence
NC	Numerical Control
CNC	Computerized Numerical Control
FFT	Fast Fourier Transform
$\|X(j\omega)\|^2$	Power Spectral Density

Preface

Part of this thesis lead to publication in journal and conference proceedings. These publications reported work carried out during my PhD researches under the supervision of Dr. Gianni Campatelli and Dr. Antonio Scippa.

Chapter 2.5 has been published as Rafanelli F., Campatelli G., Scippa A., Effects of Cutting Conditions on Forces and Force Coefficients in Plunge Milling Operations, Advances in Mechanical Engineering 2015, Vol. 7(6) 1–9.

Chapter 4 has been published in a conference proceedings: Rafanelli, F., Campatelli G., Scippa A., Development of Chatter Indices Based on Machining Sound Analysis, ICSV22 International Congress on Sound and Vibrations 22, Florence (Italy) 12-16 July 2015.

1. Introduction

1.1. The chatter problem

In modern manufacturing technologies, cutting processes are still crucial operations: it's impossible to achieve the same high level of surface quality and tolerances for general free form geometry with different technologies unless they are extremely dedicated, as for example grinding or lapping processes [1-5]. For these reasons, even if cutting processes as turning or milling are less cost efficient than net shape or near net shape processes [6-8], they are irreplaceable for task concerning high surface quality and geometrical complexity.

In the early years of the twentieth century, the main limit to productivity of this kind of manufacturing processes was the mechanical performance of the machines, in terms of Feed (F) and Spindle Speed (S). The increase of these characteristics led to an improvement of Material Removal Rate (MRR), that is the ratio of the volume of cut material per unit of time. MRR is also proportional to Radial (a_e) and Axial (a_p) Engagement and Feed per Tooth (f_{tooth}). For classical theory radial and axial engagement only depend on the mechanical stiffness of the cutter (it has to resist cutting forces with small deformations to guarantee high surface quality) while f_{tooth} is chosen based by cutting speed (V_c) that is proportional to tool diameter (D) and Spindle Speed.

Chatter, as an auto-regenerative mechanism, was known and investigated since 1907 when Taylor [9] stated that chatter was the "most obscure and delicate of all problems facing the machinist", but it has been a marginal problem until the improvement of machining performance and the developing of High Speed Milling (HSM), also known as High Speed Machining. In modern industries aero-turbine and airplane components [10] , die and mould as well [11 - 12] are typical tasks for this technology. HSM led to an higher productivity for most of the industrial cases.

This new method of production was theorized by Carl J. Salomon [13] in the early '30: the main idea of his work was to increase abruptly the typical cutting speed in order to reach a new point of cutting, as shown in Figure 1. Salomon, with a series of experimental activity, showed that the increment of V_c caused an initial increasing of cutting temperature that reached a maximal value before a new low temperature working zone, and indicated the cutting temperature as one of the main responsible for tool wear, strongly affecting tool life; increasing V_c has a direct impact on f_{tooth} and on MRR. When the capabilities of machines allowed the application of this theory (increment of maximal S and f_{tooth}), chatter arise as a main problem for cutting operations.

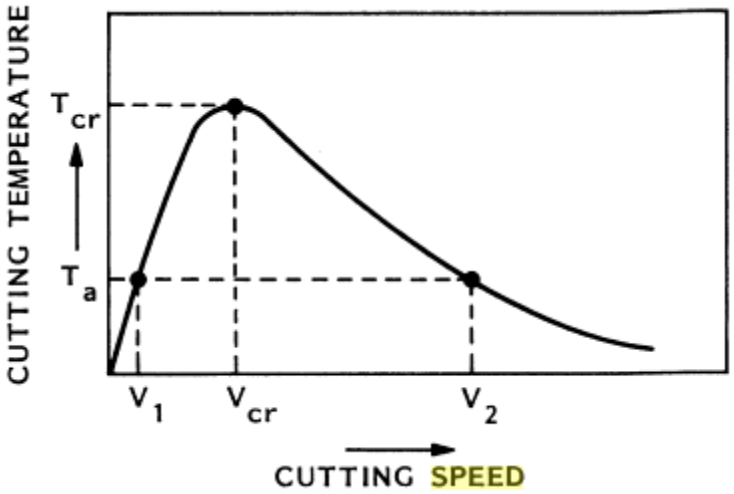

Figure 1: Salomon theory of HSM

1.2. Chatter phenomenon

Chatter is the name to indicate a particular vibration that may occur in turning or milling operations due to the fact that cutting machine, tools and workpieces are not perfect rigid body and it is cause of undesirable effects as a poor surface quality (see Figure 2). It is possible to find in literature [14] a detailed subdivision of tool tip vibrations (see Table 1)

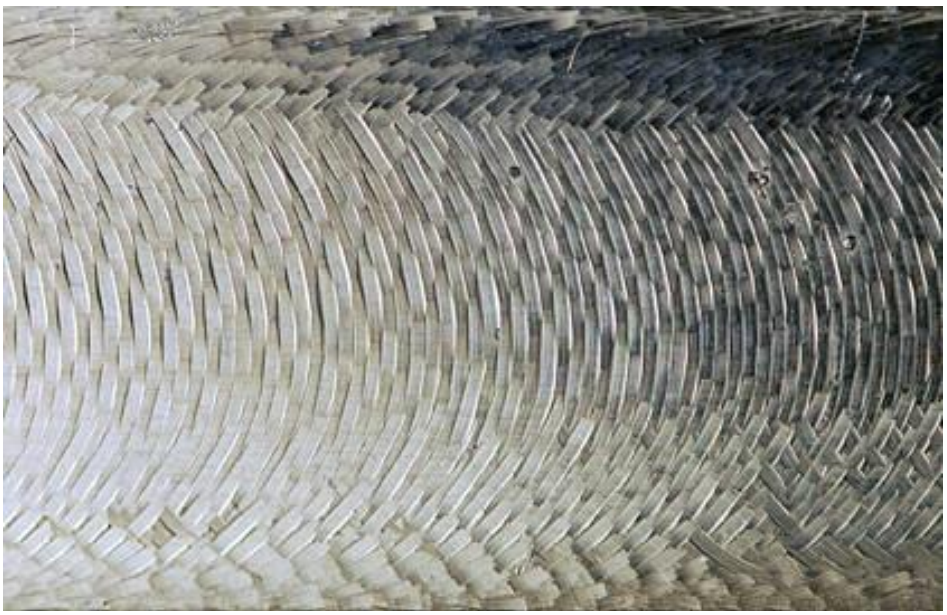

Figure 2: Chatter marks and poor surface quality

Table 1: Chatter categories

Primary	Frictional Thermo-mechanical Mode coupling
Secondary	Auto regenerative

Primary chatter is due to cutting process itself.

Frictional chatter (Figure 3) occurs when rubbing on the clearance face excites vibration in the direction of the cutting force and limits in the thrust force direction [15].

Thermo-mechanical chatter (Figure 4) occurs due to the temperature and strain rate in the plastic deformation zone [16].

Mode coupling chatter exists if vibration in the thrust force direction generates vibration in the cutting force direction and vice versa [17,18,19]. This results in simultaneous vibration in the cutting and thrust force directions. Physically, it is caused by a number of sources such as friction on the rake and clearance surfaces, chip thickness variation, shear angle oscillations and regeneration effect [16].

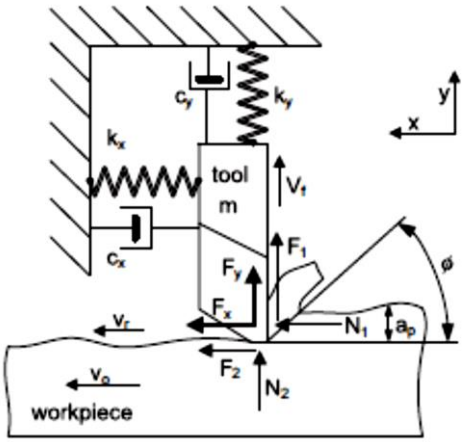

Figure 3: Turning model with friction force, here called F_2

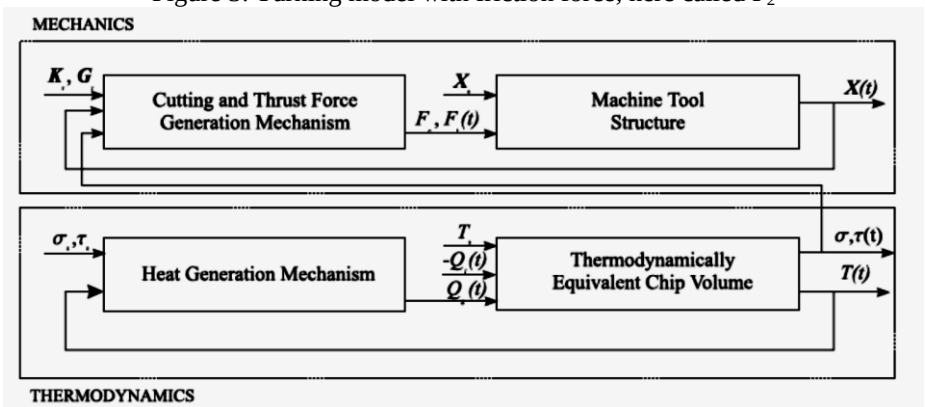

Figure 4: Effect of thermodynamics on chip volume

Secondary chatter is a form of self-excited vibration and it's a phenomenon of mechanical dynamic instability [16,20-22], also known as auto-regenerative chatter (or simply chatter) and it's the most common and severe vibration in machining. It may occurs when two overlapping cuts generate two surface waviness that are phase shifted: this cause a variation of chip thickness, followed by a variation in cutting forces that amplify the oscillation of tool tip and chip thickness (see chapter 1.2.1). This closed loop mechanism may diverge from equilibrium configuration leading to a new point of quasi-static equilibrium or to breaking of tool tip (normally) caused by excessive vibrations. This closed loop mechanism is simply described in Figure 5.

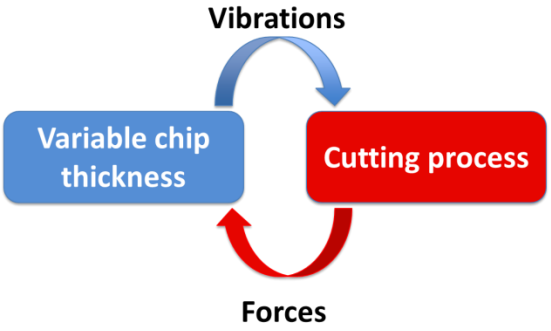

Figure 5: Closed loop mechanism of chatter

The divergence of the motion from the equilibrium configuration is influenced by cutting parameters, in particular is due to a_p and a_e and from the dynamics of the system composed by: tool, tool holder, spindle unit and machine (see Figure 6).

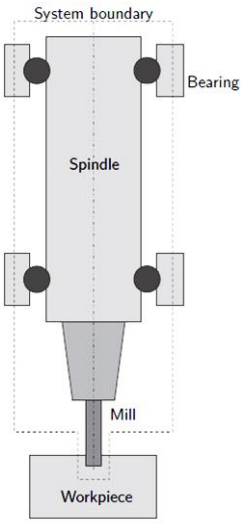

Figure 6: The mechanical system whose dynamic is primarly cause of chatter

As stated before chatter introduce a lots of problems that are listed in order of damage, from the least to the most severe, in the following table (see Table 2).

Table 2: Chatter damages, in order of severity

Excessive noise
Poor surface quality
Excessive tool wear
Tool breaking
Higher environmental impact, in terms of waste of energy and material
Machine damage

All these effects can led to a productivity loss and to an increment of the production costs. For these reasons, chatter is becoming one important argument for academic research: the papers presented on this topic are increasing, but even if great steps forward have been reported, there are still open issues.

1.2.1. **Waviness regeneration**

When a not perfect rigid body as a milling tool is excited by a not constant forces, an oscillation is generated. The amplitude and the phase of this vibration depends from the Frequency Response Function of the mechanical system (see Figure 6). Each tooth leaves a track on the surface of the workpiece that is the result of the combination of its kinematic motions and its dynamic displacements, changing the reference surface engaged by the following tooth. If a phase shift exists among the left waviness of two subsequent teeth, a change in the amplitude of the chip thickness is created [23] (see Figure 7).

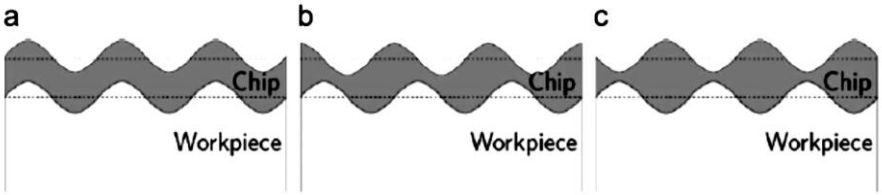

Figure 7: Effect of phase shift on chip thickness regeneration developed on a plane.
a) phase =0; b) phase = π/2; c) phase = π

If the forces in the tool tip have still small variations, the damping of the system is able to keep the tool tip in a neighborhood of the equilibrium configuration, while if the forces grew too much its motion start to diverge from it. As it's possible to understand the capability to stand around the equilibrium depends on dynamics of the system but also from cutting parameters that influences the cutting forces, such as a_p and a_e because they directly affects the magnitude of those forces.

1.3. Methods to overcome chatter

In literature, it's possible to find a lots of methods, developed in the past, used to predict or keep under control the chatter occurrence. As pointed out by Quintana in [14], all

the technique concerning chatter are categorized in four main groups, accordingly to Figure 8.

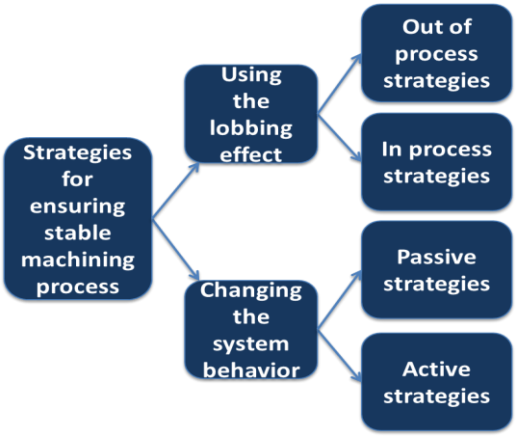

Figure 8: Research methods to overcome chatter problem

The first main division separates methods that try to forecast chatter occurrence using Stability Lobe Diagrams (SLDs) from method that try to modify the dynamics of the system, breaking the regenerative mechanism. SLDs are particular graphs: they plots critical depth of cut (e.g. Ap), that is indicated as the threshold between instability and stability, versus Spindle Speed. SLDs wants to give useful information to the CAM programmer in order to write a NC code with milling tasks that are characterized by combinations of cutting parameters placed inside the stable region of the graph (see Figure 9). SLDs try to avoid chatter to rise setting appropriate cutting parameters. Their name is derived by their typical shape, formed by a lots of lobes.

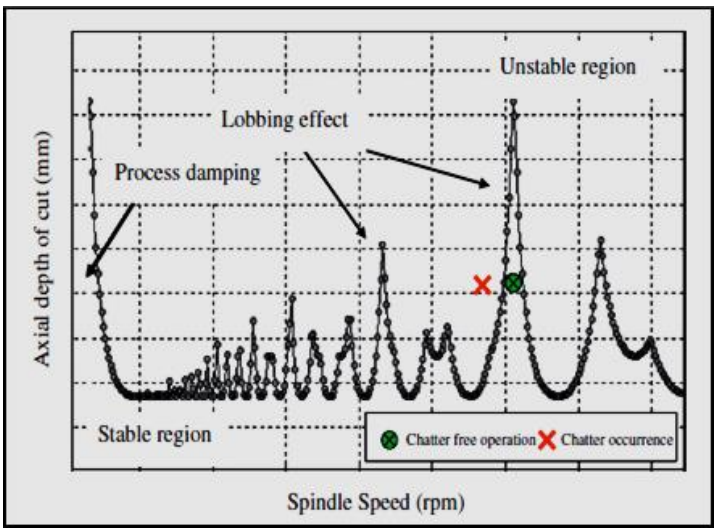

Figure 9: Example of SLD. Stability region is placed under the instability border line.

1.3.1. **Strategies based on direct experimental detection of stability**

Also known as “in process strategies”, these approaches draw SLD based on experimental activity. Usually, a series of dedicated tests are carried out for a determinate set of tool, tool holder, machine, cutting parameters and workpiece. During this experimental campaign, different type of sensors (see Figure 10, Figure 11 and Figure 12) are placed inside the working chamber and the collected data are analyzed in combination with surface finish in order to recognize chatter presence and typical features, such as chatter frequency. With this procedure is possible to draw an experimental, discrete SLD.

The main advantage of this kind of method is that it does not need knowledge of the system, cutting dynamics and process parameters, nor a modeling of the process; in particular it does not introduce errors due to approximations in process modeling. They also can be carried out in an environment that is the same, or close to the one that will be used, in operative production conditions.

The main drawback is that the SLDs obtained in this way are extremely specific for the combination of the used experimental system: a change in any part (e.g. tool or workpiece material) change the results, so that cost efficiency (time consumed and specimen costs) is sacrificed to have high precisions. With this consideration, this kind of method are useful to verify other methods or when their cost can be economically justified or amortized.

Typical sensors used in this applications are dynamometric table [24] accelerometers [25] and microphones [26-28].

Figure 10: A Kistler dynamometric table

Figure 11: Different types of PCB accelerometers

Figure 12: A Bruel & Kjaer microphone

A smart application of this methods was performed by Quintana [29], in which he perform tests on a flat incline surface (see Figure 13) where he retrieve stability limits growing a_p with a linear law.

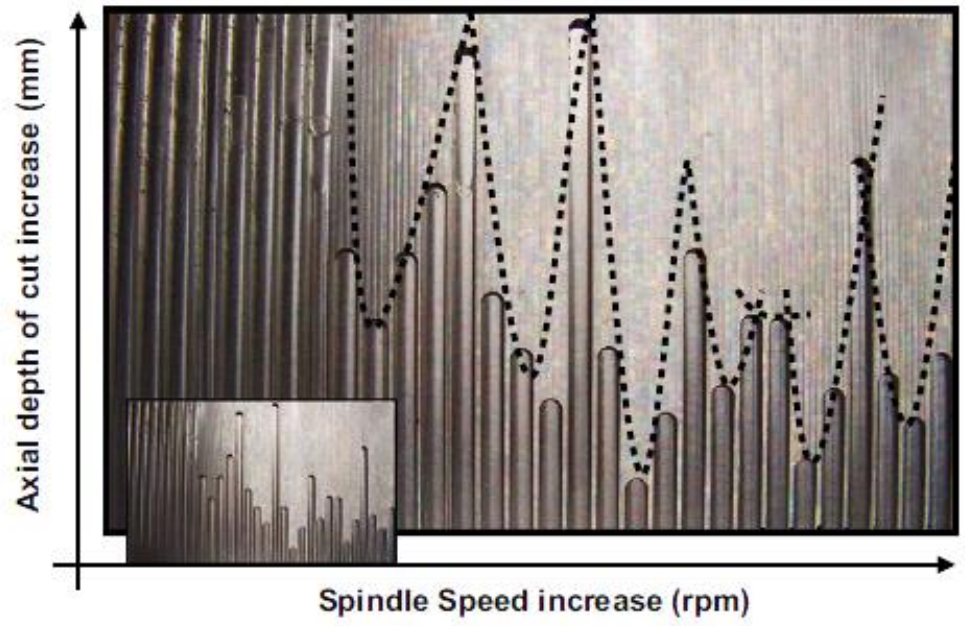

Figure 13: Quintana [29] method to obtain experimental SLD in slotting on inclined plane

1.3.2. **Strategies based on predictive algorithms**

Also known as "out of process strategies", these approaches try to predict SLDs by modeling the process (see Figure 14) with the goal not to execute experimental activity. This group of methods is the most popular and probably the category in which researchers have spent most of their efforts. Out of process strategies could be divided into three main sub-categories: Time Domain Simulations (TDS) [33-35], Laplace Domain Approach (LDA) [36-37], in particular Zeroth Order Approximation (ZOA) [38] and Semi-Discretization Method (SDM) [30-32].

The main advantages of these methods consist in predict stability limit before executing milling tasks, that allows the CAM programmer to set suitable cutting parameters to ensure the stability of the process. They are also cheaper, compared to in process strategies because they are simulations; the time of drawing a SLD depends on the type of method used. TDS is the slowest among them, because it performs a complete simulation of a simple milling task for a single set of parameters (corresponding to a single point on SLD) but is the more accurate. It can take into account more complex geometry of the tool [39 - 40] and introduce less simplifying hypothesis, solving the equation of the dynamics that model the cutting (Delayed Differential Equations, DDEs [41 - 42]). LDA, and in particular ZOA (that is a particular case of LDA in which the Laplace series that represent time-varying coefficients are approximated with their average values, that are the zeroth order ones), is the fastest. It solves the equation of the system analytically in Laplace domain and applies Nyquist criterion [37] to compute the stability border over a very width range of Spindle Speeds, but is less accurate due to simplifications. SDM is a sort of hybrid method created to solve faster DDEs system reducing them into Ordinary Differential Equations (ODEs)

approximating variable time-delayed terms with constant terms (the average values as in ZOA). Normally SDM computes SLDs for a grid of cutting parameters (correspondent to a finite number of points on the SLD) so, for this reason, is faster than TDS but slower than LDA. SDM methods were improved by Liu et Al. [134], or enchanced with Chebysev interpolation alghoritms by Totis et Al [135] The drawbacks of these methods are that they needs a lot of data to be measured, before computing stability border: in particular cutting coefficients [43 - 46] and tooltip FRFs are always needed and in some cases also tooltip geometry. This means a loss in time to acquire this data: hammer impact tests (also known as tap test, see Figure 15) for FRFs measurements and some experimental activity to compute cutting coefficients that depend from engagement parameters, tooltip geometry and workpiece material. Anyway, this data can be stored in databases and used for future applications without repeating the measures, and FRFs can also be obtained with other techniques such as receptance coupling [47 - 49], making out of process application faster and more general that in process strategies.

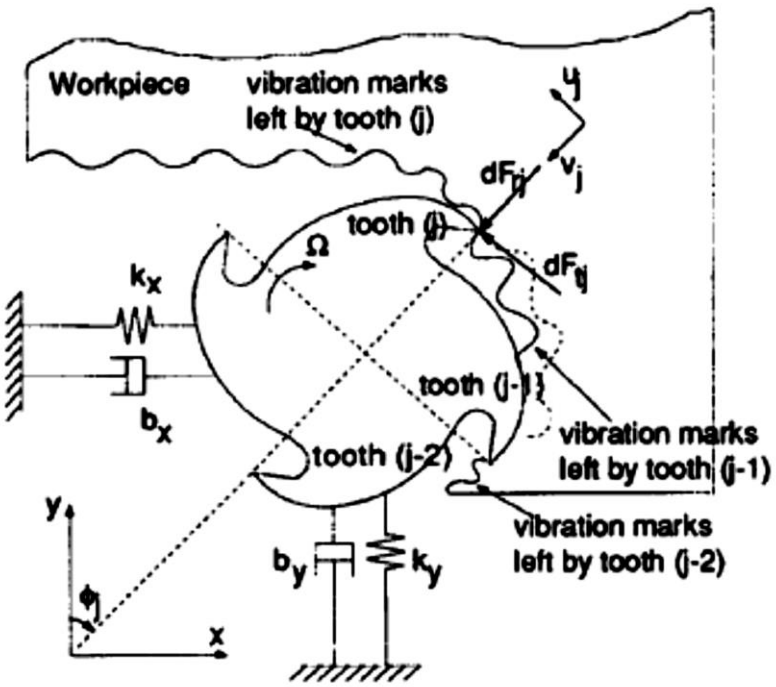

Figure 14: Planar chatter model

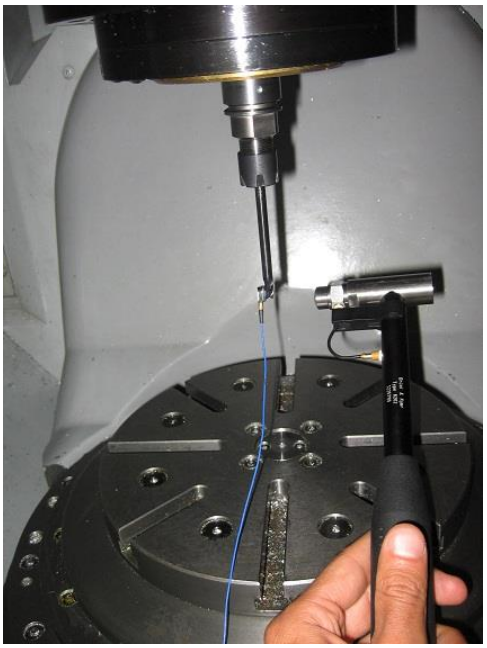

Figure 15: Impact hammer test

1.3.3. **Active methods**

Active methods are systems that try to change dynamic behavior of the tool tip or change cutting parameters in real time, with the aim to interrupt the chip regeneration mechanism. The ones that act upon the dynamics of the machine are normally systems composed by piezoelectric or electrostatic actuators that can influence the workpiece or different components of the machine, for example spindle bearings [50]. Some researchers have tried to mitigate chatter with Tunable Vibration Absorber (TVA) [51 - 52] or Tunable Mass Damper (TMD, both linear and not linear [54 - 56]). Others created special fixture known as Active Workpiece Holder (AWH, [57] see Figure 16) that try to suppress chatter introducing displacements in the system from the workpiece side, in order to nullify or minimize the phase-shift of two subsequent flute waviness to avoid chip regeneration (see chapter 1.2.1).

The common feature of active methods is their integration with sensors and software, used also to recognize the chatter presence. If instability is detected the chatter suppression device is activated or cutting parameters are changed, as in the case of Spindle Speed Selection (SSS) [58] or Spindle Speed Regulation (SSR) [133]. The last is a methods that simply change (or suggest the machine operator to change) the spindle speed, trying to find new stable operative zone.

As understandable, strong advantage of active solutions is its adaptability to virtually all the combinations of tool and workpiece, regardless the knowledge of any dynamic or force models or parameters, and the possibility to be fully automatized (especially this peculiarity made active methods very attractive for industries). Anyway, the recognition of chatter is not an easy task and consequently the velocity of response of the actuators may be not sufficient to prevent chatter damage, especially in finishing. Another drawback of these applications is the device and sensor interference inside the working chamber and the needs

of dedicated hardware and software coupled with the machine. In this direction, Okuma Corporation has developed a feature for some of their products called Machining Navi based on the principle of SSS.

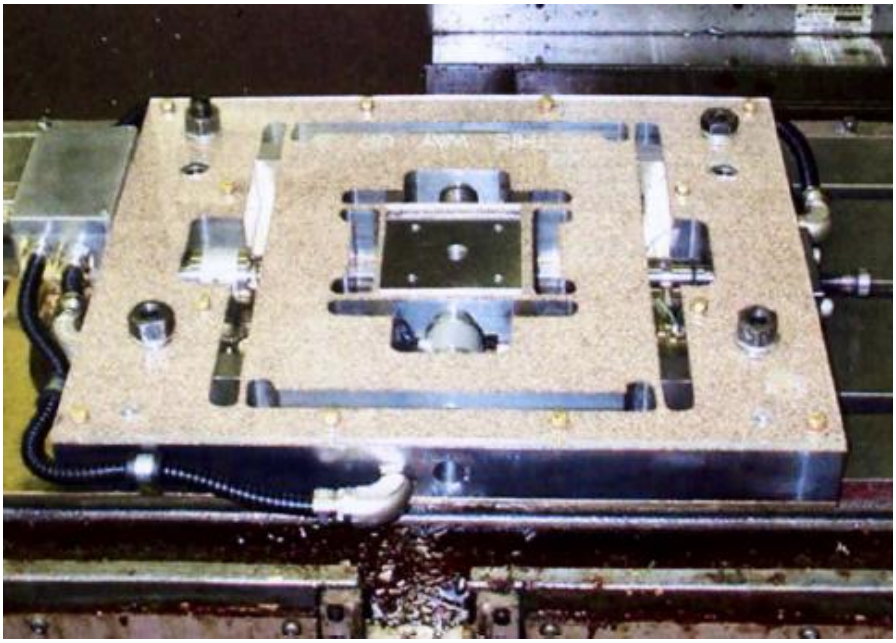

Figure 16: Active Workpiece Holder

The most known technique among active methods is Spindle Speed Variation (SSV): the interruption of auto-regenerative mechanism is obtained varying the spindle speed continuously between a maximal and a minimal value, following a mathematical law (e.g. triangular, sinusoidal) [59 - 61] as shown in Figure 17. The physical principle that stands behind this solution is to change continuously the period of the phenomenon, changing the chip thickness by acting on feed per tooth in order to avoid periodic auto-regeneration that would have led to chatter. The more is the gap between the maximal and the minimal variation, the more the SVV is effective. As drawbacks, this method shows tool overheating and wear, and spindle unit stress that lead to a shorter life of this machine component.

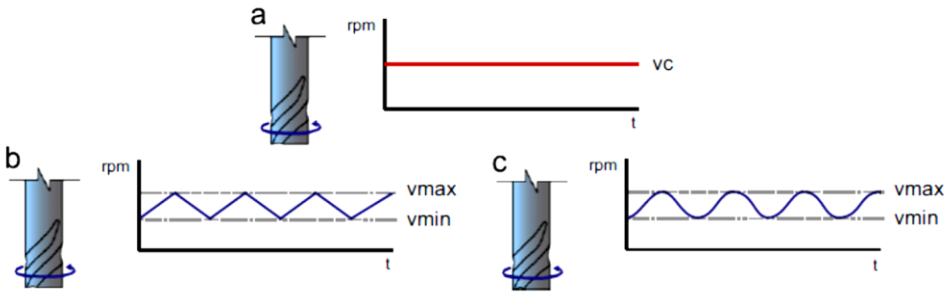

Figure 17: Spindle Speed Variation: a) No variation, b) triangular variation, c) sinusoidal variation

1.3.4. **Passive methods**

These methods, as active methods, try to change dynamic behavior of the system. The substantial difference is that these solutions change the capability of the machine to absorb vibrations, increasing its damping. Wang and Lee [62] redesigned the spindle unit, having identified it as the most critical part. Other simpler strategies involve the introduction of friction disk [63] or damper element inside machine components or inside tool [64] to dissipate chatter energy (see Figure 18).

Figure 18: Dampened anti chatter tools

The most common passive solution is to use tools with not constant spacing among the flutes (Figure 19 b), not uniform helix angle (Figure 19 c) or serrated flutes (Figure 20). It has been experimentally demonstrated [65 - 70] (and it's coherent with chatter theories) that unconventional flute spacing hinder auto-regenerative mechanism because it enlarge the period of the phenomenon.

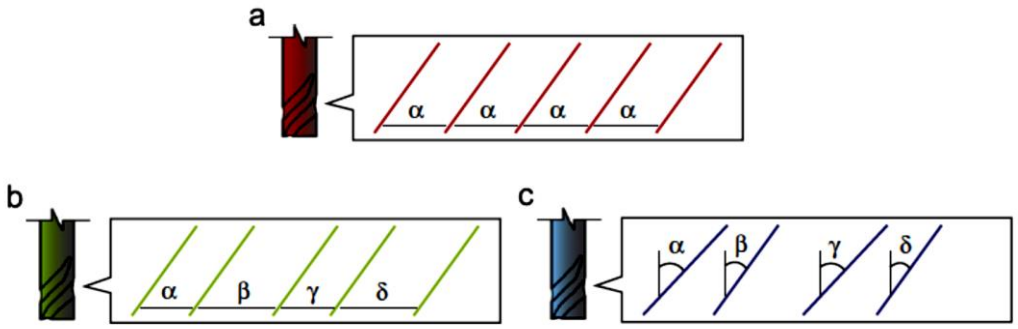

Figure 19: a) Normal tool; b,c) Anti-chatter tools with not uniform spacing or angle of the flutes

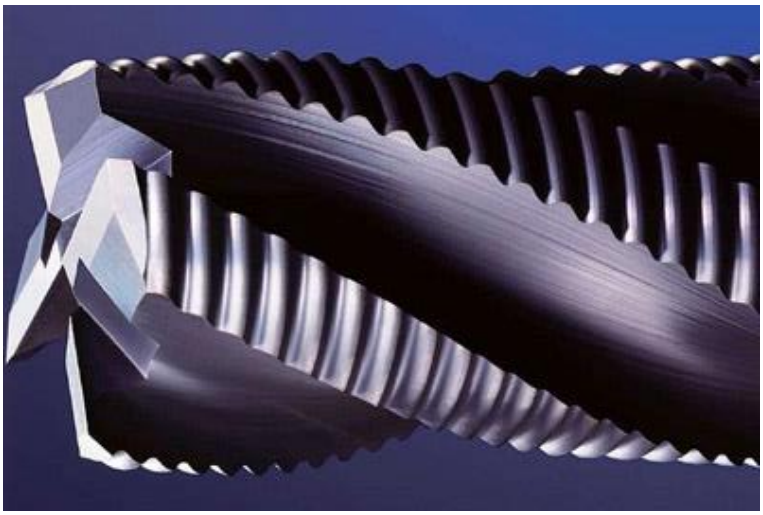

Figure 20: Serrated tool

It can be easily understood that these methods are suitable especially during the design of the components of a milling machine. Their benefits are wide, because increasing stiffness or damping is always a good factor to increase the stability zone in most of applications. The main disadvantages are the high difficulty of applying these methods on structural part on an existing machine and that they depend strictly on their design, in particular if the damped components have been developed to be optimized in a range of frequency the overall behavior outside that range can be worse than the one without it.

Obviously, these methods are more interesting for machine builder or tool maker company and these solution are less investigated at academic level.

1.4. Goals of this Thesis

After an investigation on the problem of chatter and on the approaches already adopted by the scientific community, this work propose to:

- Realize an analytical plunge milling model: plunge milling operations are specific milling operations in which the tool cut material in its axial direction (similar to drilling). For this case TDS or SDM are general solutions that can be applied, but it is needed a good description of chip geometry and surface generation. Moreover, there are a very few works regarding analytical plunge milling models and the development of a reliable model is still an open issue. The availability of such model will enable the use of analytical out of process methods described in chapter 1.3.2.
- Realize a control logic that will use mathematical index in order to create a functional active method for a fully automated chatter detection and avoidance control system.

2. Plunge milling model

2.1. Plunge milling applications in manufacturing

The demand for higher productivity in machining, in particular for chip removal processes, has imposed the machine tool manufacturers to improve the performance of their products, especially for what concerns the cutting speed and the material removal rate.

Plunge milling was neglected in the past except for specific task but now is an arising operation: it is a milling operation in which the tool plunges into the workpiece as a tip for drilling by removing material in the axial direction, being more similar to boring (with interrupted cuts) [71]. Since normally the spindle is stiffer in the axial direction, this type of machining has become very common for processing parts such as molds and geometrically complex objects as impeller for aeronautical use and energy. Such processing is used especially when the products are made of materials difficult to machine, such as high strength alloy or alloys based on nickel, or for deep cavities, such as a full milled impeller blades.

As a result of the axial motion direction, a tool used for plunge milling can show a higher stability for a certain choice of parameters than when used for flank milling. This issue allowed plunge milling to obtain higher stable removal rate than other cutting strategies; anyway, not a lot of models of plunging exist, being it a new trend. Researchers are focusing on this process only lately, since until now it has been poorly used.

As said in chapter 1.4, one of the goals of this thesis is to achieve a good analytical plunge milling model for chatter stability limit forecast.

2.2. General State of the Art on analytical chatter models for milling

The first significant works that have made a remarkable contribution to the understanding of the self-regenerative mechanism were the researches of Tobias [72] and Tlustly [73] at the turn of the fifties, concerning turning operations. Later, in the nineties, Altintas and Budak [74 - 75] proposed an analytical model for predicting the stability of working in peripheral milling and slotting; this results as a very big step forward, managing to solve for the first time with good results the problem of chatter forecast in an analytical way.

2.2.1. **Altintas and Budak model**

Budak and Altintas published their first model of planar milling in 1995 [74]. In this chapter, a brief explanation is reported.

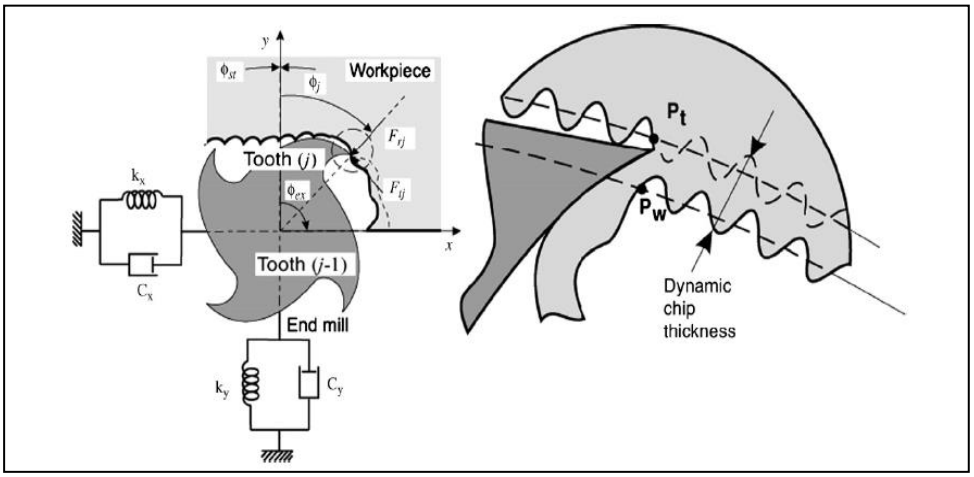

Figure 21: Altintas and Budak [74] planar milling (slotting and flank) model

In Figure 21 a planar scheme of a flank generic configuration is reported: the tool is represented as a flexible body in X and Y direction, rotating in clockwise direction. In the left part of Figure 21 the waviness regeneration is shown. To write the equation of this mechanical system three information are needed:

1. A force model
2. A waviness interaction model
3. The dynamic characterization of the system in both X and Y directions

The adopted force model is called Averaged Force Model (or Method): it is a simple model in which the force is considered linearly dependent from chip thickness, following this formula:

$$F_{c,j} = k_{cs} \mathrm{b} h_j + k_{cp} b \qquad \text{Equation 2.1}$$

Where k_{cs} is the coefficient related to tool cutting actions in tangential direction, k_{cp} is the coefficient related to tool friction effect, a is the depth of cut and h is the instantaneous cross section of the chip. Eq. 1 is valid for the three components of the force, tangential, radial and axial. To characterize all the components of the cutting forces are needed 6 coefficients, but for planar milling axial forces are neglected so only four of them are computed. These coefficients are affected by lubricant and wear conditions: increasing of the tool wear cause change to the cutting radius and mean angle of the tool [76 - 77] while the presence of lubricant alter the friction of the tool on the chip and machined surface. For this reason, they are measured in the most repeatable conditions: dry mill with brand new tooltip. Grossi et al. [46, 27] proved that these coefficients change with cutting speed in case of slotting. As a result, they provide a reliable estimation of the cutting forces only in a narrow

range of speed around the one used to acquire them; it is necessary, if your tool is used at very different spindle speed, to perform more tests and calculate the effect of cutting speed on these coefficients. In general, it is not considered the effect of other cutting parameters on the cutting coefficients.

Another important relation is the definition of chip thickness relative to a generic flute j (see Equation 2.2).

$$h_j(\phi_j) = (h_{j\ static}(\phi_j) + h_{j\ dynamic}(\phi_j))g(\phi_j) \qquad \text{Equation 2.2}$$

Whereϕ_j is the generic angular position of jth flute, with the zero on Y axis and clockwise positive direction. $h_{j\ static}(\phi_j)$ is defined as $f_{tooth}\sin(\phi_j)$: this show the direct relation between the f_{tooth} and the forces.

Function $g(\phi_j)$ is defined as follow:

$$\begin{Bmatrix} g(\phi_j) = 1 & if\ \phi_{st} \le \phi_j \le \phi_{ex} \\ g(\phi_j) = 0 & elsewere \end{Bmatrix} \qquad \text{Equation 2.3}$$

Where ϕ_{st} and ϕ_{ex} are the engaging and disengaging angle, respectively.

The procedure to measure these coefficients consist in performing a series of milling tests with constant parameters and step increasing f_{tooth}. $h_{j\ dynamic}(\phi_j)$ will not affect results because the average values of dynamic chip thickness components (due to vibration) is zero. The average value of the forces, measured by a dynamometric table, will be plotted on a chart against f_{tooth}. These data will be fitted with the best fit straight line in order to solve a linear system to compute force coefficients, see Figure 22.

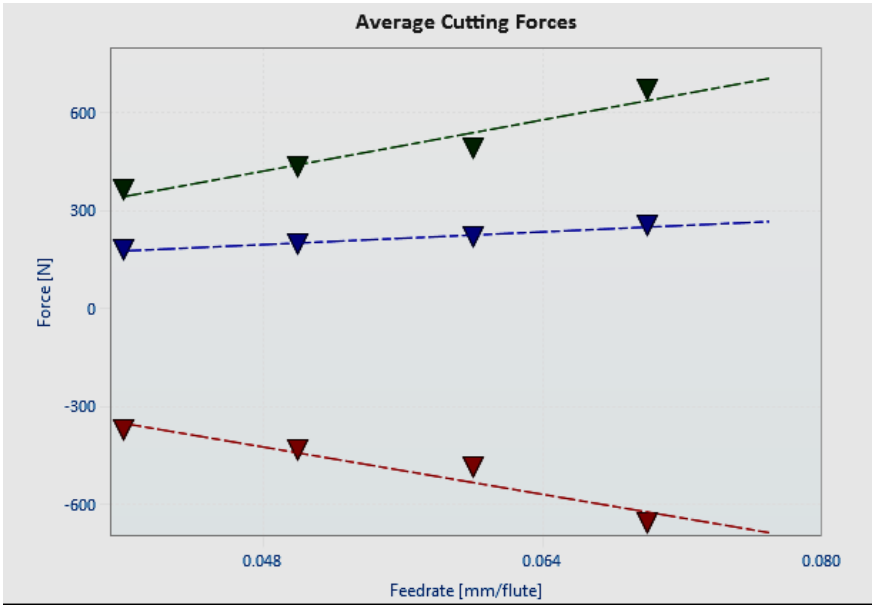

Figure 22: Best line fitting to compute cutting coefficients: X, Y, Z force components are rapresented by blue, green and red dashed lines. Data obtained with Altintas average model and CutPro software

Since the goal of the model is to predict stability, the static part of chip thickness $h_{j\ static}(\phi_j)$ does not give contribution because it is not caused by vibrations and will be neglected, dropping it from equation, leaving the dynamic part $h_{j\ dynamic}(\phi_j)$ only.

It is possible to write $h_{j\ dynamic}(\phi_j)$ as a two subsequent actual chip thickness of two flutes; substituting in Equation 2.2 it's possible to obtain:

$$h_j(\phi_j) = (v_j(t) - v_{j-1}(t-\tau))g(\phi_j) \qquad \text{Equation 2.4}$$

Where $v_j(t) - v_{j-1}(t-T)$ represents the difference between the instantaneous chip thickness of the j-th tooth and the previous (j-1)-th tooth measured at the previous period T. Showing it in its planar component, it's possible to write Equation 2.5.

$$h_j(\phi_j) = (\Delta x_j(t)\sin(\phi_j) + \Delta y_j(t)\cos(\phi_j))g(\phi_j) \qquad \text{Equation 2.5}$$

Where Δx_j and Δy_j are the components of $v_j(t) - v_{j-1}(t-T)$.

Knowing the equation of the forces and the equation of dynamic chip thickness it's possible to write and develop the equation system that model the planar milling cut, with N being the number of flutes:

$$\begin{Bmatrix} m_x\ddot{x} + c_x\dot{x} + k_x x = \sum_{j=1}^{N} F_{xj} = F_x \\ m_y\ddot{y} + c_y\dot{y} + k_y y = \sum_{j=1}^{N} F_{yj} = F_y \end{Bmatrix} \qquad \text{Equations 2.6}$$

Introducing the angular transformation from local tangential (subscript c) radial (subscript cN) coordinate system to Cartesian reference system lead to Equation 2.7.

$$\begin{Bmatrix} F_{xj} = -F_{cj}\cos(\phi_j) - F_{cNj}\sin(\phi_j) \\ F_{yj} = F_{cj}\sin(\phi_j) - F_{cNj}\cos(\phi_j) \end{Bmatrix} \qquad \text{Equation 2.7}$$

Then substituting Equation 2.5 in Equation 2.1 and then the result in Equation 2.7, summing all the j-th components as in Equations 2.6:

$$\begin{Bmatrix} F_x \\ F_y \end{Bmatrix} = \frac{1}{2} a K_c \begin{bmatrix} a_{xx} & a_{xy} \\ a_{yx} & a_{yy} \end{bmatrix} \begin{Bmatrix} \Delta x \\ \Delta y \end{Bmatrix} \qquad \text{Equation 2.8}$$

Where a is the axial depth of cut and the coefficient are defined as follows:

$$a_{xx} = \sum_{j=0}^{N-1} -g(\phi_j)\left[\sin(2\phi_j) + K_{cN}\,(1 - \cos(2\phi_j))\right] \qquad \text{Equation 2.9}$$

$$a_{xy} = \sum_{j=0}^{N-1} -g(\phi_j)\left[(1 + \cos(2\phi_j) + K_{cN}\sin(2\phi_j)\right] \qquad \text{Equation 2.10}$$

$$a_{yx} = \sum_{j=0}^{N-1} g(\phi_j)\left[(1 - \cos(2\phi_j) - K_{cN}\sin(2\phi_j)\right] \quad \text{Equation 2.11}$$

$$a_{yy} = \sum_{j=0}^{N-1} g(\phi_j)\left[\sin(2\phi_j) - K_{cN}\,(1 + \cos(2\phi_j))\right] \quad \text{Equation 2.12}$$

These equations (from Equations 2.9 to 2.12) contain engaging function $g(\phi_j)$, reference system transformation (Equation 2.7), dynamic chip thickness an radial force coefficient, defined as a ratio of the actual radial coefficient on tangential one. The matrix defined by these coefficients is called Orientation Matrix. It is possible to rewrite Equation 2.8 in a matrix form as follows:

$$\{F(t)\} = \frac{1}{2} a K_c [A(t)]\{\Delta(t)\} \quad \text{Equation 2.13}$$

Because all the variables are dependent from angle ϕ_j that is a time dependent variable. Equation 2.13 is periodic of a period τ, so it can be expanded in a Fourier series (operator $\mathcal{F}$) as follows:

$$\mathcal{F}\{F(t)\} = \frac{1}{2} a K_t \mathcal{F}([A(t)]) * \mathcal{F}(\{\Delta(t)\}) \quad \text{Equation 2.14}$$

Developing the second part (that is $\mathcal{F}(\{\Delta(t)\})$) and defining vector $\{\Delta(t)\}$ as difference of vectors $\{Q\} - \{Q_0\}$:

$$\{Q\} = \begin{Bmatrix} x(t) \\ y(t) \end{Bmatrix} \quad \text{Equation 2.15}$$

$$\{Q_0\} = \begin{Bmatrix} x(t-T) \\ y(t-T) \end{Bmatrix} \quad \text{Equation 2.16}$$

With equation 2.17, it's possible to derive equation 2.18:

$$\{Q(\omega)\} = [\Phi(i\omega)]\{F(\omega)\} \quad \text{Equation 2.17}$$

$$\mathcal{F}(\{\Delta(t)\}) = [1 - e^{-i\omega T}][\Phi(i\omega)]\{F(\omega)\} \quad \text{Equation 2.18}$$

Where Equation 2.17 is the relation between displacements and forces in frequency domain. The $[\Phi(i\omega)]$ matrix is the FRF Matrix (Receptance Matrix). Now, developing the first part of Equation 2.13 (that is $\mathcal{F}([A(t)]) = A(\omega)$) leads to

$$\mathcal{F}[A(t)] = \sum_{r=-\infty}^{\infty} [A_r]\delta(\omega - r\omega_T) = \sum_{r=-\infty}^{\infty} [A_r]e^{ir\omega_T t} \quad \text{Equation 2.19}$$

$$[A_r] = \frac{1}{T}\int_0^T [A_t]e^{-ir\omega_T t}\,dt \quad \text{Equation 2.20}$$

Where $T = \frac{2\pi}{\omega_T}$ is the period, δ is the Dirac delta function operator, ω_T is the tooth passing frequency and r is the harmonic number. Changing integration variable to ϕ, where $d\phi = \frac{dt}{\Omega}$ and Ω is the angular velocity and ϕ_p is the pitch angle, Equation 2.20 becomes:

$$[A_r] = \frac{1}{\Omega T}\sum_{j=0}^{N-1}\int_{j\phi_p}^{(j+1)\phi_p}\begin{bmatrix}a_{xx,j} & a_{xy,j}\\ a_{yx,j} & a_{yy,j}\end{bmatrix}e^{-irN\phi}d\phi \quad \text{Equation 2.21}$$

That can be reduced in this form, with the assumption that the flutes are cutting only between ϕ_{st} and ϕ_{ex}:

$$[A_r] = \frac{N}{2\pi}\int_0^{2\pi}\begin{bmatrix}a_{xx}^r & a_{xy}^r\\ a_{yx}^r & a_{yy}^r\end{bmatrix}e^{-irN\phi}d\phi \quad \text{Equation 2.22}$$

The coefficient of Orientation Matrix developed in this way became:

$$a_{xx}^r = \frac{i}{2}\left[-c_0K_re^{-irN\phi} + c_1e^{-ip_1\phi} - c_2e^{ip_2\phi}\right]\Big|_{\phi_{st}}^{\phi_{ex}} \quad \text{Equation 2.23}$$

$$a_{xy}^r = \frac{i}{2}\left[-c_0K_re^{-irN\phi} + c_1e^{-ip_1\phi} + c_2e^{ip_2\phi}\right]\Big|_{\phi_{st}}^{\phi_{ex}} \quad \text{Equation 2.24}$$

$$a_{yx}^r = \frac{i}{2}\left[c_0K_re^{-irN\phi} + c_1e^{-ip_1\phi} + c_2e^{ip_2\phi}\right]\Big|_{\phi_{st}}^{\phi_{ex}} \quad \text{Equation 2.25}$$

$$a_{yy}^r = \frac{i}{2}\left[-c_0K_re^{-irN\phi} - c_1e^{-ip_1\phi} + c_2e^{ip_1\phi}\right]\Big|_{\phi_{st}}^{\phi_{ex}} \quad \text{Equation 2.26}$$

Where $p_1 = 2 + Nr$, $p_2 = 2 - Nr$ and $c_0 = 2/Nr$, $c_1 = (K_r - i)/p_1$ and last $c_2 = (K_r + i)/p_2$

Altintas and Budak model assumes that the cutting can be described with good numerical approximation by the average component of its Fourier expansion. This fact has been proven later to be more accurate when the engaging angle is large [78]. With this hypothesis, the Equations 2.23 to 2.26 are developed only for r=0 as shown here:

$$a_{xx}^0 = \frac{1}{2}\left[\cos(2\phi) - 2K_r\phi + K_{cN}\sin(2\phi)\right]\Big|_{\phi_{st}}^{\phi_{ex}} \quad \text{Equation 2.27}$$

$$a_{xy}^0 = \frac{1}{2}\left[-\sin(2\phi) - 2\phi + K_{cN}\cos(2\phi)\right]\Big|_{\phi_{st}}^{\phi_{ex}} \quad \text{Equation 2.28}$$

$$a_{yx}^0 = \frac{1}{2}\left[-\sin(2\phi) + 2\phi + K_{cN}\cos(2\phi)\right]\Big|_{\phi_{st}}^{\phi_{ex}} \quad \text{Equation 2.29}$$

$$a_{yy}^0 = \frac{1}{2}\left[-\cos(2\phi) - 2K_r\phi - K_{cN}\sin(2\phi)\right]\Big|_{\phi_{st}}^{\phi_{ex}} \quad \text{Equation 2.30}$$

And Equation 2.22 is reduced to:

$$[A_0] = \frac{N}{2\pi}\int_0^{2\pi}\begin{bmatrix} a_{xx}^0 & a_{xy}^0 \\ a_{yx}^0 & a_{yy}^0 \end{bmatrix} \quad \text{Equation 2.31}$$

Finally, it is possible to insert Equation 2.18 and Equation 2.31 in Equation 2.14:

$$\{F(\omega)\} = \frac{1}{2}aK_c\left\{[A_0][1-e^{-i\omega T}][\Phi(i\omega)]\{F(\omega)\}\right\} \quad \text{Equation 2.32}$$

With $[A_0]$ being now a time-invariant (but radial depth of cut dependent) matrix. Because the average value of cutting force is independent from helix angle, this relation is valid also for helical end mills.

Cross terms of FRF matrix can be neglected normally because their effect is negligible, in order to simplify calculations.

The system will be critically stable by vibrating at chatter frequency ω_c if the roots of the characteristic equation satisfy this relation:

$$det\left[[I] - \frac{1}{2}aK_c(1-e^{-i\omega_c T})[A_0][\Phi(i\omega)]\right] = 0 \quad \text{Equation 2.33}$$

To simplify the notation two relations are introduced, Orientated FRF matrix and eigenvalue of Equation 2.33:

$$\Phi_0(i\omega) = [A_0][\Phi(i\omega)] \quad \text{Equation 2.34}$$

$$\Lambda = -\frac{N}{4\pi}aK_c(1-e^{-i\omega_c T}) \quad \text{Equation 2.35}$$

Therefore, that Equation 2.33 can be written in this form:

$$det\big[[I] + \Lambda[\Phi_0(i\omega)]\big] = 0 \quad \text{Equation 2.36}$$

In addition, the characteristic equation becomes:

$$a_0\Lambda^2 + a_1\Lambda + 1 = 0 \quad \text{Equation 2.37}$$

Solving Equation 2.37:

$$\Lambda = -\frac{1}{2a_0}\left(a_1 \pm \sqrt{a_1^2 - 4a_0}\right) \quad \text{Equation 2.38}$$

Λ is an complex value. It can be written as a summation of a real part and an imaginary part: $\Lambda = \Lambda_R + i\Lambda_I$. With Euler formula, it's possible to substitute inside Equation 2.38: $e^{-i\omega_c T} = \cos(\omega_c T) - i\sin(\omega_c T)$, obtaining a_{lim}:

$$a_{lim} = -\frac{2\pi}{NK_c}\left[\frac{\Lambda_R(1-\cos(\omega_c T)) + \Lambda_I \sin(\omega_c T)}{1-\cos(\omega_c T)} + i\frac{\Lambda_I(1-\cos(\omega_c T)) - \Lambda_R \sin(\omega_c T)}{1-\cos(\omega_c T)}\right] \quad \text{Equation 2.39}$$

The imaginary part of a_{lim} must vanish because it's a real value:

$$\Lambda_I(1-\cos(\omega_c T)) - \Lambda_R \sin(\omega_c T) = 0 \quad \text{Equation 2.40}$$

From Equation 2.40, it is possible to define as follows:

$$\kappa = \frac{\Lambda_I}{\Lambda_R} = \frac{\sin(\omega_c T)}{1-\cos(\omega_c T)} \quad \text{Equation 2.41}$$

It's finally possible to write the final solution equation for a_{lim}:

$$a_{lim} = -\frac{2\pi\Lambda_R}{NK_c}[1+\kappa^2] \quad \text{Equation 2.42}$$

To find the corresponding spindle speed S at the given chatter frequency we use the phase shift ψ of the eigenvalues Λ_I, that is:

$$\psi = \tan^{-1}(\kappa) \quad \text{Equation 2.43}$$

In addition, this relation identifies the phase distance in a period:

$$\omega_c T = \pi - 2\psi + 2k\pi \quad \text{Equation 2.44}$$

Where k is an integer number of full vibration waves in a revolution of the mill and $\pi - 2\psi$ is the phase shift between inner and outer modulation.

The spindle speed can be calculated from Equation 2.44 by computing T in this way:

$$S = \frac{60}{NT} \quad \text{Equation 2.45}$$

To compute an SLD, these steps has to be followed:

1. Choose a value of k
2. Choose a value of ω_c
3. Solve Equation 2.33
4. Find a_{lim} with Equation 2.42
5. Find S with Equations 2.43, 2.44, 2.45
6. Repeat from Step 2 to Step 5 until all wanted ω_c are computed
7. Repeat from Step 1 to Step 6 until all wanted k are computed

The inputs of this model are:

- Complex FRF Matrix: $\Phi(i\omega)$
- Angular engage: ϕ_{ex} and ϕ_{st}
- Number of flutes N
- Force coefficients: K_t and K_r

2.3. State of the Art on analytical plunge milling chatter models

The pioneers of plunge milling modeling in an analytical way were in 2006 Altintas and Ko [79] but since then, few literature is present. They developed a model for this process on the basis of planar milling model, adjusting relations and equations for the new milling task.

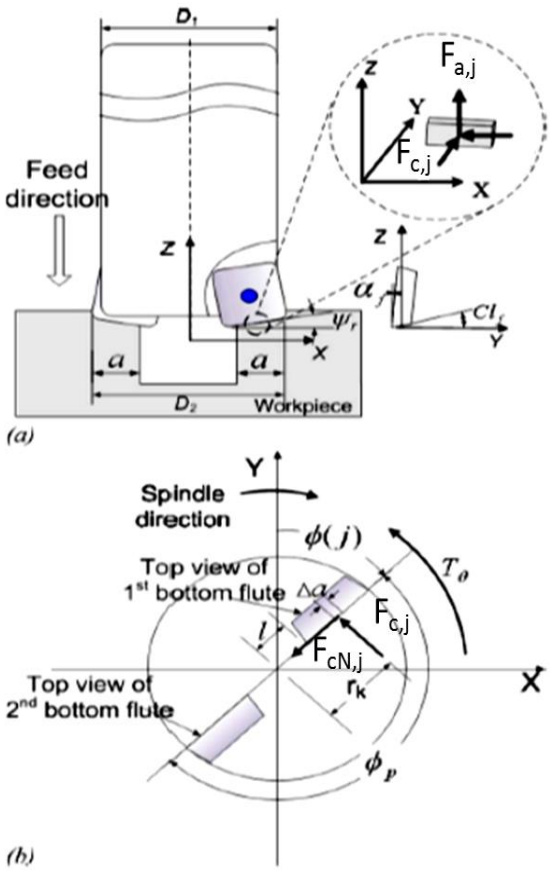

Figure 23: a) Lateral view of the tool [79]. b) Top view of the tool

Figure 23 describe one of the possible new configurations of the plunge milling task: Feed direction is parallel to tool axis direction and its direction is towards the bottom. It can be used to make holes, enlarge holes or can remove material form a vertical surface. There is a limited literature on this peculiar process; most of the effort are concentrated on studying the best cutter geometry [80 - 81], Tlustly and Ismail describe a dynamic model of plunge

considering helix angle [82], DeVor et al. presented a paper about plunging cutting forces where runout and static deflection were present [83]. Researchers studied extensively the mechanics of ball end mills, tapered helical ball end mills, and serrated cutters are also by using time domain models of the process [ref 84 - 87].

This model is a 4 DOF model, taking into account also the dynamics equation in axial and torsional direction. The force model used is the same as in planar milling (Average Force Method). As analogy as flank milling Equation 2.2, chip thickness can be described as a summation of a static part due to kinematics and a dynamic part due to vibrations. For this reason, it is possible to write this equation:

$$\begin{Bmatrix} x_c(t) \\ y_c(t) \\ z_c(t) \\ \theta_c(t) \end{Bmatrix}_{center} = \begin{Bmatrix} R\sin(\phi) \\ R\cos(\phi) \\ (Nc\Omega t)/2\pi \\ \Omega t \end{Bmatrix}_{kinematic} + \begin{Bmatrix} x(t) \\ y(t) \\ z(t) \\ \theta(t) \end{Bmatrix}_{vibrations} \qquad \text{Equation 2.46}$$

Where in this case R is the tool radius, c is f_{tooth}. As done in planar milling, an analytical form of the dynamic component of chip thickness is needed. First, the dynamic chip thickness in plunge milling is defined and identified along Z direction as depicted in Figure 24.

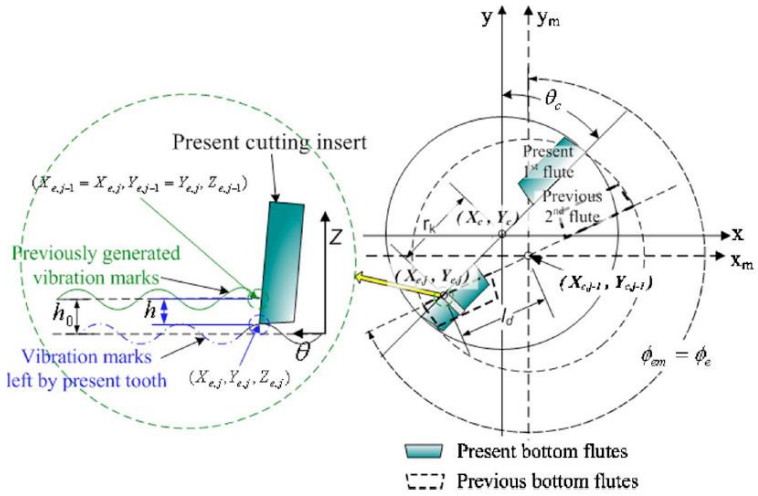

Figure 24: Chip thickness description along Z axis [79]

For a complete analytical description of dynamic chip thickness components, Figure 25, Figure 26 and Figure 27 are taken as a reference.

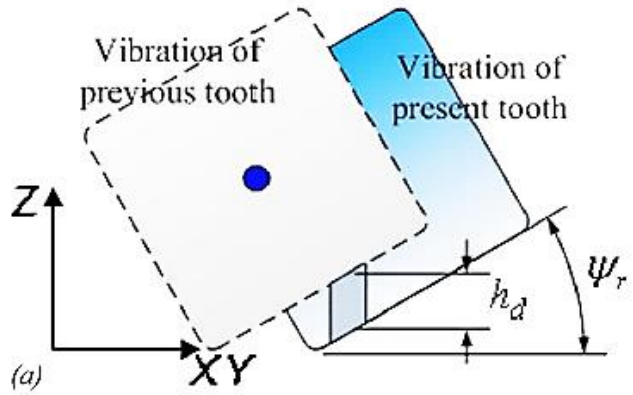

Figure 25: chip thickness component due to lateral vibrations

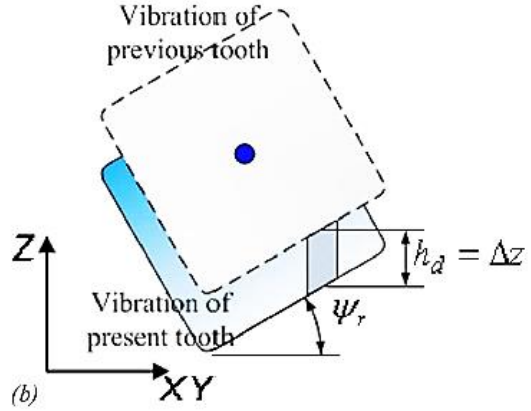

Figure 26: chip thickness component due to axial vibrations

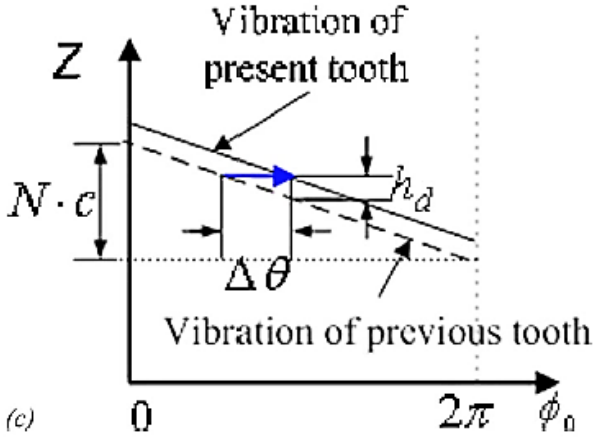

Figure 27: chip thickness component due to torsional vibrations

Knowing how a general vibration affects chip thickness Equation 2.47 can be written:

$$\{h_{j\ dynamic}(\phi_j)\} = \begin{Bmatrix} sin(\phi_j)\, tan(\psi_r) \\ cos(\phi_j)\, tan(\psi_r) \\ 1 \\ -\dfrac{c}{\phi_p} \end{Bmatrix} \qquad \text{Equation 2.47}$$

Where ψ_r is the angle measured between XY plane and the tool flute. As done in flank milling, is possible to write a system (in this case not a 2 DOF but a 4 DOF) that describe the dynamic of plunge milling, dropping the kinematic part of the motion:

$$\begin{Bmatrix} F_x(t) \\ F_y(t) \\ F_z(t) \\ T_\theta(t) \end{Bmatrix} = a_e K_c \sum_{j=0}^{N-1} \begin{Bmatrix} -\cos(\phi_j) - K_{cN}\sin(\phi_j) \\ \sin(\phi_j) - K_{cN}\cos(\phi_j) \\ K_a \\ (D+2l)/4 \end{Bmatrix} \begin{Bmatrix} sin(\phi_j)\, tan(\psi_r) \\ cos(\phi_j)\, tan(\psi_r) \\ 1 \\ -\dfrac{c}{\phi_p} \end{Bmatrix}^T \begin{Bmatrix} \Delta x_j(t) \\ \Delta y_j(t) \\ \Delta z_j(t) \\ \Delta\theta(t) \end{Bmatrix} \qquad \text{Equation 2.48}$$

Where outside the summation operator it's possible to find the radial depth of cut a_e and the tangential cutting force coefficient K_c, while inside the summation operator there are three vectors. The first one is the orientation vector and it is used to switch from a local tangential radial axial system to an external Cartesian reference system (l is the length of the central not cutting zone of the tool), taking into account also radial and axial cutting force coefficients K_{cN} and K_a respectively (as in planar milling expressed as a ratio between the real value and K_c). The second vector is the dynamic chip thickness component vector described in Equation 2.47. The third vector is displacement vector and can be rewritten as follow:

$$\begin{Bmatrix} \Delta x_j(t) \\ \Delta y_j(t) \\ \Delta z_j(t) \\ \Delta\theta(t) \end{Bmatrix} = \begin{bmatrix} \Phi_{xx} & \Phi_{xy} & \Phi_{xz} & \Phi_{x\theta} \\ \Phi_{yx} & \Phi_{yy} & \Phi_{yz} & \Phi_{y\theta} \\ \Phi_{zx} & \Phi_{zy} & \Phi_{zz} & \Phi_{z\theta} \\ \Phi_{\theta x} & \Phi_{\theta y} & \Phi_{\theta z} & \Phi_{\theta\theta} \end{bmatrix} \begin{Bmatrix} F_x(t) \\ F_y(t) \\ F_z(t) \\ T_\theta(t) \end{Bmatrix} \qquad \text{Equation 2.49}$$

That is the results of the product between the FRFs matrix $[\Phi(i\omega)]$ and forces vector $\{F(\omega)\}$.

This system can be reduced to a close synthetic matrix form as Equation 2.32 and 2.33, but it is a 4 DOF system and oriented matrix $[A_0]$ is a 4x4 matrix whose coefficients have been computed with the same technique described in chapter 2.2 (From Equation 2.19 to Equation 2.22), computed for zeroth order and reported here (because these coefficients will be used inside the plunge model proposed in this thesis):

$$A_{xx}^0 = \frac{1}{4} tan(\psi_r)\, [\cos(2\phi) + K_{cN}\sin(2\phi) - 2K_{cN}\phi]\Big|_{\phi_{st}}^{\phi_{ex}} \qquad \text{Equation 2.50}$$

$$A_{xy}^0 = \frac{1}{4} tan(\psi_r)\, [-\sin(2\phi) - 2\phi + K_{cN}\cos(2\phi)]\Big|_{\phi_{st}}^{\phi_{ex}} \qquad \text{Equation 2.51}$$

$$A_{xz}^0 = [-\sin(\phi) + K_{cN}\cos(\phi)]|_{\phi_{st}}^{\phi_{ex}} \qquad \text{Equation 2.52}$$

$$A_{x\theta}^{0} = \frac{c}{\phi_p}[\sin(\phi) - K_{cN}\cos(\phi)]\Big|_{\phi_{st}}^{\phi_{ex}} \quad \text{Equation 2.53}$$

$$A_{yx}^{0} = \frac{1}{4}tan(\psi_r)\,[2\phi + K_{cN}\cos(2\phi) - \sin(2\phi)]\Big|_{\phi_{st}}^{\phi_{ex}} \quad \text{Equation 2.54}$$

$$A_{yy}^{0} = \frac{1}{4}tan(\psi_r)\,[-2K_{cN}\phi - \cos(2\phi) - K_{cN}\sin(2\phi)]\Big|_{\phi_{st}}^{\phi_{ex}} \quad \text{Equation 2.55}$$

$$A_{yz}^{0} = [-\cos(\phi) - K_{cN}\sin(\phi)]|_{\phi_{st}}^{\phi_{ex}} \quad \text{Equation 2.56}$$

$$A_{y\theta}^{0} = \frac{c}{\phi_p}[\cos(\phi) + K_{cN}\sin(\phi)]\Big|_{\phi_{st}}^{\phi_{ex}} \quad \text{Equation 2.57}$$

$$A_{zx}^{0} = [-K_a\,tan(\psi_r)\cos(\phi)]|_{\phi_{st}}^{\phi_{ex}} \quad \text{Equation 2.58}$$

$$A_{zy}^{0} = [K_a\,tan(\psi_r)\sin(\phi)]|_{\phi_{st}}^{\phi_{ex}} \quad \text{Equation 2.59}$$

$$A_{zz}^{0} = [K_a\phi]|_{\phi_{st}}^{\phi_{ex}} \quad \text{Equation 2.60}$$

$$A_{z\theta}^{0} = \left[-\frac{c}{\phi_p}K_a\phi\right]\Big|_{\phi_{st}}^{\phi_{ex}} \quad \text{Equation 2.61}$$

$$A_{\theta x}^{0} = \left[-\frac{D+2l}{4}tan(\psi_r)\cos(\phi)\right]\Big|_{\phi_{st}}^{\phi_{ex}} \quad \text{Equation 2.62}$$

$$A_{\theta y}^{0} = \left[\frac{D+2l}{4}tan(\psi_r)\sin(\phi)\right]\Big|_{\phi_{st}}^{\phi_{ex}} \quad \text{Equation 2.63}$$

$$A_{\theta z}^{0} = \left[\frac{D+2l}{4}\phi\right]\Big|_{\phi_{st}}^{\phi_{ex}} \quad \text{Equation 2.64}$$

$$A_{\theta\theta}^{0} = \left[-\frac{c}{\phi_p}\frac{D+2l}{4}\phi\right]\Big|_{\phi_{st}}^{\phi_{ex}} \quad \text{Equation 2.65}$$

To solve the system the same eigenvalues problem is solved but being a 4 DOF system the solution is obtained not trough a close form equation but with a specific MATLAB® function.

In 2013, Zhuang et al. published a paper [88] about a possible modification of the plunge milling configuration used by Altintas in its work. To make the model more similar to real plunge applications, Zhuang modified the general configuration as visible from top view of the tool in Figure 28; so, he added a new variable to take into account that is the distance between two subsequent plunge cutting, indicated in Figure 28 with the variable a_s. This will be called later in this thesis, Stepover, as industrially used from plunging process. It represents is the overlapping surface due to a lateral displacement of two subsequent cuts, and define the real shape of the chip. Differently from flank model, Zhuang point out that the red triangle in Figure 28 identified by the point ABC cannot be neglected and that the chip thickness need a finer mathematical description to model the forces. The rest part of the work of his was focused on identify starting and exit angles, ϕ_{st} and ϕ_{ex}.

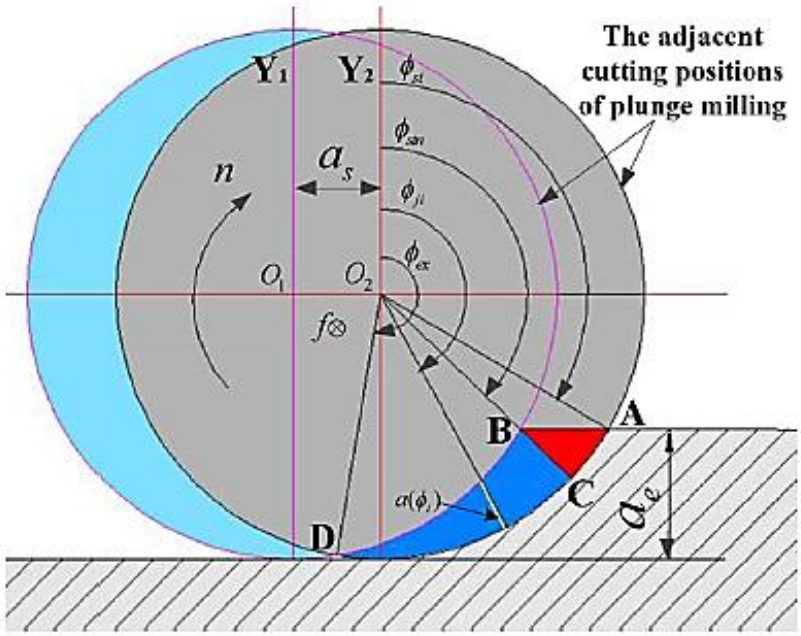

Figure 28: Top view of the tool and 2 consecutive tool positions in plunge [88]

2.4. Criticalities of state of the art models

Altintas plunge model cannot deal with a real plunge configuration, suggested by Zhuang. Anyway, this second real configuration was not developed to an exhaustive description, that is a complete angular engagement ($a_e = D$). Moreover, both models do not take into account that in plunge milling the real cutters are the frontal ones placed on the flat tip of a generic end mill, and not the peripheral ones as in planar milling. These cutters may have different geometries from the peripheral ones and different interactions with the workpiece: this fact can be seen as a variability of the cutting force coefficients. A model/method to measure and adapt them is needed. It will be shown (see chapter 2.5.3) that plunge milling coefficients change with radial depth of cut. For this reason a too simple description of cutter geometry with just one angle ψ_r is not sufficient to take into account the cutter edge effect: to solve this problem a more complex tool edge description is needed.

To complete the input parameters, a method to measure axial and torsional effect is needed as well. The answer of this point was found in literature and will be described in chapter 2.7, together with the relative experimental activity, applications and measures.

The last feature that both of the models can't deal is the impossibility to take into account the existing geometrical relation between the angular engagement (that is an input for the model, in the form of ϕ_{st} and ϕ_{ex}) and the Radial Depth of Cut a_e (that is the output of the model). They make the assumption that a_e is independent from the input configuration but actually is uniquely defined by the inputs, with the sole exception of hole enlarging, where angular engagement is fixed to be 360° as definition. Knowing this pointed out that this kind of model could be used to verify a stable condition but not to find the stability limit. A configuration is stable if predicted $a_{e\,lim}$ is greater than geometrical a_e, or unstable

otherwise. An iteration system to reach convergence and physical coherence between geometrical a_e and predicted $a_{e\,lim}$ is needed. To see all the differences look Table 3: Differences between literature and proposed model.

Table 3: Differences between literature and proposed model

Model	Real plunge configuration	Hole enlarging/ boring	Cutter edge geometry	Convergence between geometrical configuration and theoretical chatter limit
Altintas	No	Yes	No	No
Zhuang	Partial	No	No	No
Proposed	Completed	No	Yes	Yes

2.5. Plunge force coefficients method

2.5.1. Introduction on plunge milling force models.

The first step to represent a machining process is the definition of a cutting force model. An analysis of the literature shows that there exist mainly three cutting force models: lumped-mechanism model, dual-mechanism model and ternary-mechanism model. In the lumped-mechanism model, the effect of both shearing and friction at the cutting edge are described with a single coefficient. This is a simple model that produce reasonably good results with the advantage of its fast implementation in an industrial context. This approach has been developed by many researchers, that have included flat end mill and ball end mill. The most popular models are from Kline [89], Altintas and Spence [90], Lazoglu [91], who extended this concept to the prediction of cutting forces to ball-end mill. Later, more complex models have been developed, taking into account different coefficients for both the shearing and friction contribution at the cutting edge, these are usually called dual mechanics approaches. In particular, Budak et al. [92] developed a general approach that could fed the model with data extracted from orthogonal cutting tests. Then Altintas and Lee [93 - 94], Altintas and Yucesan [95] and Engin and Altintas [96] presented general models that could be used for the reliable prediction of cutting forces for a general end mill, often used to obtain stability lobe diagram with zero-th order approximation. The last is still the basis for more recent models that include other features such as the introduction of the effect of the runout [97] (Wan et al.). A detailed comparison of the most actual approaches to model the cutting force have been carried out by Wan and Zhang [98] which include also different solutions to carry out one of the most crucial step in force modeling, the calibration of the model. Some authors like Imani et al. [99] studied also the influence of different process parameters such as the axial depth on the cutting coefficients. At the end, the ternary mechanisms models [100] (Wan et al.) identifies and models the contributions of flank shearing, flank rubbing and bottom cutting effects; the coefficients could be calculated considering together chip load, chip width and bottom contact width.

It must be reported that, although the analytical methods are still the most used approaches to determine the cutting forces, due to the ever increasing computing capabilities of modern workstations and the availability on the market of commercial software able to

simulate the cutting process using FE approach, some researchers [101 -103] used simulation to predict the cutting force. Another interesting and arising approach, able to provide a faster result than FE modeling, is provided by the use of slip line field [104] (Altintas et al.). This approach is based on the strain, strain rate and temperature-dependent flow stress of the material and friction coefficient.

It is important to notice that the cutting force models are dependent from the tool geometry and the machining process approach, so the choice or definition of optimal cutting model could not be a trivial task. To solve this issue are arising both approaches that are oriented to have an unified model for cutting [105] based on a complete description of tool geometry or to create specific cutting models for each operation. Some example of this trend are the development of a model specific for the threading operation [106] and the development of a mathematical method to geometrically define a general tool as a flat tool with geometry variables or cutting inserts [107] or alternatively a multi-purpose tool [108].

Most of the cutting models are specific for the flanking and slotting operations: only few authors investigated the mechanics of plunge milling [79]. Plunge milling is similar to boring (with interrupted cuts) [109], so a different method to measure the cutting force coefficients must be developed. In this following sub-chapter a new simple method to obtain experimentally the cutting coefficients for traditional end mills is proposed. The proposed method is faster and more reliable than traditional approaches and it could fed the required data to a plunging chatter model; this will improve the industrial usability of such approach.

The proposed method is based on the average force method that is normally used for slotting and flank milling. Starting from this background, new relations to determine the average chip thickness and average coefficients in end mills plunging tasks have been developed. Those relationships are used to predict the cutting forces thanks to a model of the interaction between the material and the main rake angle (in plunge is the frontal one, not the peripheral one). Since the developed approach proposes a simple strategy to obtain the coefficients, it is possible to replicate the tests in order to evaluate the effect of the cutting parameters, such as the radial engagement, on their values. Some example of the experimental tests will be provided and discussed in this thesis.

2.5.2. **Average force model description**

The model developed is based on average cutting force model, where the cutting forces are proportional to feed per tooth and to chip thickness. The average cutting force model is one of the most adopted thanks to its simplicity and the good accuracy of prediction. However, must be reported that there are also more complex models that consider non-linear relationship between force and feed per tooth [110], obtaining more precise results. The choice of the average cutting force model has been motivated by the larger diffusion and its adaptability to analytical models, however the developed geometrical relations could be used also for more complex models. The average cutting force model uses the following description for the cutting forces:

$$F = k_{cs} f_{tooth} L + k_{cp} L \qquad \text{Equation 2.66}$$

Remembering that k_{cs} is the coefficient related to tool cutting actions, k_{cp} is the coefficient related to tool friction effect, f_{tooth} is the feed per tooth (in plunge equals to kinematic chip thickness h) and L is the instantaneous cross section of the chip. Equation 2.66 is valid for the three components of the force, tangential (the main one), radial and

axial. To characterize all the components of the cutting forces are needed 6 coefficients. These coefficients are affected by lubricant and wear conditions: increasing of the tool wear cause change to the cutting radius and mean angle of the tool [24,25] while the presence of lubricant alter the friction of the tool on the chip and machined surface. For this reason they are measured in the most repeatable conditions: dry mill with brand new tooltip. Grossi et al. [111 - 112] proved that these coefficients could change with cutting speed in case of slotting. As a result, they provide a reliable estimation of the cutting forces only in a narrow range of speed around the one used to acquire them; it is necessary, if a tool is used at very different spindle speed, to perform more tests and calculate the effect of cutting speed on these coefficients. In general it is not considered the effect of other cutting parameters on the cutting coefficients; however, the tests carried out in this research highlighted that this could not be assumed true for plunging operations.

The developed model starts taking into account the geometric position of a tool engaging a workpiece and from the cutting force model.

Figure 29 and Figure 30 describe a generic configuration of the tool and workpiece respect to a Cartesian reference system placed with Z-axis coincident with tool axis. The red segment h indicates the instantaneous chip thickness of the j-th cutter in a generic position that is identified by the angle φ_j respect to Y-axis. In plunge operation, the main cutters are the frontal ones not the peripheral ones as in slotting or flanking: so they are substantially straight cutter that operate with a different radial engagement for each angular positioning.

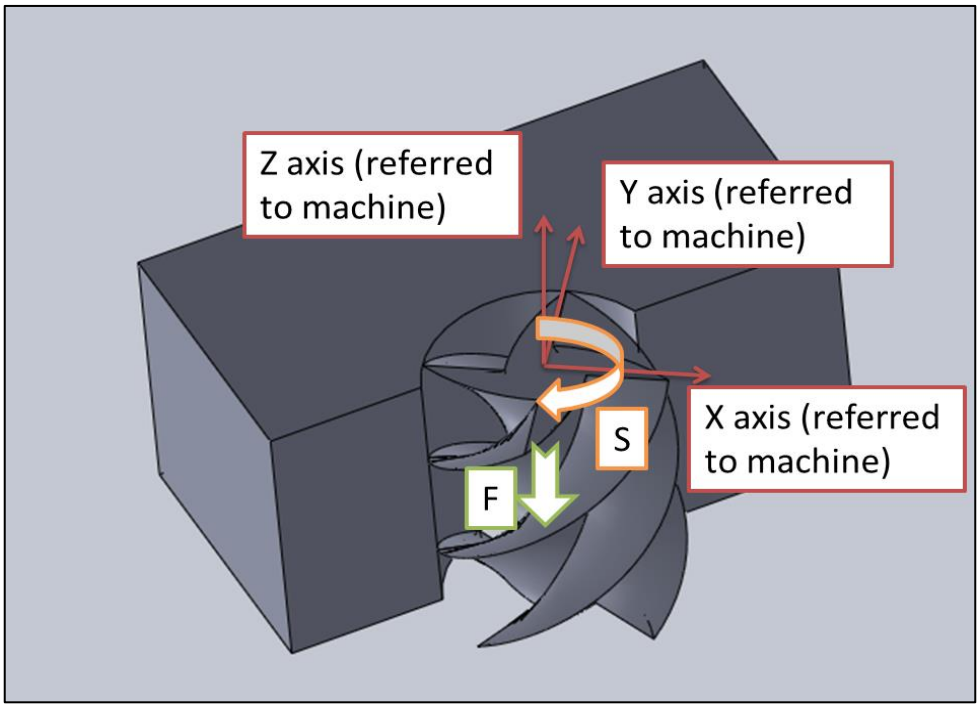

Figure 29: Generic relative tool-workpiece position cutting a vertical wall. The center of the reference system is coincident with the tool axis, while axis direction are coincident to an external fixed coordinate system, for example machine system

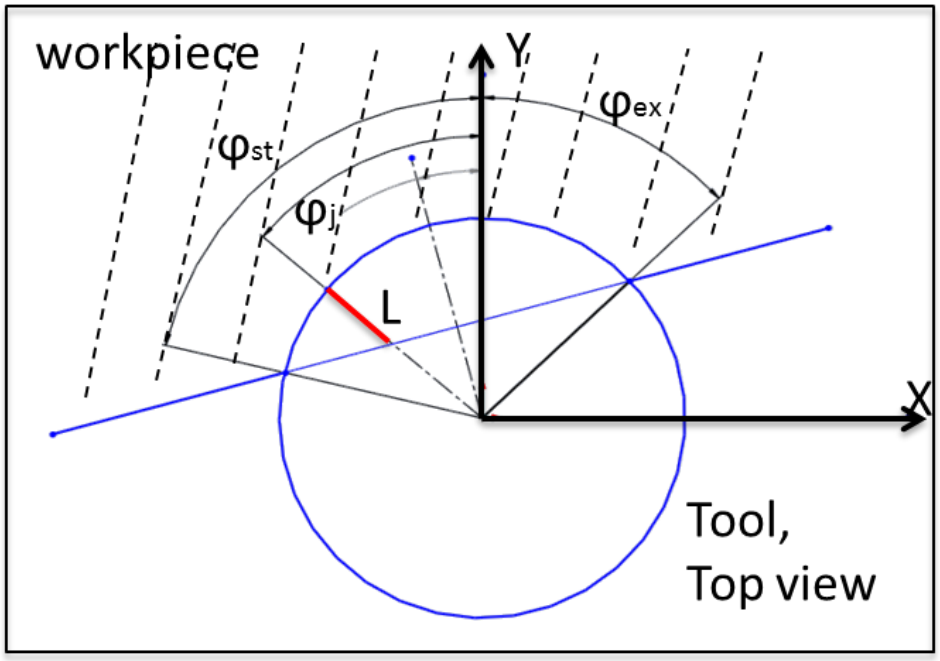

Figure 30: Top view of a tool-workpiece position cutting a vertical wall

It is possible to define the angle α as follow:

$$\alpha = \frac{\varphi_{ex} - \varphi_{st}}{2} \qquad \text{Equation 2.67}$$

Consequently, it is possible to indicate the length of segment L (the instantaneous chip cross section) as a summation of the M-th elements Δa that are engaging the material. L can be expressed also analytically with geometrical and trigonometrical relations, as shown in Equation 2.68 using Equation 2.67:

$$L = \sum_{k}^{M} \Delta a = R - \frac{R\cos\alpha}{\cos(\varphi_j - \alpha - \varphi_{st})} \qquad \text{Equation 2.68}$$

Where R is the radius of the tool. L reach its maximal value when φ_j is equal to α, that is the mean engage angle; L is defined as zero outside the interval φ_{st} and φ_{ex}. It's also possible to introduce a rotational matrix to switch from tangential, radial axial reference system to the tool Cartesian one. Axial axis is coincident to Z axis for definition.

$$\begin{Bmatrix} F_x \\ F_y \end{Bmatrix} = \begin{bmatrix} -\cos(\varphi_j) & -\sin(\varphi_j) \\ \sin(\varphi_j) & -\cos(\varphi_j) \end{bmatrix} \begin{Bmatrix} F_c \\ F_{cN} \end{Bmatrix} \qquad \text{Equation 2.69}$$

With Equation 2.69 is possible to write, in discrete form in the Cartesian reference system the forces at the tooltip.

$$F_x = \sum_{j=1}^{N}\sum_{k=1}^{M} \Delta a \left\{ -\left[K_{c_s} f_t + K_{c_p}\right] \cos\varphi_j - \left[K_{cN_s} f_t + K_{cN_p}\right] \sin\varphi_j \right\} \quad \text{Equation 2.70}$$

$$F_y = \sum_{j=1}^{N}\sum_{k=1}^{M} \Delta a \left\{ \left[K_{c_s} f_t + K_{c_p}\right] \sin\varphi_j - \left[K_{cN_s} f_t + K_{cN_p}\right] \cos\varphi_j \right\} \quad \text{Equation 2.71}$$

$$F_z = \sum_{j=1}^{N}\sum_{k=1}^{M} \Delta a \left\{ \left[K_{a_s} f_t + K_{a_p}\right] \right\} \quad \text{Equation 2.72}$$

Applying the definition of average forces:

$$F_{average} = \frac{1}{\varphi_{pitch}} \int_0^{2\pi} F(\varphi) d\varphi \quad \text{Equation 2.73}$$

And by substituting the analytical form of eq. 3 in eq. 5, 6 and 7, knowing that this integral is non-zero only between the angles φ_{st} and φ_{ex} and that the flutes are evenly spaced by the pitch angle, we can write the final formula of the method:

$$F_{x-ave} = -\frac{RN}{2\pi} \varepsilon_1 \left[K_{c_s} f_t + K_{c_p}\right] - \frac{RN}{2\pi} \varepsilon_2 \left[K_{cN_s} f_t + K_{cN_p}\right] \quad \text{Equation 2.74}$$

$$F_{y-ave} = \frac{RN}{2\pi} \varepsilon_2 \left[K_{c_s} f_t + K_{c_p}\right] - \frac{RN}{2\pi} \varepsilon_1 \left[K_{cN_s} f_t + K_{cN_p}\right] \quad \text{Equation 2.75}$$

$$F_{z-ave} = \frac{RN}{2\pi} \varepsilon_3 \left[K_{a_s} f_t + K_{a_p}\right] \quad \text{Equation 2.76}$$

Where ε variables are expressed by the following formulas:

$$\varepsilon_1 = \int_{\varphi_{st}}^{\varphi_{ex}} \cos\varphi - \frac{\cos\alpha \cos\varphi}{\cos(\varphi - \alpha - \varphi_{st})} d\varphi \quad \text{Equation 2.77}$$

$$\varepsilon_2 = \int_{\varphi_{st}}^{\varphi_{ex}} \sin\varphi - \frac{\cos\alpha \sin\varphi}{\cos(\varphi - \alpha - \varphi_{st})} d\varphi \quad \text{Equation 2.78}$$

$$\varepsilon_3 = \int_{\varphi_{st}}^{\varphi_{ex}} 1 - \frac{\cos\alpha}{\cos(\varphi - \alpha - \varphi_{st})} d\varphi \quad \text{Equation 2.79}$$

To compute the force coefficients a series of plunge tests must be executed with different cutting parameters: these must be chosen in order to achieve a stable cutting. For each test, the 3 components of the forces must be measured, normally with a dynamometric table. The tests must have different values of the feed per tooth. In accordance with to the model, the forces are proportional to feed per tooth; so if a linear increment of feed per tooth is chosen, also the forces (and their average values) must follow this trend. For these measures, there is no need of compensating the dynamics of the dynamometric table [113] because it does not affect the average values of the measured forces.

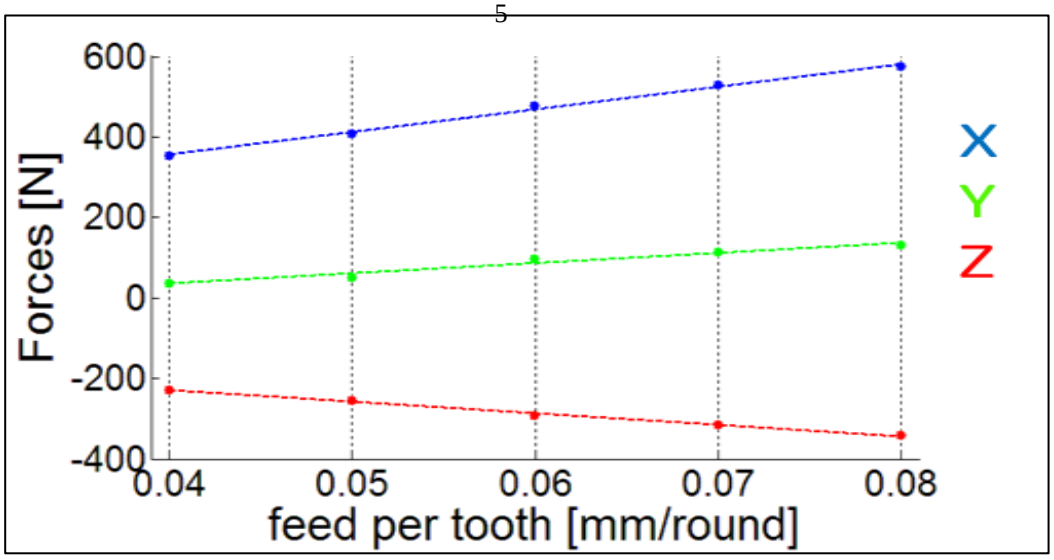

Figure 31: Example of measurement and data interpolation to obtain force coefficient

As shown in Figure 31, the average values of the forces are plotted using as variable the feed per tooth. A regressive model is then used to compute the six cutting force coefficients, using the Equations 2.70, 2.71 and 2.72.

2.5.3. **Experimental set up and tests**

In order to verify the effectiveness of the proposed model a set of experimental tests has been carried out. The test piece consists of a rectangular piece of aluminum clamped with a couple of screws to a dynamometric table (Figure 32). Additionally, a microphone was used to verify the stability of the process [25, 114 - 115].

Figure 32: Example of setup with a steel workpiece and detail of plunge test on aluminum

The chosen tool was a Mitsubishi Carbide Mill I MX1n 2S3A 12010 ET2020 12 that has 12 mm of diameter and 3 flutes, the shank was a Mitsubishi EF I MX12 U12N017L080C, the tool holder was a Big Mega New Baby Chuck MGN13 Daishowa Seiki

Co.L.Td and the milling machine was a Mori Seiki NMV 1500. It has been chosen to use a spindle speed of 8000 rpm and to maintain it constant in every test to avoid the problem of coefficient changes with cutting speed [116]. It also has been chosen to perform the coefficient measurements for four different radial depths of cut: 0.5 mm, 1 mm, 2 mm and 3 mm. For each radial depth of cut a set of five different feed per tooth have been tested: from 0.03 mm/tooth to 0.07 mm/tooth spaced by 0.01 mm/tooth.

The results in term of average forces and force coefficient are presented Table 4: Force cutting coefficient in aluminum for different radial engagement and Table 5: Force edge coefficient in aluminum for different radial engagement.

Table 4: Force cutting coefficient in aluminum for different radial engagement

AE [mm]	$K_{c,s}$ [N/mm^2]	$K_{cN,s}$ [N/mm^2]	$K_{a,s}$ [N/mm^2]
0.5	1249.04	496.0457	298.9652
1	843.1247	230.6405	9.895345
2	750.193	222.4607	112.8966
3	847.9039	404.52	303.0117

Table 5: Force edge coefficient in aluminum for different radial engagement

AE [mm]	Kc,p [N/mm]	KcN,p [N/mm]	$K_{a,p}$ [N/mm]
0.5	19.49199	6.663548	18.96992
1	25.52482	5.775643	29.11762
2	20.60815	0.148353	21.32309
3	18.23892	11.11235	19.52395

Every test made was checked and all the operations resulted to be stable, with no chatter evidence not on the surface not in signal analysis. A first results is that the average force method provide a good approximation of the mean cutting force, as proven by the very good accuracy of the linear regression model used to interpolate the experimental data. In this case, the behavior of the cutting force could be considered linear, respect to the chip area.

The tests carried out highlighted also another trend in the cutting force data: the cutting force coefficients change for different radial engagement. This trend is reported in **Errore. L'origine riferimento non è stata trovata.** and **Errore. L'origine riferimento non è stata trovata.**, where the not linear behavior of the coefficients is evident.

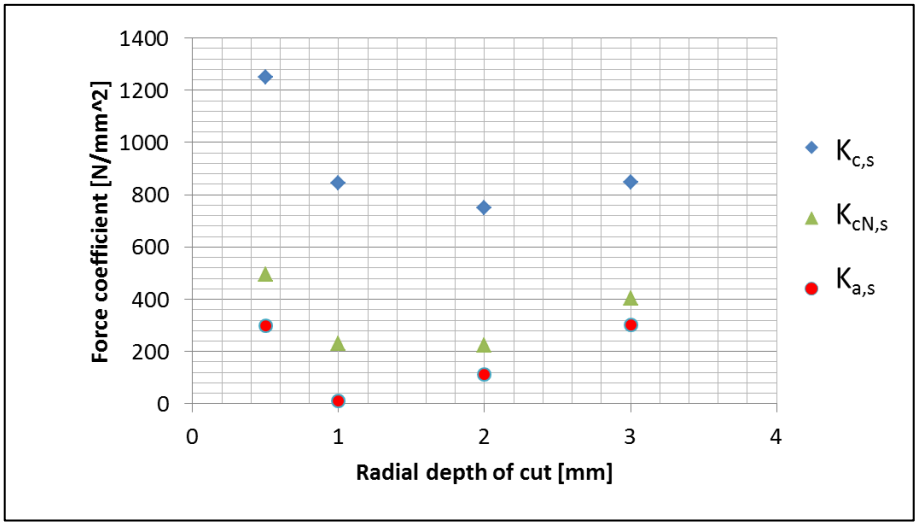

Figure 33 : Trend of cutting force coefficients

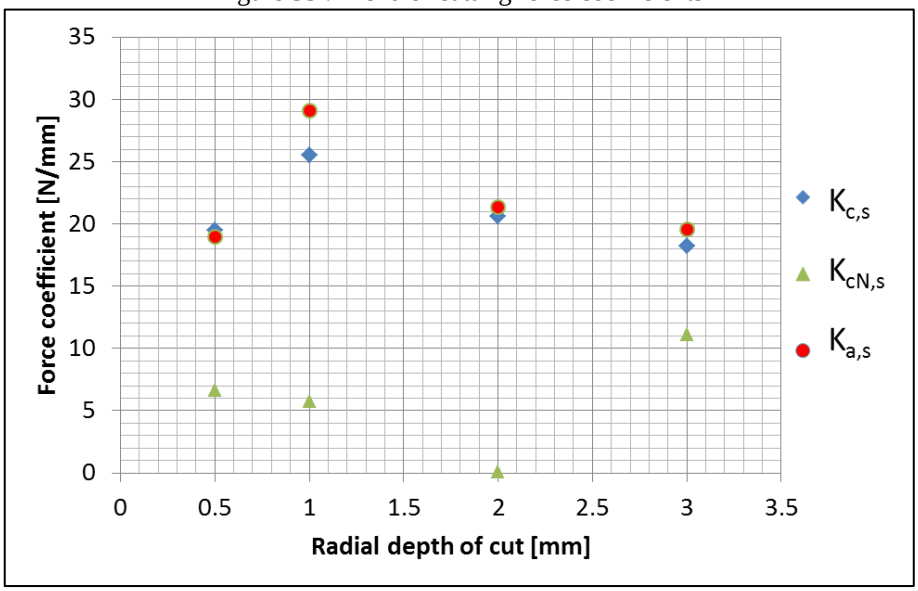

Figure 34: Trend of edge force coefficients

It is possible to notice that for reduced radial engagement the cutting coefficient become higher when the dimension of radial depth of cut is small; this is probably due to the influence of the corner radius of the cutter [117]. It is possible to confirm that forces are proportional to feed per tooth but the value of the constant change with cutting parameter. In this case, the cutting coefficients show a minimum value for radial depth of cut within the range of 1 to 2 mm. Edge coefficients are usually relevant on the computation of the cutting forces only in case of low feed per tooth, when using greater feed per tooth their contribution to the total cutting force is reduced. However, these coefficients do not have a trend as relevant as the cutting coefficients. The values of force coefficient have been used in a

kinematic simulation of the cut to test their capacity of describing and foresee the cutting force. Here (Figure 35, Figure 36 and Figure 37) is reported as an example one of the results obtained for spindle speed of 8000 rpm, feed 960 mm/min and radial immersion of 3 mm:

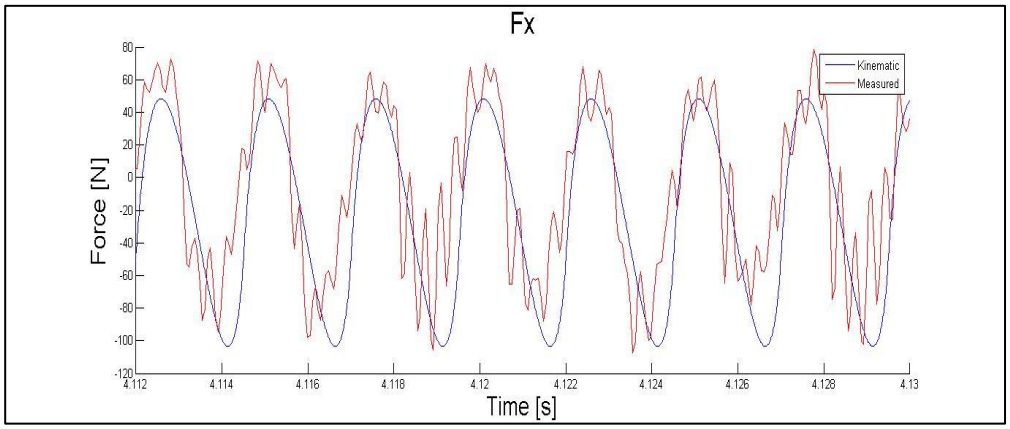

Figure 35: Comparison between kinematic X forces (blue) and measured X forces (red)

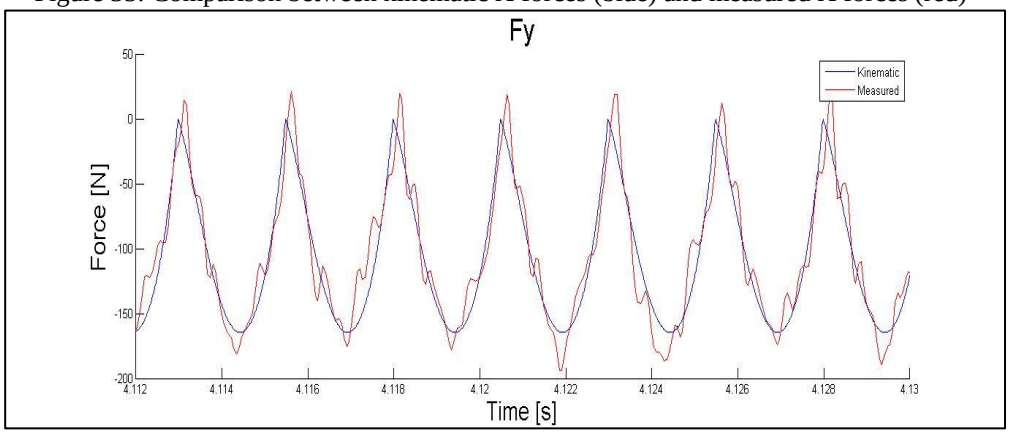

Figure 36: Comparison between kinematic Y forces (blue) and measured Y forces (red)

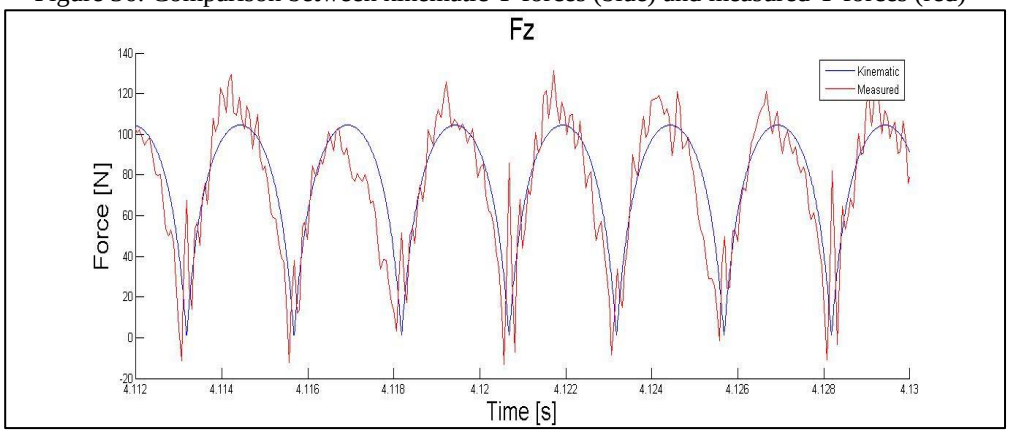

Figure 37: Comparison between kinematic Z forces (blue) and measured Z forces (red)

This comparison have been carried out just using a kinematic model, that it is not able to consider the dynamics of the system, responsible for the high frequency variation of the measured forces. In conclusion, the proposed model correctly represents the general trend of the cutting forces.

2.6. Geometrical description of cutting edge

Reliable cutting force coefficients are crucial for a correct prediction of the cutting forces. This could be used to design the fixture and the tooling, and to have a reliable estimation of the stability of the process. The use of an analytical solution to forecast the arising of chatter [79] makes possible to create a stability lobe diagram to represent graphically the stable and unstable zones. In Figure 38 is reported the SLD of a plunging operation, as obtained with model [79] with 3 different radial engagements in witch is possible to see the difference of taking constant cutting coefficients referred to a standard group of coefficient measured at 2mm of radial depth of cut (blue line in Figure 38).

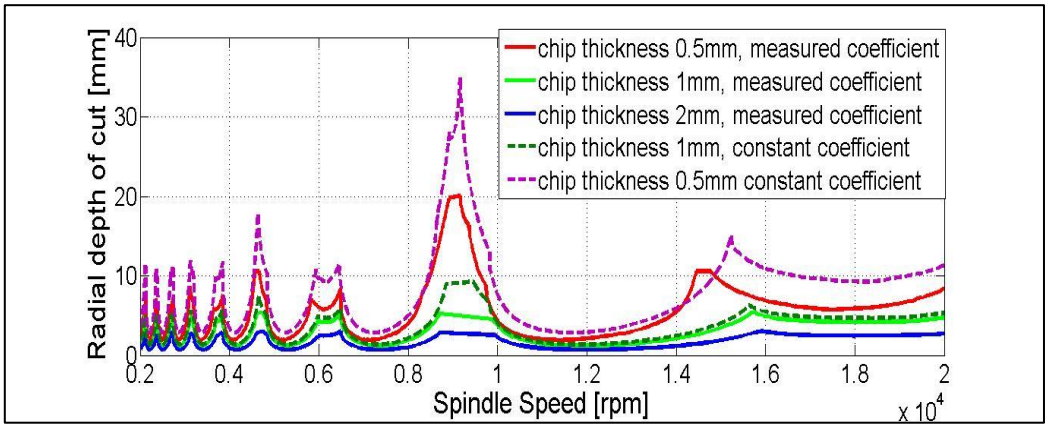

Figure 38: Continuous lines: SLD with measured coefficients; dashed lines: SLD computed with 2mm coefficients taken as a constant standard

Figure 38 reports that not using a force model able to take into account radial engagement varying cutting coefficients bring to relevant differences in the prediction of stability. The standard approach is to consider these coefficients independent from this value: this leads to a not negligible error that is related to the user chosen a_e.

To obtain a better accuracy, from exposed data (**Errore. L'origine riferimento non è stata trovata.** and Figure 34), the best approach is an exhaustive series of tests with a fine radial depth of cut step in order to characterize the force coefficients for an high number of values. This approach will guarantee the best performance in computing SLD by using the more suitable coefficients values every time. Anyway, in this thesis different model based on a more detailed description of cutting edge chamfer (and not only the inclination angle ψ_r and non-cutting length zone l) is developed. This choice was made in order to decrease the number of characterization tests to be carried out, with a little expense of precision. Moreover, this approach can guarantee a faster experimental phase for gathering all the inputs needed to the model, making the procedure more suitable with industrial time

scheduling. This modeling choice was made to fulfill an requests of one of University of Florence industrial partner that was co-promoter of this research activity.

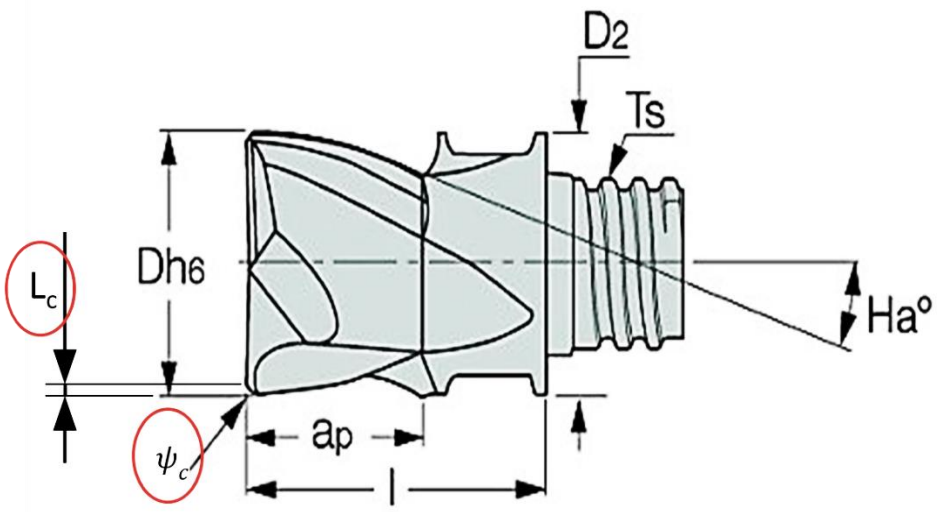

Figure 39: circled in red the new variable of geometric description. From Iscar website

Observing Figure 39 is possible to see highlighted the geometric description of a general tool edge: it has been modeled as a chamfer with length L_c and inclination ψ_c. Also fillets radius has been modeled as chamfer with ψ_c= 45°. This approximation gives good prediction results.

This particular geometrical modeling allows the model to take into account the geometrical influence of inclination angle in dynamic chip component vector for very small stepovers; for this reason this will be included in the final model.

This is based on Zeroth Order Approximation for stability border computing, so a mathematical method to compute the average value of the inclination angle is needed. For this reason a mathematical description of engaged instantaneous chip thickness has been developed, taking Figure 40 as reference. The equations derive from geometrical and trigonometrical considerations.

The following geometrical definitions are introduced:

$$\phi_{ex} = \pi + \tan^{-1}\left(\frac{a_s}{D}\right) \qquad \text{Equation 2.80}$$

$$\phi_{st} = \pi - \cos^{-1}\left(1 - \frac{a_e}{\frac{D}{2}}\right) \qquad \text{Equation 2.81}$$

$$\phi_{stn} = \pi - \tan^{-1}\left(\frac{\sqrt{D a_e - a_e^2} - a_s}{\frac{D}{2} - a_e}\right) \qquad \text{Equation 2.82}$$

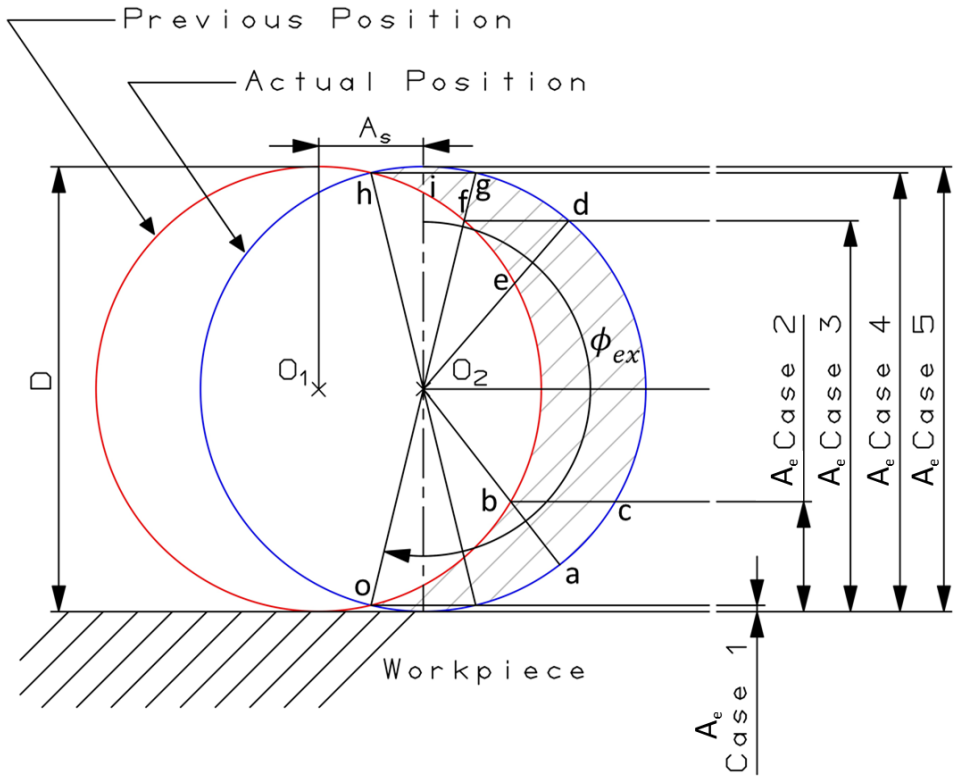

Figure 40: Possible plunge milling configurations

Case 1: $a_e \leq \frac{D}{2}(1-\cos(\phi_{ex}-\pi))$; in this case the value of $a_e$never exceeded point o in Figure 41 . The equation of chip thickness becomes:

$$h(\phi) = \frac{D}{2} - \frac{D}{2}\left(\frac{\cos(\alpha)}{\cos(\phi-\alpha-\phi_{st})}\right) \qquad \text{Equation 2.83}$$

Case 2: $a_e \geq \frac{D}{2}(1-\cos(\phi_{ex}-\pi))$ *and* $a_e \leq \frac{D}{2}$; in this case almost triangular part abc (Equation 2.84) must be taken in account as well as the round part abo (Equation 2.85)

$$h(\phi) = \frac{D}{2} - \frac{a_e - \frac{D}{2}}{(\cos(\phi+\phi_{st}))} \qquad \text{Equation 2.84}$$

$$h(\phi) = \frac{D}{2} - \sqrt{\left(\frac{D}{2}\right)^2 - (a_s\cos(\phi+\phi_{stn}))^2} + a_s\sin(\phi+\phi_{stn}) \qquad \text{Equation 2.85}$$

Equation 2.84 is not used if $a_e = \frac{D}{2}$ exactly.

Case 3: $a_e \leq \frac{D}{2}(1-\cos(\phi_{ex}-\pi))\ and\ a_e \geq \frac{D}{2}$; in this case triangle def (Equation 2.88) and the upper circular part from de to $\pi/2$ (Equation 2.89), having introduced the definition of variable X and Y (Equations 2.86 and2.87)

$$X = \frac{-a_s + \sqrt{{a_s}^2 - (1+\tan(\frac{\pi}{2}-\phi+\phi_{st}))^2\left({a_s}^2 - \left(\frac{D}{2}\right)^2\right)}}{(1+\tan(\frac{\pi}{2}-\phi+\phi_{st}))^2} \quad \text{Equation 2.86}$$

$$Y = \tan(\frac{\pi}{2}-\phi+\phi_{st})X \quad \text{Equation 2.87}$$

$$h(\phi) = \frac{a_e - \frac{D}{2}}{\cos(\phi+\phi_{st})} - \sqrt{X^2+Y^2} \quad \text{Equation 2.88}$$

$$h(\phi) = \frac{D}{2} - \sqrt{X^2+Y^2} \quad \text{Equation 2.89}$$

For the remaining part from $\pi/2$ to ϕ_{ex} case 2 is taken as reference (see Equation 2.85).

Case 4: $a_e \geq \frac{D}{2}(1-\cos(\phi_{ex}-\pi))\ and\ a_e < D$; in this case the triangular part O_2gh is divided into three parts, one is described by Equation 2.90, one described by Equation 2.93, one described by Equation 2.96. The remaining part over $\pi/2$ is described by Equation 2.97.

$$h(\phi) = \frac{D}{2} - \sqrt{X^2+Y^2} \quad \text{Equation 2.90}$$

$$X_1 = \frac{-a_s + \sqrt{{a_s}^2 - (1+tan(\frac{\pi}{2}-\phi+\phi_{stn}))^2\left({a_s}^2 - \left(\frac{D}{2}\right)^2\right)}}{(1+tan(\frac{\pi}{2}-\phi+\phi_{stn}))^2} \quad \text{Equation 2.91}$$

$$Y_1 = \tan(\frac{\pi}{2}-\phi+\phi_{stn})X_1 \quad \text{Equation 2.92}$$

$$h(\phi) = \frac{a_e - \frac{D}{2}}{\cos(\phi-\phi_{st})} - \sqrt{{X_1}^2+{Y_1}^2} \quad \text{Equation 2.93}$$

$$X_2 = \frac{-a_s + \sqrt{{a_s}^2 - (1 + \tan(\frac{\pi}{2} - \phi))^2 \left({a_s}^2 - \left(\frac{D}{2}\right)^2\right)}}{(1 + \tan(\frac{\pi}{2} - \phi))^2}$$ Equation 2.94

$$Y_2 = \tan(\frac{\pi}{2} - \phi) X_2$$ Equation 2.95

$$h(\phi) = \frac{a_e - \frac{D}{2}}{\cos(\phi)} - \sqrt{{X_1}^2 + {Y_1}^2}$$ Equation 2.96

$$h(\phi) = \frac{D}{2} - \sqrt{{X_1}^2 + {Y_1}^2}$$ Equation 2.97

The last part is defined by Equation 2.85.

Case 5: $a_e = D$; this is a special case in which the equation of case 4 can be reduced to a symmetrical engagement than case 2 for $a_e = \pi/2$.

With this formulation is possible to solve a simple numerical algorithm to compute the average inclination angle $\psi_{ave}(\phi)$ by calculating the engagement for each angular position (starting from the knowledge of a_e, for each angular increase $d\phi$), then calculate its relative mean inclination angle and, at last, calculating the average value ψ_{ave} on all over the radial engagement from ϕ_{st} to ϕ_{ex}.

2.7. FRFs measurements

The relation between the machining process and tool-tool holder-spindle unit dynamics is well known: tooltip forces are the causes of displacements that are the origin of vibrations and regenerative effect. Frequency Response Functions describe the description of interaction between displacements and forces.

There are both experimental and numerical technique in literature able to measure these functions. While experimental techniques, such as impact testing, may often be applied to determine the required receptances directly, in some instances this approaches may be too time-consuming (such as a large production facility with many hundreds of tooling combinations) or inconvenient due to physical restrictions (slender, flexible tools and micromills). In these situations, a preferred alternative is to implement a predictive technique based on tool-structure models. Challenges to this paradigm include for example damping estimation (particularly at interfaces) contact stiffness determination (in rolling element bearings) and full geometric knowledge of commercial components, such as spindles. In literature, the Receptance Coupling Substructure Analysis (RCSA) is the common procedure to obtain numerically tooltip FRFs. This technique was developed [118 – 122] by building on the receptance coupling principles detailed by Bishop and Johnson [123]. Using RCSA, models of the tool and holder (relative easy to model) are coupled to a measurement of the spindle machine (more difficult to model) to predict the assembly's bending receptances.

This information may then be used, together with milling models, to predict the stability [74, 124] and forced vibration behavior [125].

In this thesis, the objective is not derive the theory of RCSA for FRFs computing nor derive a method to measure axial and torsional FRFs (to deepen its principles read as example the paper of Schmitz [126]). Anyway, it has been chosen to synthetically present the measurement procedure and an example of results because FRFs measurements are a crucible input to the plunge model. The choice of measuring FRFs over computing them was made with the purpose to decrease or avoid modeling ad numerical errors as far as possible in order to be sure of the inputs before checking results and validate the models.

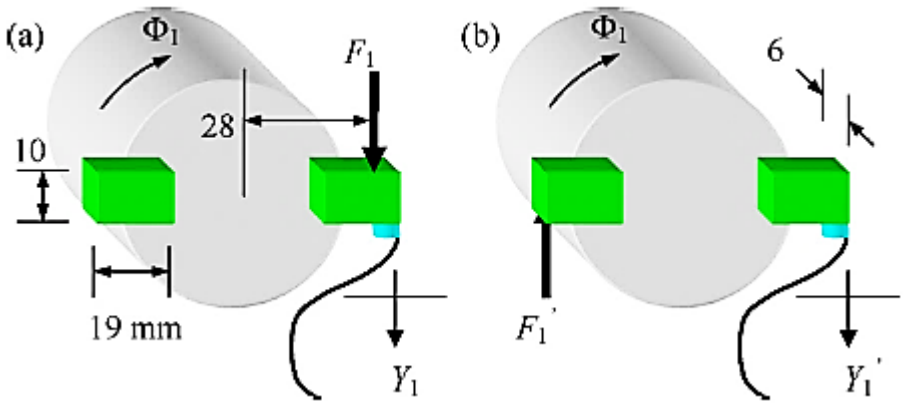

Figure 41: Description of torsional measurement with bending compensation

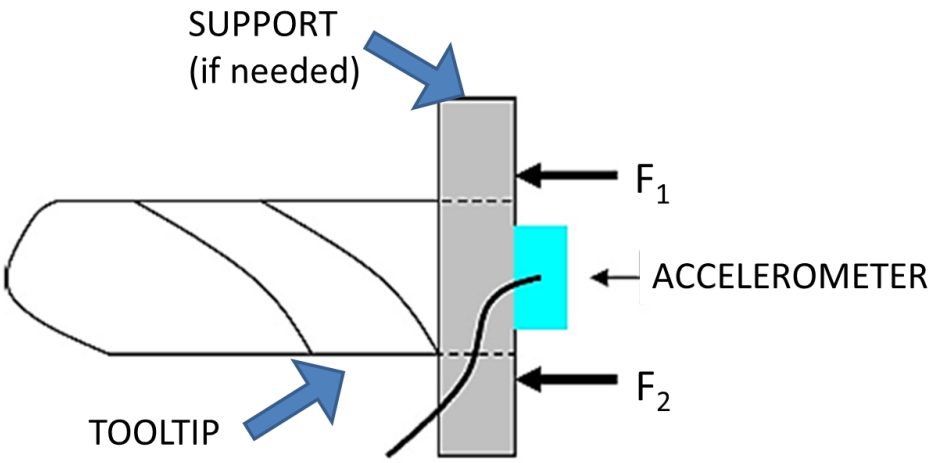

Figure 42: Description of axial measurement with bending compensation

Figure 41 and Figure 43 describe the configuration to perform torsional and axial FRFs measurement. In both cases an additional adapter is fixed at the end of the tool to create enough space to fix the accelerometers and to have a planar surface to strike with an instrumented hammer. If the tool is big and present planar insert surfaces is possible to avoid

the use of the adapter: it is fundamental for small tool to place the measure instrumentation. The effect of the adapter on FRFs is then removed with reverse RCSA techniques.

Both measurements have in common the problem of measure alteration caused by bending effect: this effect is inevitably introduced when the tooltip structure is excited by an hammer hit whose direction is lateral or axial (but not collinear with tool axis). This flection will affect results by introducing the bending modes inside axial or torsional FRFs, as if they were effectively due to these dynamic behaviors. For this reason two measure must be performed: the hammer will excites the structure in two point in order to introduce the same axial or torsional component (in terms of direction) but an opposite bending. If the measures are well performed, by averaging the results, the pure torsional or axial FRFs are obtained because the bending modes will be compensated in the average computing.

The position of the accelerometer and of force impact point (R_P) must be carefully measured in order to having the same amplitude of torque and bending to be compensated and to convert forces into torques and linear displacements into angular ones (for FRF concerning angles or torques). After having complete the measure this simple formulas can be used to retrieve the real FRFs in the right physical unit: Equation 2.98 is used to obtain torsional FRF, Equation 2.99 is used for cross- talk axial-torsional FRF.

$$\frac{\theta}{T}(\omega) = \frac{{}^{Y}/_{R_P}}{FR_P} = \frac{Y}{F}(\omega)\frac{1}{{R_P}^2} \qquad \text{Equation 2.98}$$

$$\frac{\theta}{T}(\omega) = \frac{Y}{FR_P} = \frac{{}^{Y}/_{R_P}}{F} = \frac{Y}{F}(\omega)\frac{1}{R_P} \qquad \text{Equation 2.99}$$

To understand how compensation by averaging bending contribution works Figure 43 and Figure 44 (relative to a rectangular aluminum specimen used as a trial test) are reported as an example.

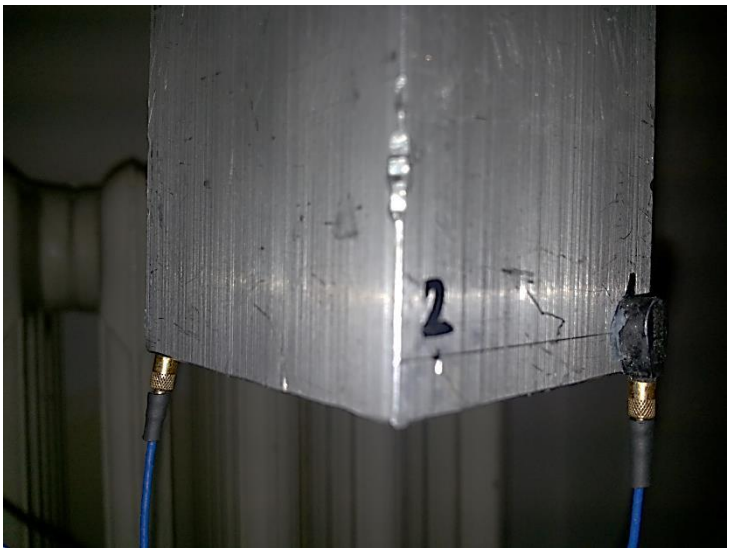

Figure 43: free-free configuration of aluminum steel block specimen

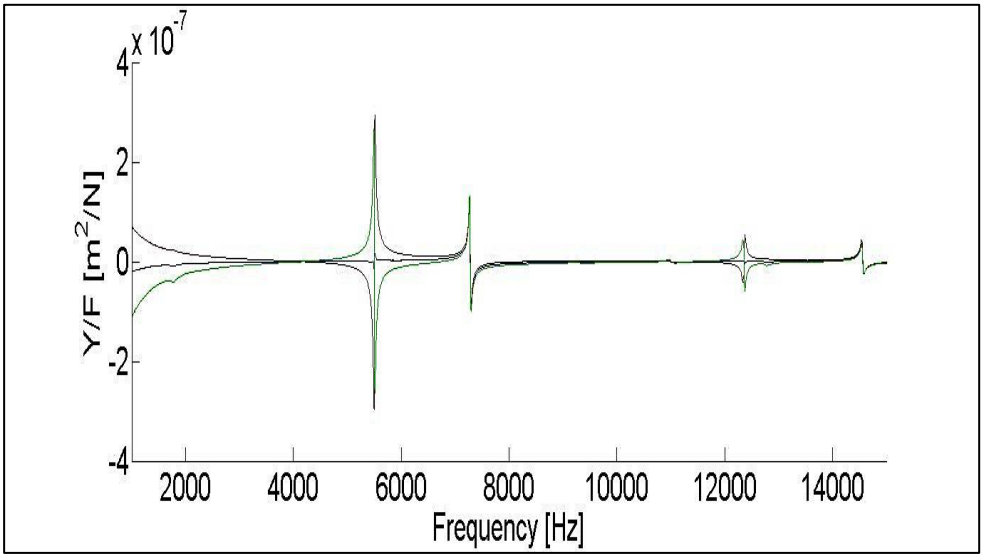

Figure 44: Example of bending effect on real part: opposite spikes with same amplitude are the bending effect (around 5500 Hz and 12000 Hz), while torsional modes (around 7200 Hz and 14500 Hz) have same direction and amplitude

For higher accuracy and repeatability, more than one measure have been carried out. This method has the same criticalities as the classic bending FRF measurement: it's affected by the capability of the operator to strike with high precision on a marked hit point while maintaining as far as possible the instrumented hammer parallel to the required direction (for example X direction if X direction FRF is wanted), and in the errors that lies in the accelerometer positioning. If the accelerometer has a mass not negligible respect the structural dynamic behavior, also a mass loading compensation [127] must be taken into account. The measure of the correct position of accelerometer and hammer hit points is fundamental and can lead to errors in the computing of torsional FRF from a linear measure.

For a complete report, an example of results on a Iscar plunge tool E93CN D25-2-M12-10 is reported: see from Figure 45 to Figure 48. From this data it can be seen that some errors can anyway be found in a frequency range placer in low frequency, as normal can happen in this kind of measurements.

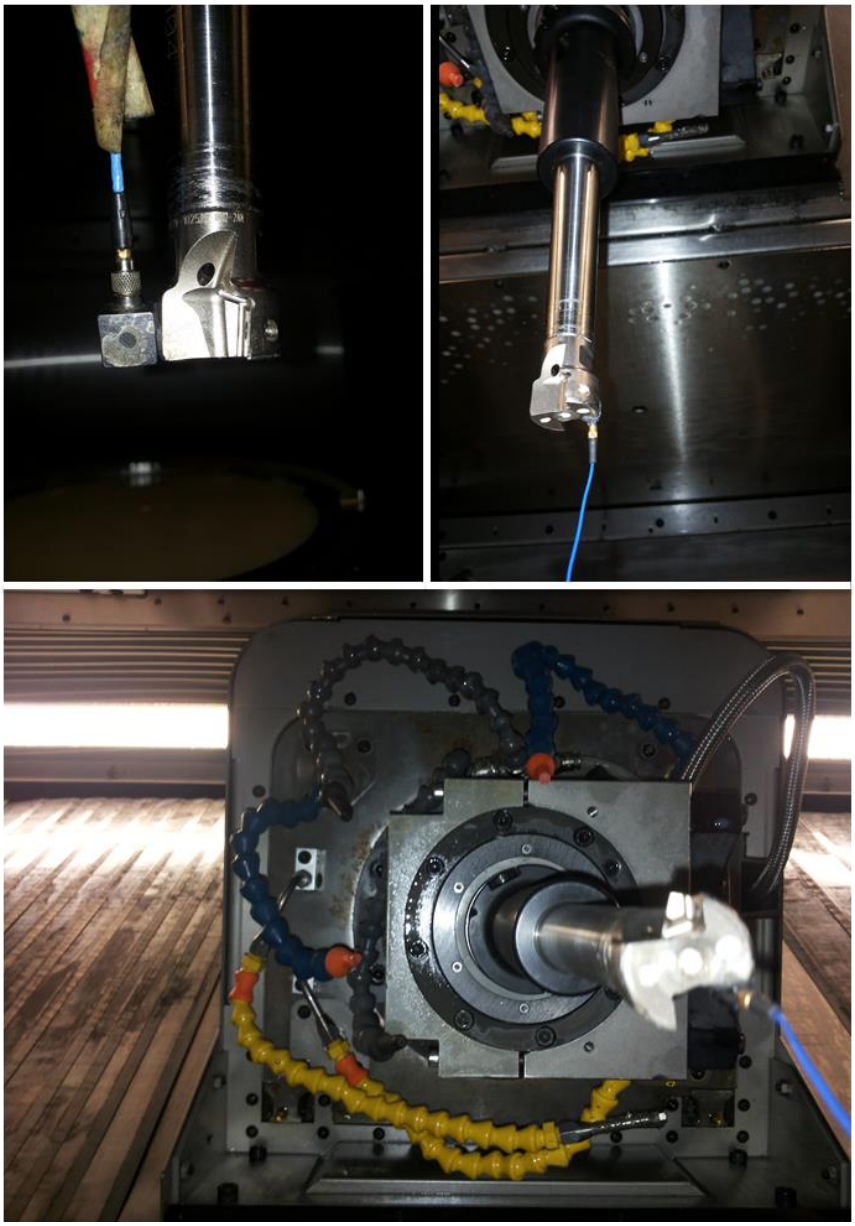

Figure 45: Tooltip and marks relative to accelerometer positions and hammer hitpoints

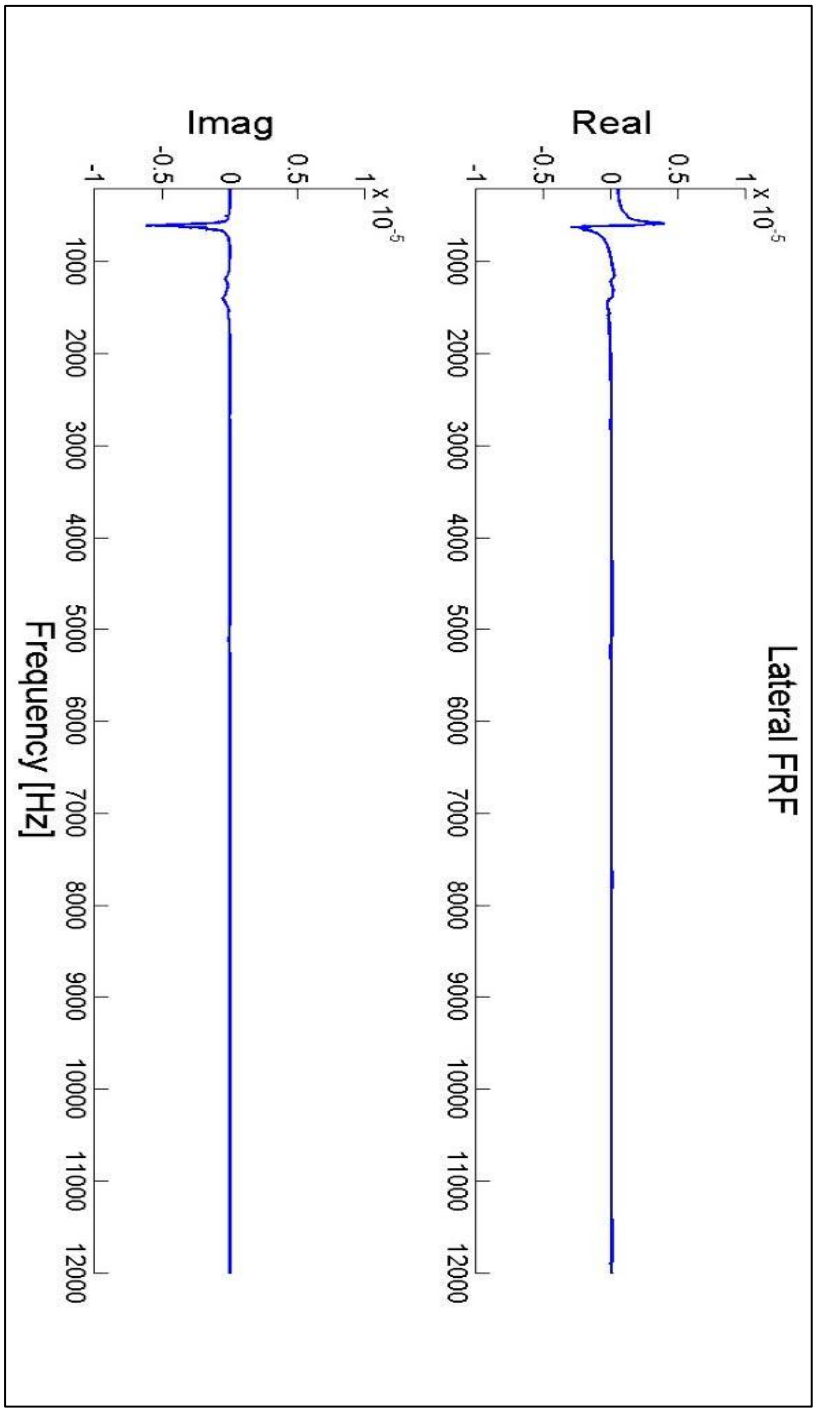

Figure 46: XX and YY FRFs. The machine exhibits a symmetrical dynamic behavior on the horizontal plane. Displacements are expressed in metres [$^{m}/_{N}$]

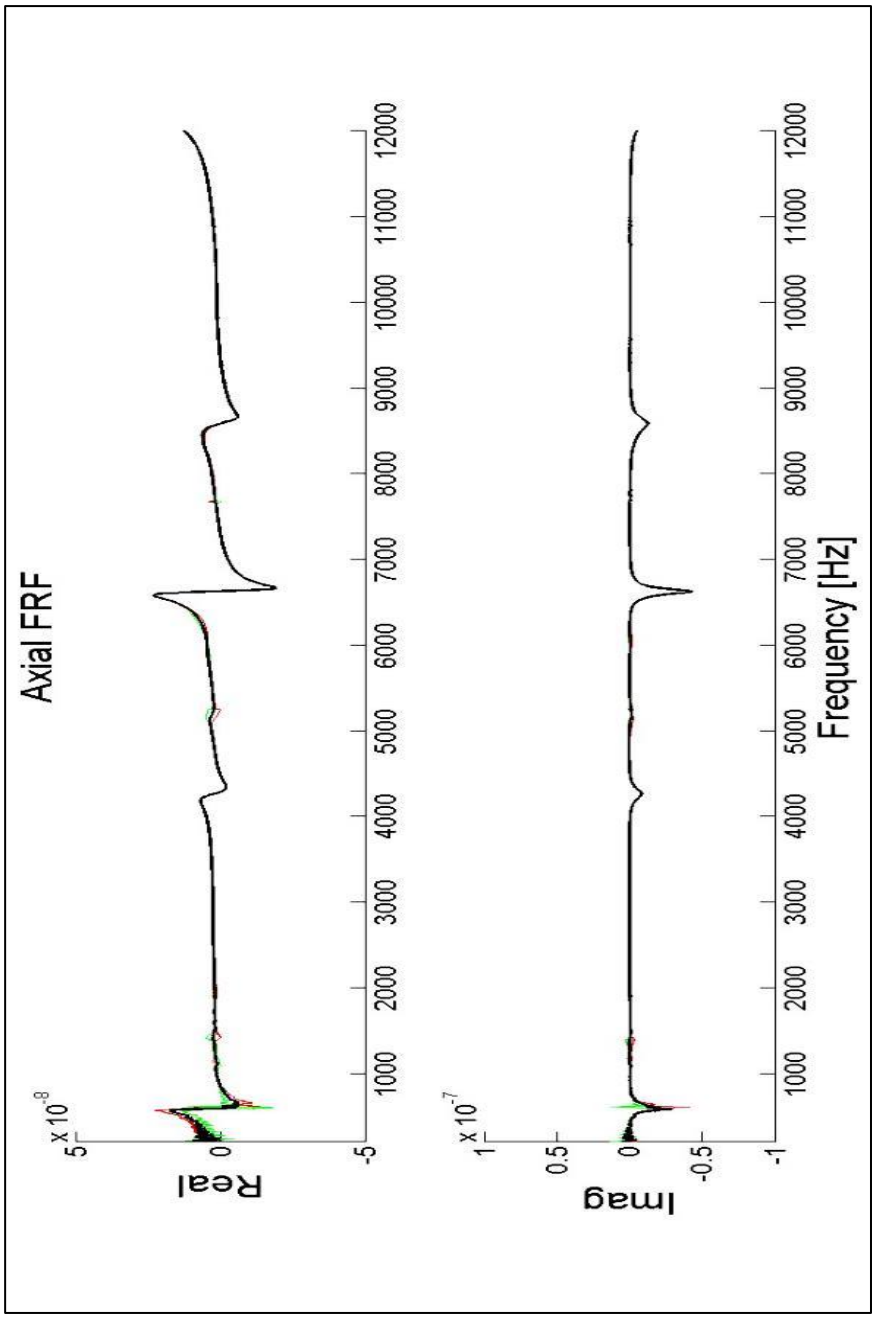

Figure 47: Axial averaged FRF (black line). Displacements are expressed in metres [$^{m}/_{N}$]

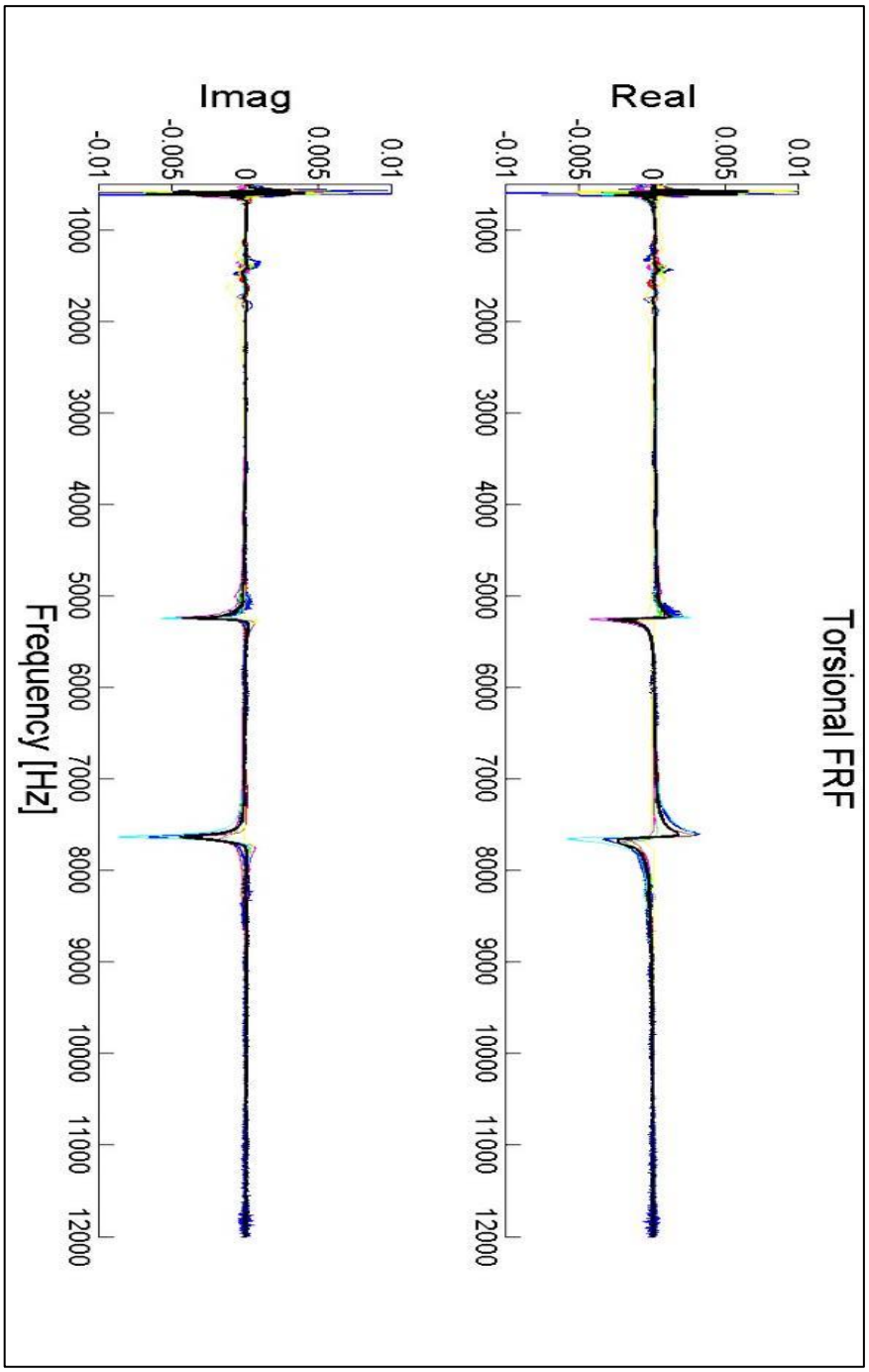

Figure 48: Torsional averaged FRF (black line). Displacements are expressed in [$^{rad}/_{Nm}$]

2.8. Plunge milling solution algorithm

After having defined all model inputs, in this chapter it will be shown how the main algorithm work for taking into account the geometrical consistency between the predicted critical radial depth of cut $a_{e\,lim}$ and the geometrical imposed one a_e.

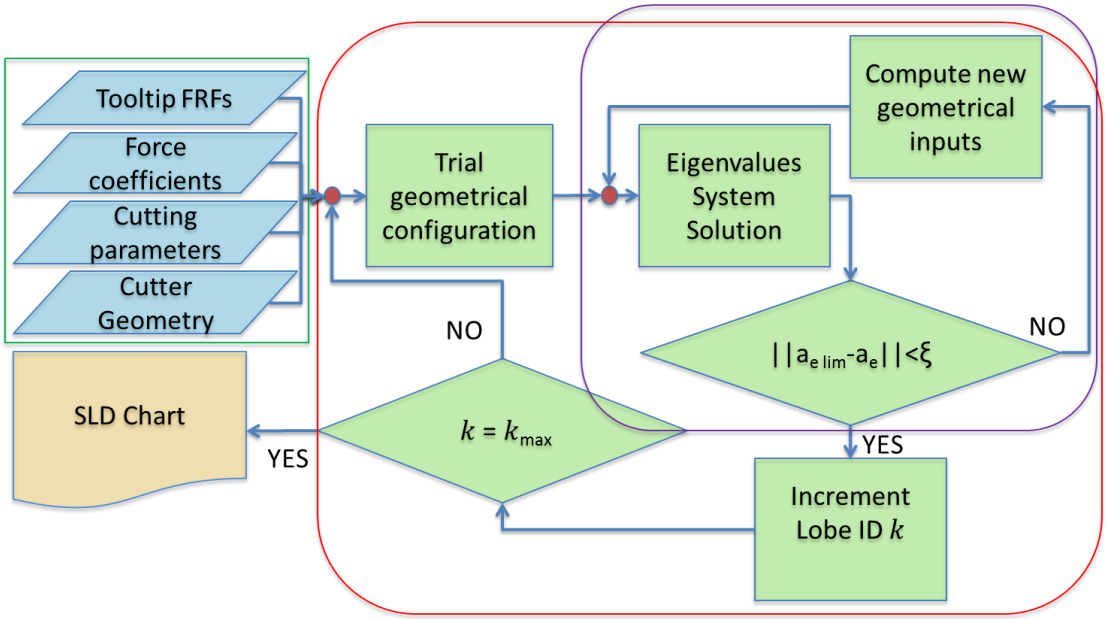

Figure 49: Solution algorithm flow chart

The principle of this algorithm is simple. The inputs are highlighted in the green square in Figure 49 and have been described in the previous chapters. The inputs are processed in a first attempt starting from a trial configuration, using the equation relatives to plunge milling model (see chapter 2.3). The algorithm is composed by two nested main loop: the external loop (red square) is the same described at the end of chapter 2.2 and it works as the same way as flank milling model. The internal one (violet square), solve the eigenvalue solution of Equations 2.48 and 2.49, computing the critical radial depth of cut. A control verifies if the calculated $a_{e\,lim}$ is contained within a certain error ξ (that can be chosen by the user) respect the trial geometry. If this happen, the internal loop ends: these phases are repeated until the external loop is completed and SLD are drawn.

If the congruency between the computed and the geometrical inputs are not verified, two scenarios can arise:

- $a_{e\,lim} < a_e$
- $a_{e\,lim} > a_e$

If the first scenario is met, it means that chatter conditions have been already satisfied with actual tool engagement: therefore this configuration will results in an instable one and the radial engagement must be reduced.

If the second scenario is met, it means that instability condition are far from being reached. For this reason radial engagement can grow. In this case a second attempt is try a complete immersion, with $a_e = D$. This represent the geometrical limit condition for every tool with a fixed stepover a_s. If the new iteration repeats the second scenario, it means that this tool is always stable for the chosen value of a_s on that material at that computed frequency and the internal loop iteration ends. If stepover or forces coefficients are too small or the tool is exceptionally rigid, it may happen at the end of calculations that the results of SLD is a straight line placed at $a_{e\,lim} = D$: this means that the stepover for that specific tool can be augmented: the limit of stepover augmentation is the cutter length that is equal to $D/2 - l$.

After a cycle of internal loop both of the two scenarios lead to a new calculation of configuration: the new value of radial depth of cut is chosen by bisection method between the first attempt value and the corresponding extreme limit (that are $a_e = 0$ for the first scenario and $a_e = D$ for the second one). After that a new calculation of $a_{e\,lim}$ is completed and the geometrical congruency is checked again. The previous step value of a_e will substitute the upper or the bottom limit if $a_{e\,lim} < a_e$ or $a_{e\,lim} < a_e$ respectively. This fact leads normally to alternations of scenarios until the convergence condition is satisfied, ending the internal loop.

The error value that has been chosen for all computation was 0.01mm that is a very small value of tolerance. With this value the computing time is about 10-15 minutes in average, that is acceptable, also for industrial time scheduling.

3. Experimental activity

In this chapter a short but significant summary of all experimental activity (composed by many tests with different combination of tool kits and workpiece material) is given. Experimental test had flanked step by step all the development of the models and have led to its final solution formulation.

3.1. Confirmation of literature model

The first step was to test Altintas plunge model in order to verify its prediction capability but also eventual author errors in interpretations of his model. For this reason, the very first test was computed using data from its paper just to obtain the same SLD. This preliminary result was achieved.

Initial tests have been carried out at Department of Industrial Engineering of Florence (DIEF) laboratory, using different systems: machine, tool, tool holder and workpiece.

The used machine was a Mori Seiki MNV1500, that is a 5 axis high speed milling machining center, see Figure 50. The used tool was an Iscar MultiMaster EC120 E09 R05 CF - 4T08 -IC908 (see Figure 52), that is a 4 flute end mill with an overhang of 50 mm from the tool holder end (shank was an Iscar MM S-A-L070-C12-T08-C), and the tool holder was a Daishowa BIG HSK 32 Er20 (see Figure 51).

The work piece was a rectangular steel block of S275yc prepared for performing hole enlarging milling. Force coefficients have been measured with the method described in chapter 2.5.2. In Table 6 force coefficients are reported. The purpose of chapter 3.1 is to verify the literature model or quantify its errors, so the coefficients were kept constants. They were computed for an $a_e = 1\ mm$.

Table 6: cutting forces coefficient in preliminary tests: Iscar Multi Master on S275yc steel block

Kc,s [N/mm^2]	KcN,s [N/mm^2]	Ka,s [N/mm^2]	Kc,p [N/mm]	KcN,p [N/mm]	Ka,p [N/mm]
2610.80	429.71	1328.60	42.16	3.09	34.70

Figure 50: Mori Seiki NMV1500

Figure 51: Tool kit of preliminary test

The edge inclination angle was set to be ψ_r=45° to model the edge chamfer. The tool was too small to measure torsional and axial FRFs, so the contribution of these dynamics was not taken into account for SLD computation (in this phase of model developing) having at least the accuracy to use took kit not too rigid in bending direction.

The lateral FRF can be seen in Figure 52.

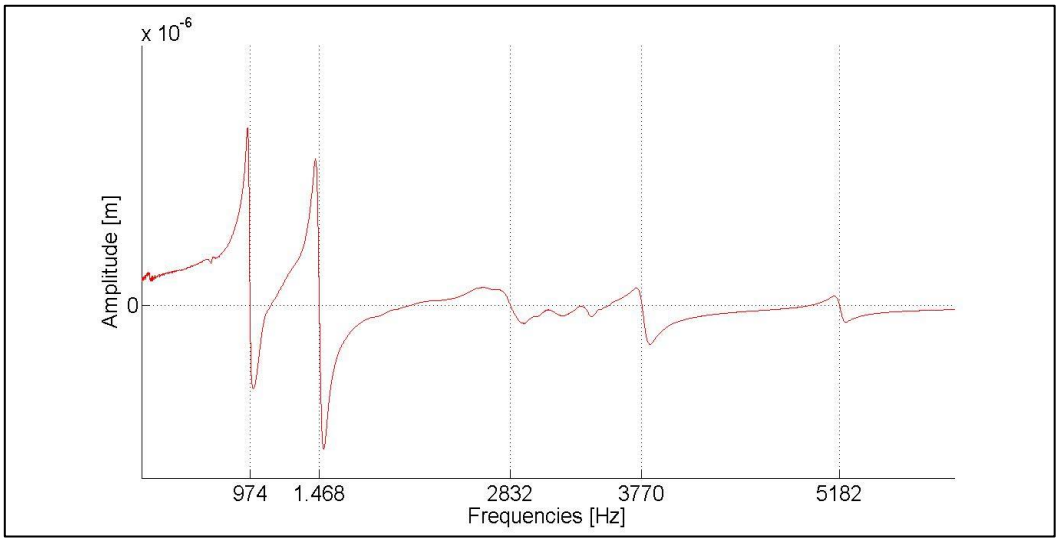

Figure 52: preliminary test tool kit lateral FRF

The preliminary workpiece was milled with a series of holes to obtain incremental radial depth of cut for different spindle speed as shown in Figure 54. This test was tried in accord to SLD to verify the predicted chatter limit. To control the instability insurgence the steel block was clamped on a Kistler dynamometer Type 9257A.

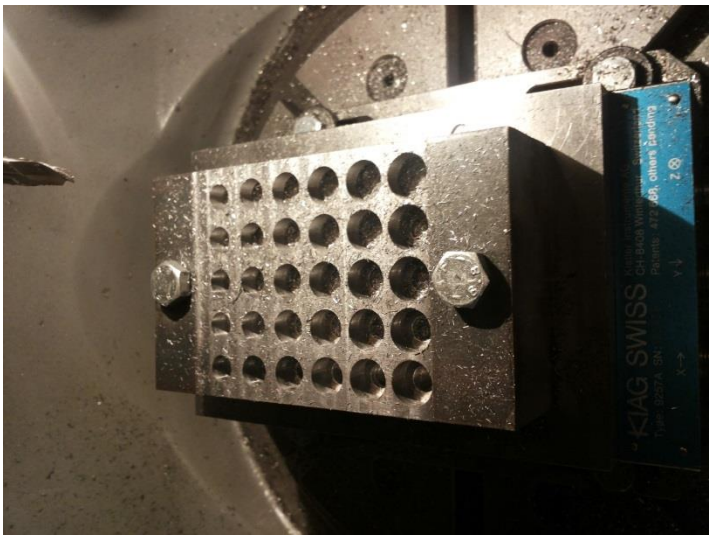

Figure 53: Steel block assembly on Kistler dynamometer

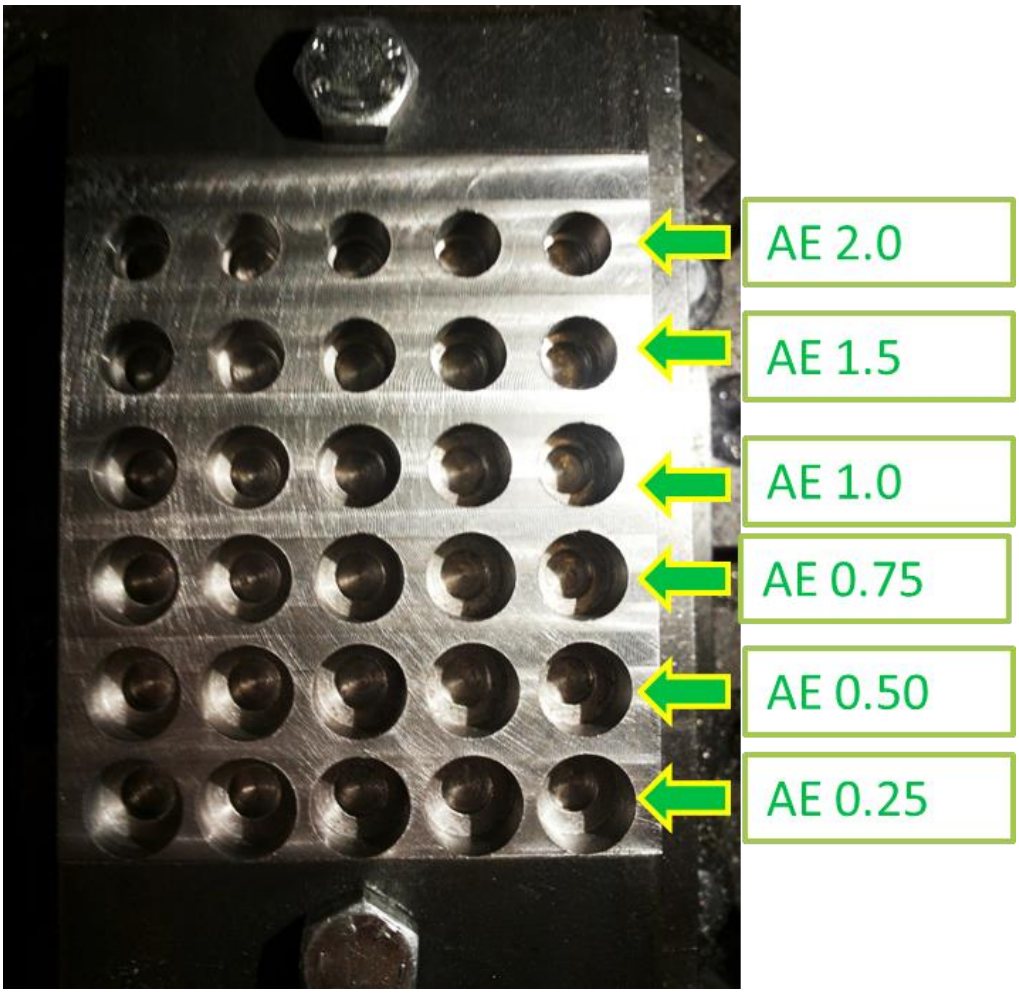

Figure 54: Steel block preparation with incremental radial depth of cut.

Each column was milled keeping a fixed spindle speed S from smallest radial depth of cut to the maximal one, or when chatter was detected, as reported in Figure 55. Finally, the $a_{e\ lim}$ was reported on the computed SLD as shown in Figure 56.

Milling larger preparation hole means higher radial engagement for real tests.

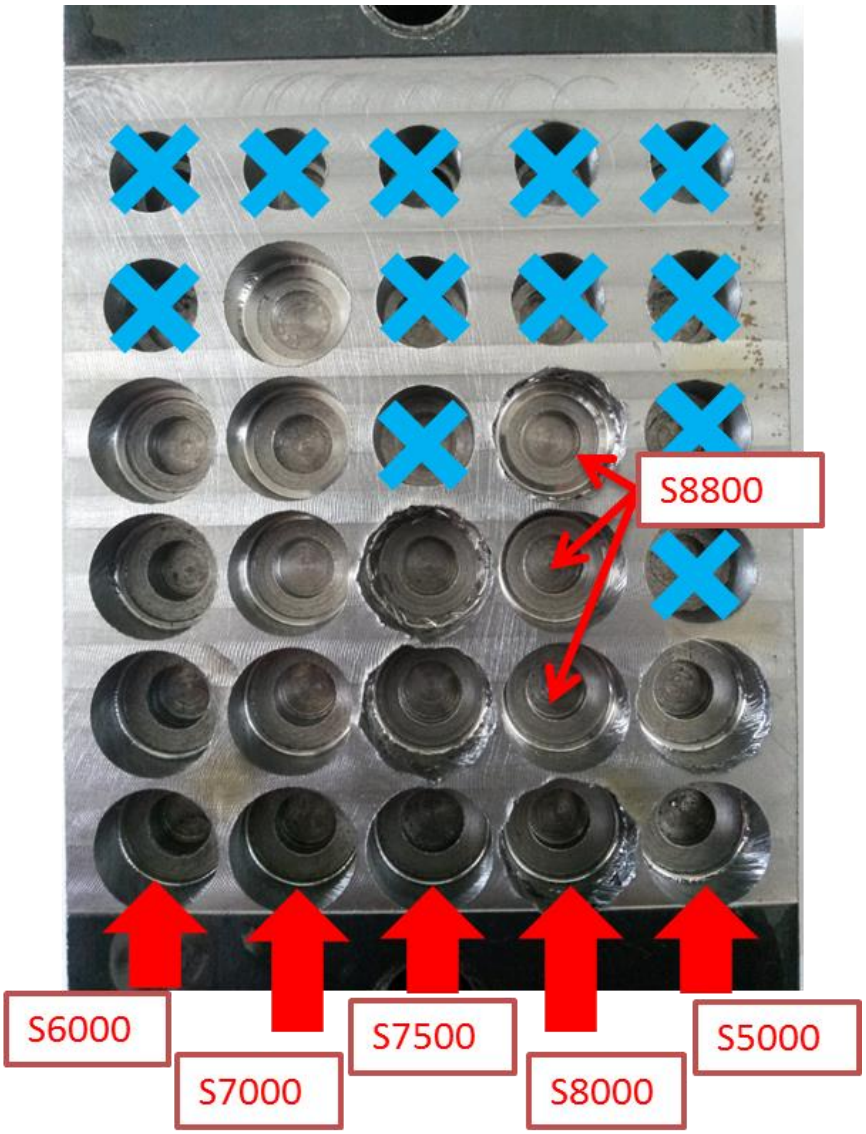

Figure 55: Milling schedule and results: blue X in the figure are not milled holes

It is possible to see from Figure 55 how the chatter can be very severe for certain combination of Spindle speed and radial depth of cut, while in other combination it is present but the surface is anyway good.

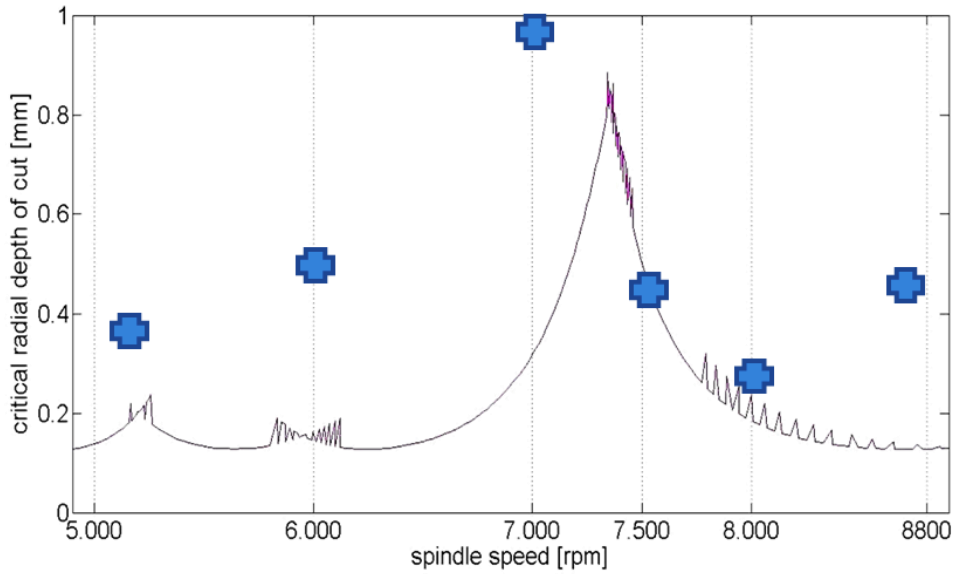

Figure 56: predicted SLD and measured $a_{e\ lim}$. Small peaks are numerical errors in enveloping the lobes. Blue + represent measured chatter limit

From Figure 56 it can be observed a shift towards left of the real lobe position and a shift towards the bottom of the chart of the predicted SLD respect to real SLD. The first phenomenon is not uncommon, and can be originated from a shift in the frequency of the dominant modes due to the normal discrepancy that can be found between the static FRF measurement (hammer test with not rotating spindle unit) and the real dynamic behavior while the spindle unit is in motion. A shift of frequency (from few Hertz to dozen Hertz) can be reflected as a displacement in spindle speed (about dozens or hundreds rpm) in the SLD. This is a phenomenon that is already been evidenced in literature [128] and depends from the structure and form the joint ad bearing dynamic behavior at different rotation speed. The second shift can be due from the inclination angle:45° is the value of the chamfer while the value of the average inclination change (decrease) with immersion because the tool is a flat and mill: it's possible to solve this problem with an accurate geometric description as described in chapter 2.6.

For a complete report of this test, the measured forces for 8000 rpm and 7000 rpm are reported and analyzed using SCADAS acquisition system and TestLab® software.

Figure 57 report the forces for a_e=0.25 and S=8000, while Figure 58 is a spectrogram of the force in Z direction. From Figure 57 it can be observed that the value of the forces exceed the upper limit of the measure, being heavily affected by chatter. In particular from spectral analysis of Figure 58 (even not properly correct being the measure out of scale because of instability), it can be seen that the main harmonic in the spectrum is placed around 4100 Hz; this frequency is not comparable with bending modes but is coherent with torsional one, This fact means that the intuition of Altintas (about the needing for plunge milling to take into account a 4 DOF model) was exact.

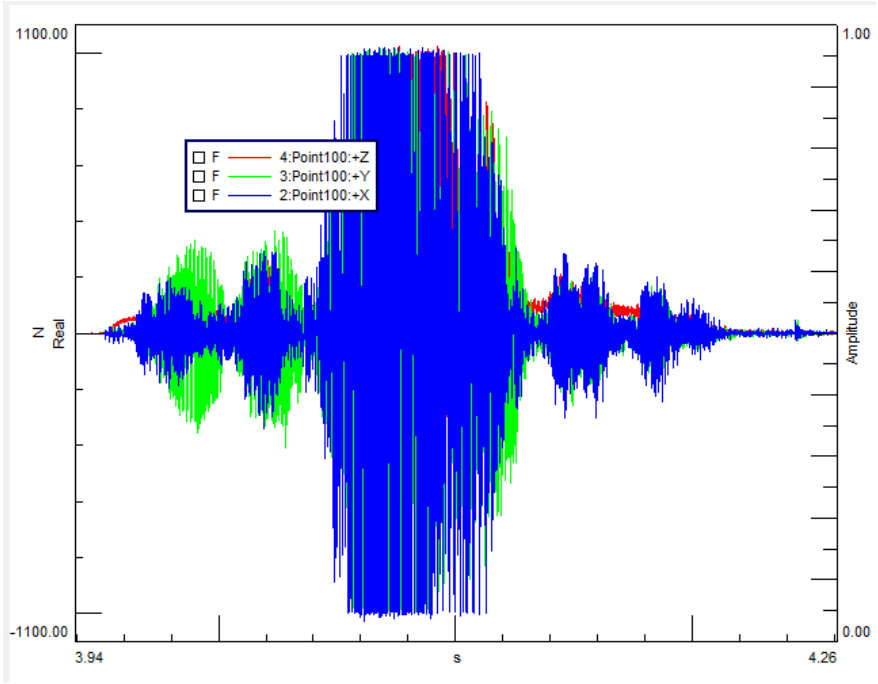

Figure 57: Measured forces [N] versus Time [s] for a_e=0.25 and S=8000 test

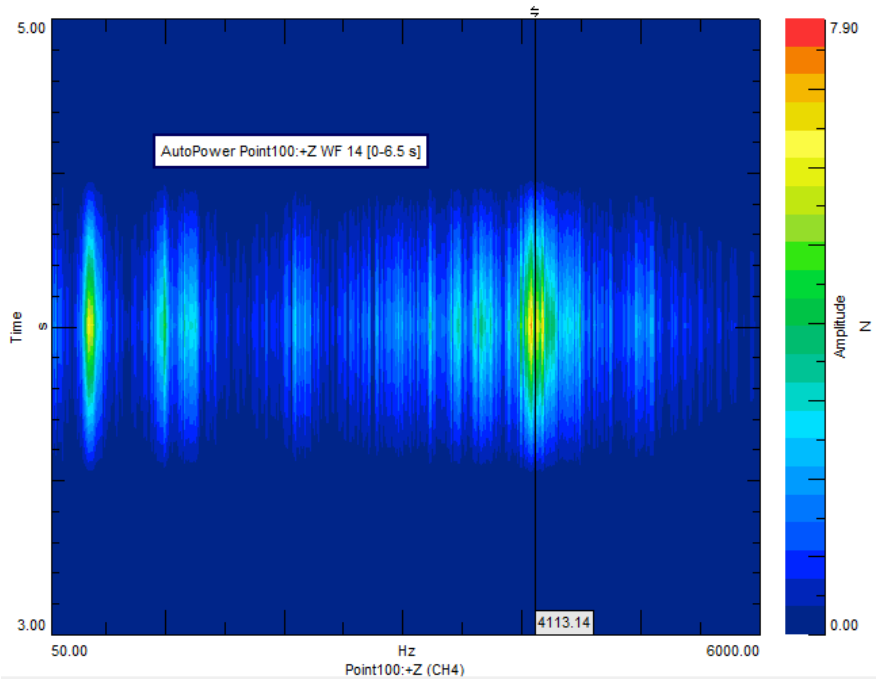

Figure 58: Spectrogram of Z force in a_e=0.25 and S=8000 test

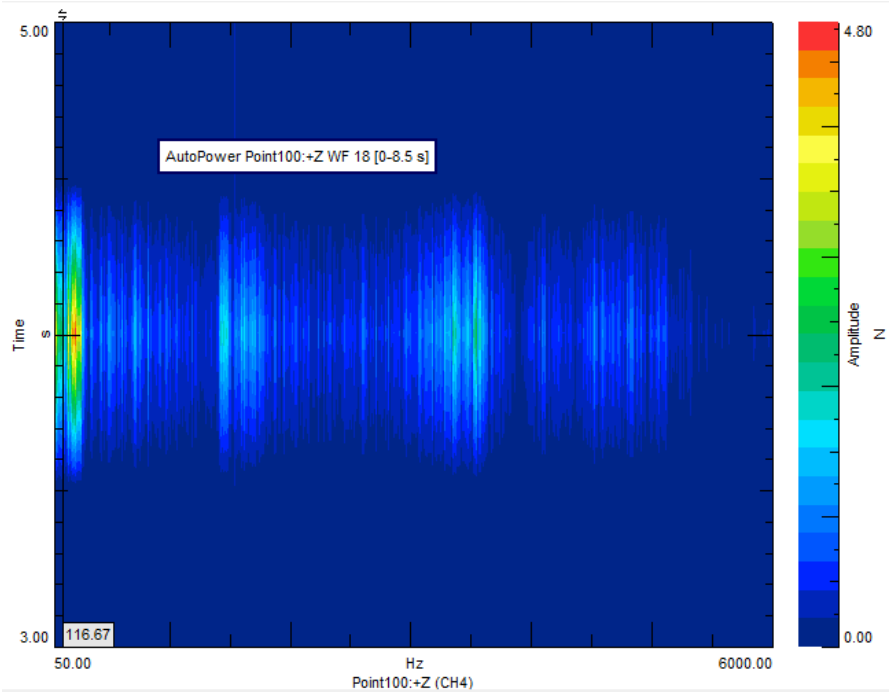

Figure 59 Spectrogram of Z force in a_e=1.00 and S=7000 test

In Figure 59 the spectrogram (spectrogram) in Z direction of a_e=1.00 and S=7000 test is reported. The second harmonic of rotation frequency is the most relevant harmonics; the dynamometer has a mode in the table in Z direction around 3200 Hz (measured with hammer test); it can be seen the main contribution to chatter given by a frequency around 1500 Hz, that is compatible with bending mode.

As a conclusion of this preliminary test, it can be said that Altintas model is built in a good way and can be used as a starting point, but it needs more input to overcome its limits, in particular to describe the inclination of the main cutters and to be applied to a real plunge configuration.

3.2. Angular engagement influence tests

To verify the influence of angular engagement (the difference between $\phi_{ex}$and ϕ_{st}) for a new configuration and to test the iteration part of the solving algorithm described in chapter 2.5.6, a series of intermediate test was executed. To reach this intermediate development goal a special test was designed. It consist in a plunge milling with incremental angular engagement but keeping constant the maximal chip thickness.

The specimen is a rectangular steel block mounted on a dynamometer with a certain degree of inclination respect to vertical position, see Figure 60. The workpiece is pre milled in order to create e cave that grew its radial engagement in a linear way with the height of the block.

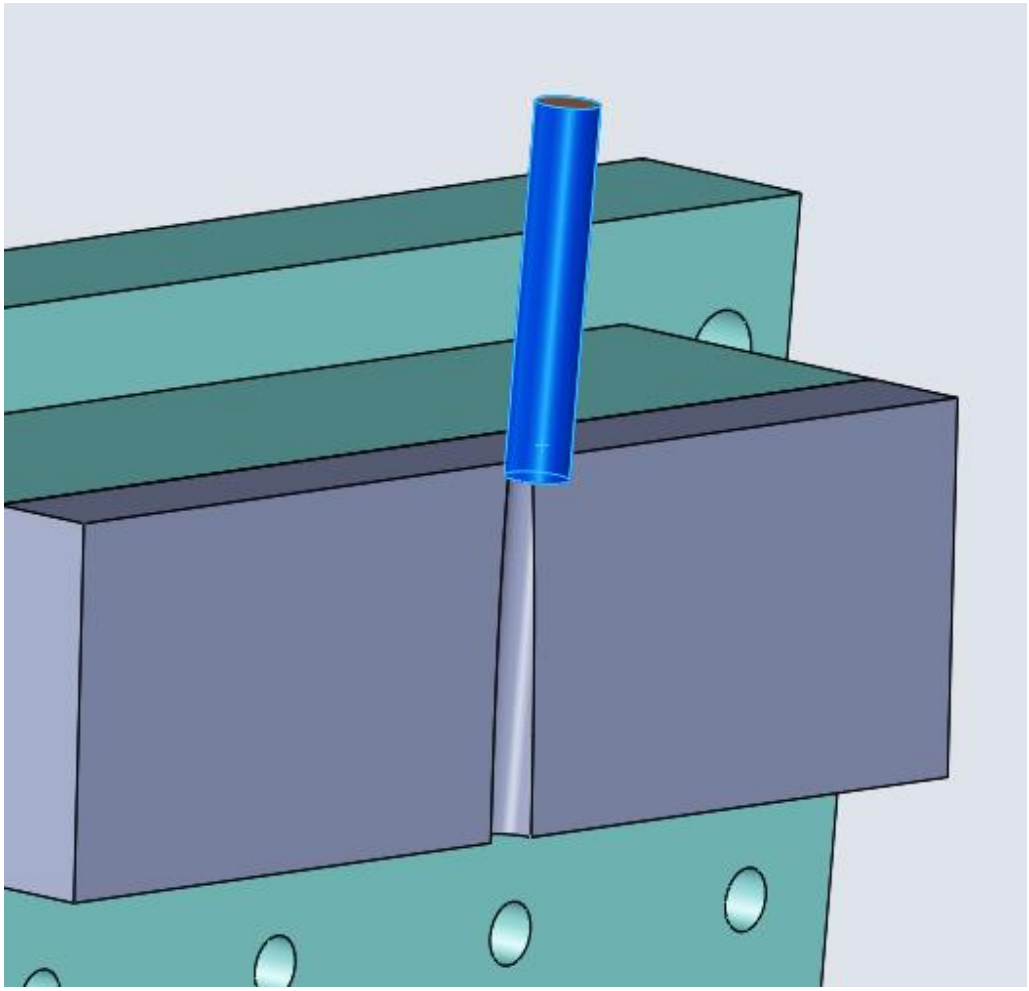

Figure 60: Blue cylinder represent the tool, grey block represent the workpiece and green solid represent the dynamometer

The creation of the cavity on the workpiece can be delicate and lead to instability, so it needs a particular attention. Moreover, a good surface finish must be obtained (to be confidant of radial slope): repeated machining tasks at nominal geometry are an optimal solution to obtain sufficient precision. After the specimen preparation, the real test can be accomplished with a specific NC program that maintain the parallelism between Feedrate vector and the cavity direction. It is important to provide at the tool an angle respect to the specimen normal in order to avoid collisions between workpiece and tool holder or spindle unit (a common incident in plunging if not controlled), as described in Figure 62.

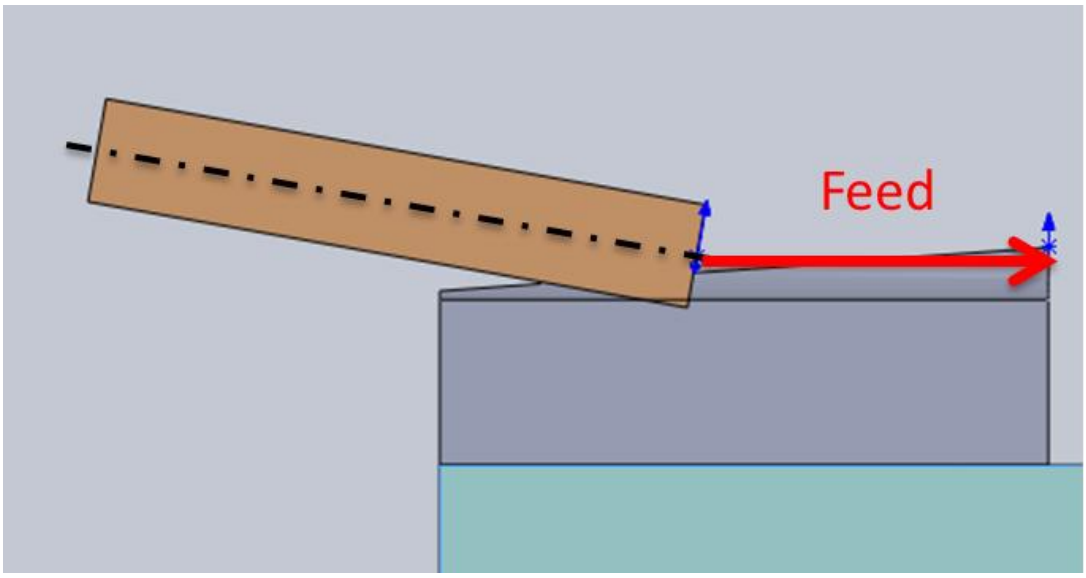

Figure 62: Section of the milling test: orange cylinder represent the tool, grey block represent the workpiece and green solid represent the dynamometer

With this test it is possible to maintain constant the maximal chip thickness in the center of the chip while augmenting the angular engagement without increasing too much the chip area because the adding part are thinner than the part in the middle of the section. As reference, Figure 61 is reported.

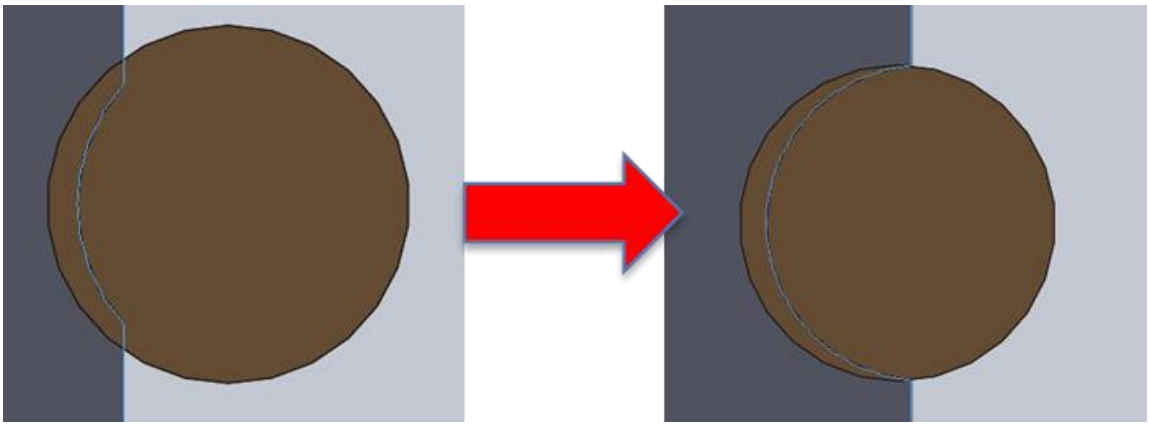

Figure 61: Left part is the chip section at the top of workpiece, right part is the section at the end of the milling task

This test was performed with the same tool kit and steel block described in chapter 3.1 (see Table 5 for force coefficients) with the same machine (see Figure 62 and Figure 63).

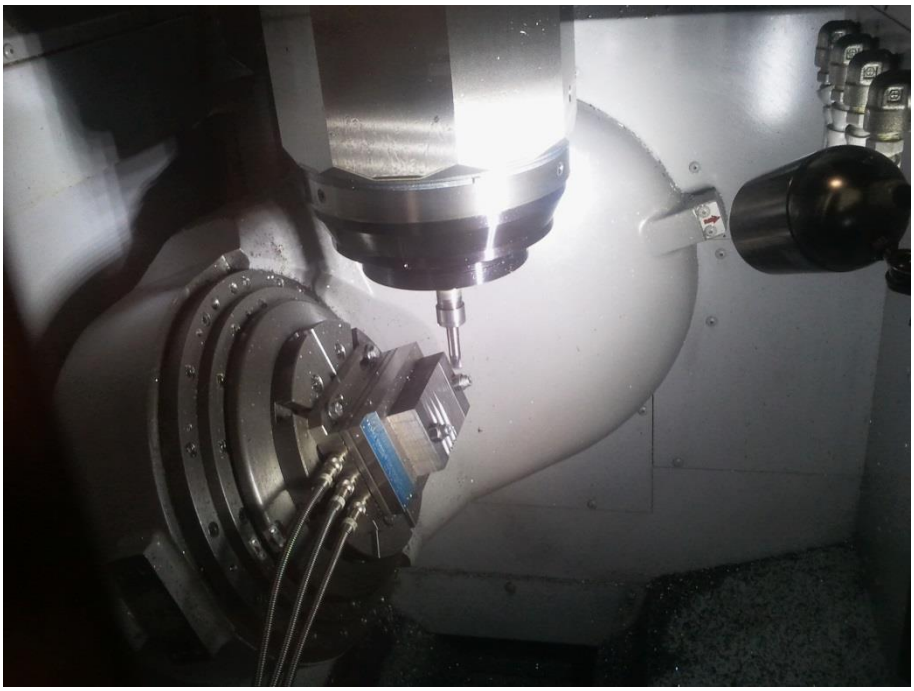

Figure 62: Ramp test example

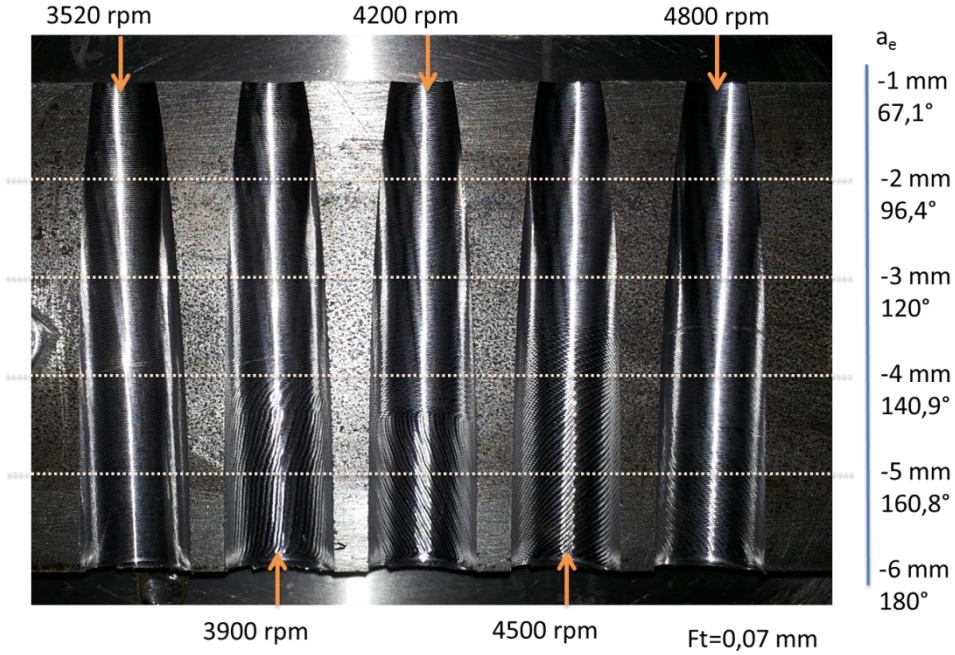

Figure 63: Example of result relative to test in Figure 62. It can be seen the insurgence of instability for different spindle speed at different angular engagement, being the chip area almost the same

This tests gave good results in terms of understanding the behavior of the tool with the sole changing of angular engagement because it creates negative upside-down real SLD on the steel block; Figure 64 report the predicted upside-down SLD versus the axial distance from the top of the workpiece. In this figure the critical angular engagement was transformed in the relative linear coordinate on the experimental steel block by applying geometrical relations.

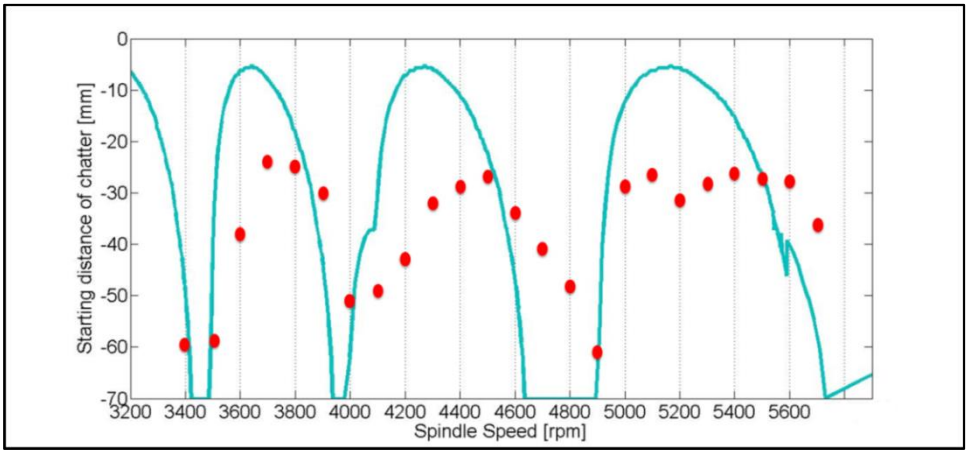

Figure 64: Red rot are the measured instability starting points. Light blue line is the upside-down SLD in which the $a_{e\,lim}$ is transformed (using geometrical relations) in the linear distance from the engaging point (set as zero)

From Figure 64 it's possible to observe that the lobes position is well predicted, a little shift towards the left of the real data is present as in test 3.1, and the problem of under-estimating the $a_{e\,lim}$ for low a_e due to an approximate geometry description is still present.

3.3. Real plunge test in final configuration

This chapter reports a real plunge milling test, executed in DIEF laboratory, using the same tool kit and workpiece as chapter 3.1. See Figure 65.

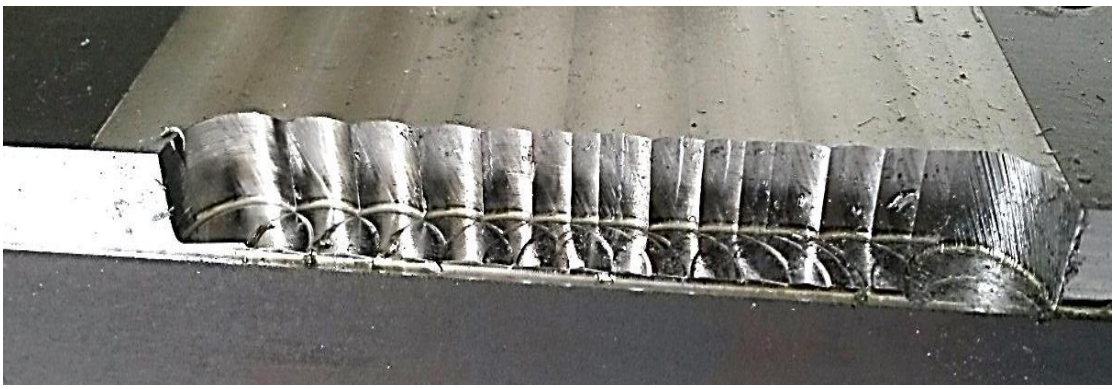

Figure 65: Example of plunge tests relative to chapter 3.3

For a comparison, these tests were executed at the same experimental points as tests reported in chapter 3.1. For a reference to force coefficients and bending FRFs see Table 5 and Figure 52. The SLD and the measured instable radial depth of cut are reported in Figure 66. The model used to perform the chatter forecast is the final one, taking into account also the geometrical description of the flutes and all the parameters introduced so far.

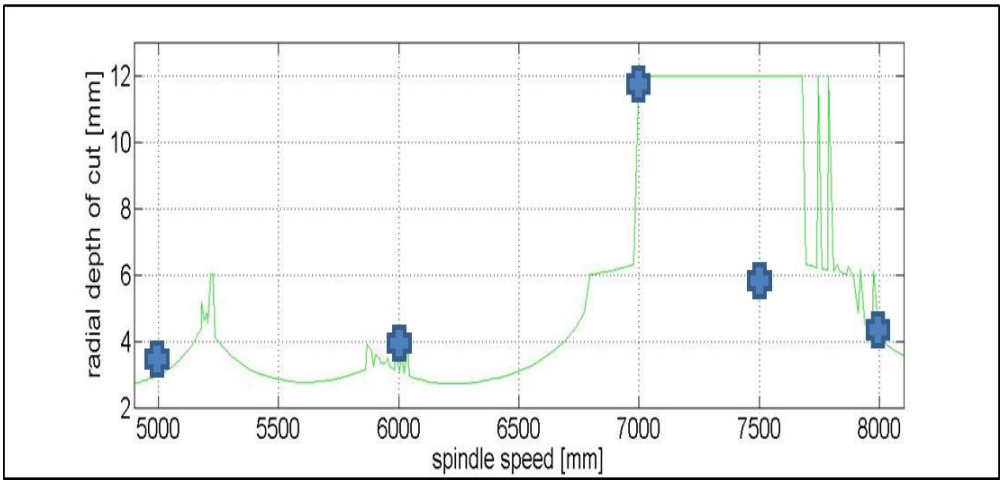

Figure 66: SLDs of experimental test of chapter 3.3: top chart pluts maximal chip thickness vs spindle speed, bottom chart plots radial depth od cut vs spindle speed

As possible to see from Figure 66 (especially in comparison with Figure 57), the new predicted SLD is substantially correct, matching the experimental results. Anyway, a small lobe shift (to the right of the chart) is seen: this phenomenon is a common issue of analytical SLD prediction and it's due to the differences between the measured FRFs in static condition and the real FRFs when the spindle is turning. With these engagement and configuration the torsional effect appear to be less influent. Figure 67 and Figure 68 report spectrogram for 8000 rpm and a_e =4mm and 7000 rpm and a_e=12mm respectively, as reported for tests in chapter 3.1.

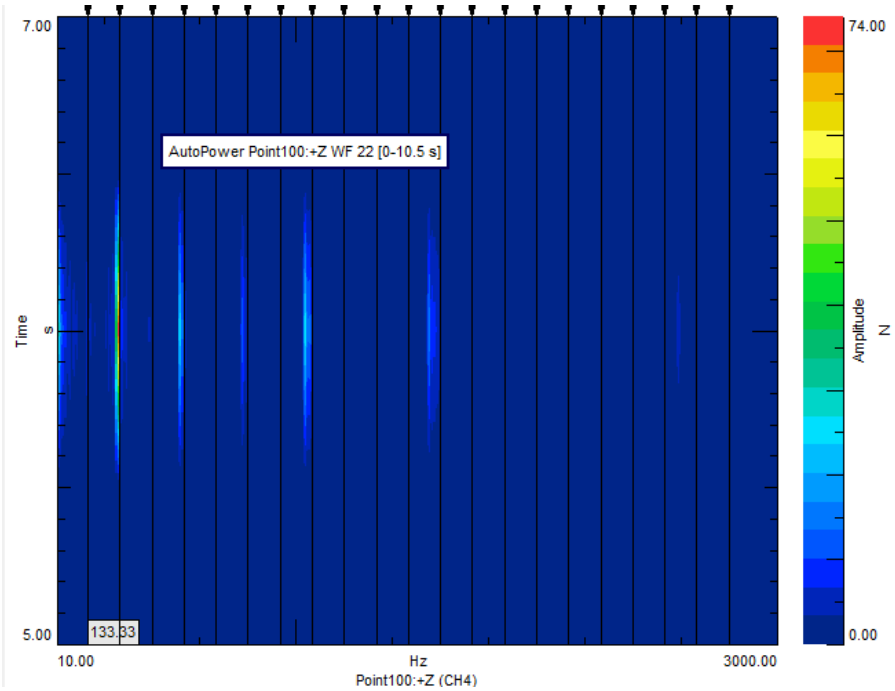

Figure 67: Spectrogram of Z force of test in chapter 3.3. Chatter frequency around 1060 Hz. Black lines are rotation frequency and tooth passing frequency harmonics

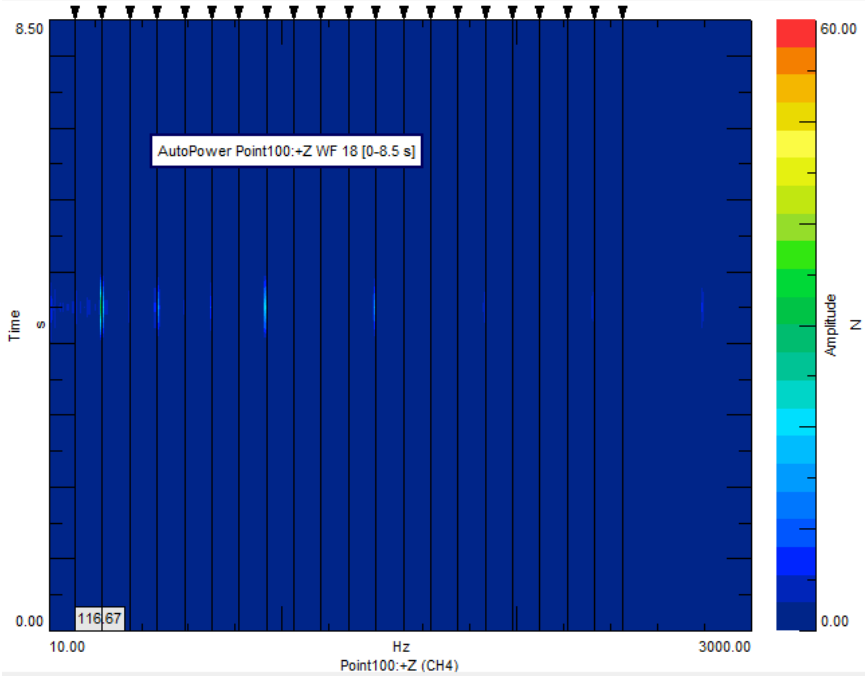

Figure 68: Spectrogram of Z force of test in chapter 3.3. No chatter has been detected. Black lines are rotation frequency and tooth passing frequency harmonics

3.4. Model final validation.

To perform the final validation all inputs of the model are required. For this reason, and to change completely all their values to check its reliability, final test was performed outside department laboratory, within the infrastructure of one of DIEF industrial partner. They dispose of a bigger milling machine able to mount a tool holder HSK 63a: this allow us to use a bigger tool that has sufficient space to place accelerometers and perform torsional and axial FRFs measurements. For FRFs and tool description, chapter 2.7 is taken as reference. Other information (example material, cutting coefficients, etcetera) are covered by non-disclosure agreement. Figure 69 report final results.

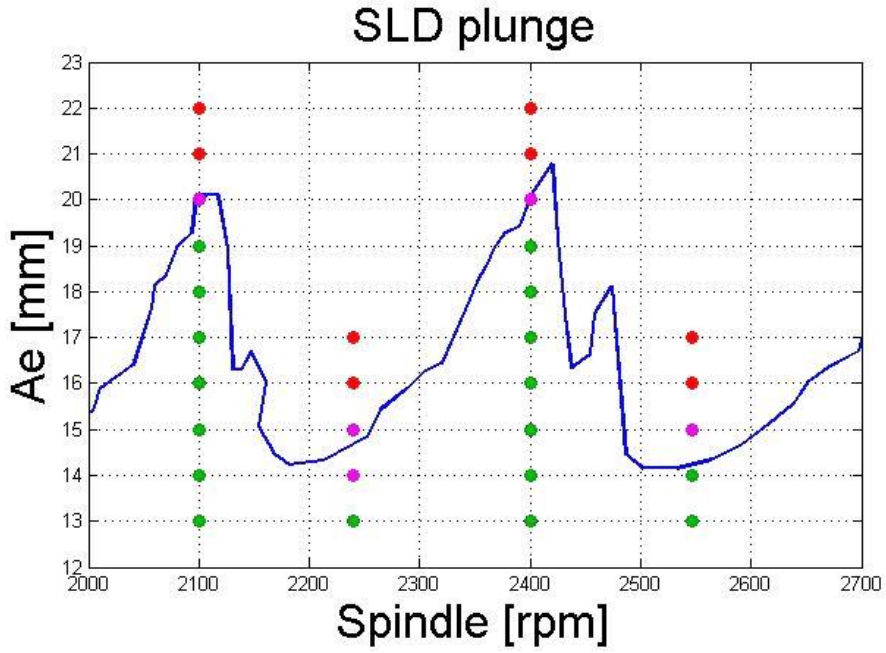

Figure 69: Final results of validation test. Green dots are stable, violet dots ar uncertain, red dots are unstable.

A notable remark of this test is the absence of modes shift probably due to relative low spindle speed. The model prediction and the experimental results agree in a very good way: considering that all the inputs have been changed the model can be considered validated.

4. The active chatter control techniques

The main goal of this part of the thesis is to obtain new, mathematical defined indices that can be used as chatter detectors, being capable to be used as a control logic for a full automated chatter control.

4.1. State of the art on chatter detection

Due to the complexity and uncertainties of the mathematical models and the expensive series of experimental tests needed to define the used forecast algorithm constants, the research pushed forward enchanting more complex simulations methods, , as semi-discretization method by Insperger and Stepan [30, 31] or FEM models [129, 130]. Anyway most difficulties of the out-of-process strategies remain, as well as the very long simulation time required to fully compute a full time domain cutting simulation and the fact that, normally, parameters and cutting features change during the cutting operation.

In-process methods are focused on the real-time control of the machining operation. Rahman and Ito [115] were among the firsts to suggest this approach: their idea was based on the monitoring with an optic sensor of the deflection of the workpiece. Liao and Young [24] analyzed a force signal measured with a dynamometric table with the workpiece clamper on. Kuljanic [25] combined the dynamometric table force signal with two ones obtained from two accelerometers placed on the spindle. Among the variety of sensors, the microphone is used in this work. The milling sound generated in the workpiece cutting offers the possibility to analyze the stability of the process. Delio [26] was one of the first researchers to use an acoustic signal to monitor the chatter. He tried to compare the sound information with the ones of a tri-axial accelerometer. Schmitz [27,28] developed a method based on statistic evaluations executed upon an acoustic signal and an IR sensor directed to the tooltip. Ismail [131] used the microphone to set a stability threshold for specific and repetitive tasks; this requires a preliminary set of experimental tests. Moreover, the acoustic sensor is also cheaper than other type of sensor, it can be placed in the working chamber easily and it doesn't interfere with the moving part of the machine.

One of the limit of all in-process approaches is the time that elapses between the instability insurgence, its recognition and the intervention on the machine; this time lapse can lead to unacceptable surface, especially in finishing. In chapter 4.4, novel indices are proposed and tested to verify which is the best, in terms of instability identification; also a method is tested to reduce chatter recognition time lapse. An interesting prospective is the application of these indicators for a real time chatter monitoring, maybe integrated in software that can suggest the operator new chatter-free parameters. In literature it's possible

to find attempts in this direction; as example Fassen [132] has proposed a software that can directly and automatically change CNC parameter, in particular spindle speed. The importance of in-process method is testified also by machine builder company who are challenging with this approaches, as Okuma and its CNC feature called Machining Navi®. The indices proposed in chapter 4.4 allow to identify not only the chatter arousal (in combination with literature ones), but also the phase of cutting task (air cutting, tool engage and disengage), in order to be useful for a future automation of real time chatter active control, that can be independent from the machine NC and applicable to every milling machine.

4.2. Signal acquisition and process

The idea of this research is to develop method able to identify the arising of chatter using numerical indices that are also suitable for real time monitoring. To achieve this goal, the emitted sound must be sampled with a Nyquist frequency that is sufficiently high: at least higher than the highest frequency expected within the signal, including any eventual chatter frequency. Moreover, to have indices that change rapidly enough, a time period T must be defined: this time period identifies a buffer of a portion of the signal that has to be analyzed. So is possible to observe along the timeline the evolution of the chatter indices. The higher frequency f_{max} that can be observed inside the portion of the signal is related the sampling frequency Equation 4.1.

$$f_{max} <= \frac{f_s}{2} \qquad \text{Equation 4.1}$$

f_{max} must be less or equivalent to Nyquist frequency (f_s is the sampling frequency). The right choice of f_s affects the capability of the indices to work correctly: as a general approach if you don't know nothing about the dynamics of the system you are monitoring, f_s must be chosen as high as possible (considering the milling machine used for test in this thesis, dominant modes of tools can be found between 1 and 2 kHz). After that, a Hann window is applied to avoid leakage errors. The average value of the signal must be subtracted from the signal itself before the Hann window, than that value must be added again to avoid introducing errors in the signal. In this way each index is computed once, within a period T; if the period T is too large (bigger than the transitory between stable and unstable cutting), this method can't be applied in real time applications. To increase the number of indices within a period T a simple method has been implemented described in Figure 70. Instead of starting with the successive sound acquisition after the period T, it will start each successive sampling after a shorter time T_{shift}, So indices are computed T/T_{shift} times within each period, virtually decreasing T without losing accuracy and waveform spectral resolution. The waveform resolution ΔR is the minimal distance between two peaks in the spectrum that can be detected; this value depends only from the value of time step T, accordingly to Equation 4.2.

$$\Delta R = \frac{1}{T} \qquad \text{Equation 4.2}$$

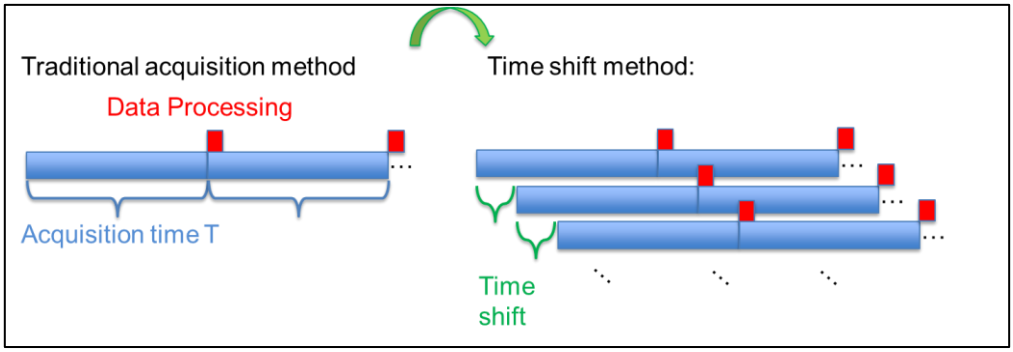

Figure 70: Comparison between traditional adquisition and time shift method

Introducing the T_{shift} method allows to maintain the best resolution without being forced to choose a compromise solution between sampling frequency and period T at the expense of more memory resources.

4.3. Frequency domain process

In accordance to chatter theory, the chatter frequency normally is found around one of the dominant modes of the tooltip. If the cutting is stable, the only frequencies that can be found in the forces spectra are the tooth passing frequency and the rotation frequency (due to an eventual tool runout or not uniform angular spacing of the teeth), and their higher harmonics. Normally, indices search for frequencies that are not related to tooth passing or rotation frequency. These frequency domain features are present also in the acoustic signal so it's possible to create classical chatter indices for microphone signal as well. The basic idea is to separate the spectrum of each signal with stop-band and pass band notch filter in order to obtain two different spectra: one called Stable Spectrum, containing tooth passing, rotational frequency and their harmonics and one called Unstable Spectrum, containing the remaining harmonics.

$$f_{tp} = \frac{NS}{60} \qquad \text{Equation 4.3}$$

The tooth passing frequency, f_{tp} (normally the main one, with the greater amplitude) depends from the number of teeth N, and from the spindle speed S (expressed in rpm). One problem is that the CNC maintains the imposed value of spindle speed constant within a minimal error respect to the nominal value. It's important to find the real value of spindle speed to position correctly the notch filter. It's possible to overcome this problem searching for the higher frequency peak around a small neighborhood of the nominal tooth pass frequency: the neighborhood value depends on CNC. The identification of the true spindle speed is fundamental because it avoid errors in the separation between Stable and Unstable Spectrum, leading to a misinterpretation of the stability of the process (for example an harmonic of f_{tp} is included in the Unstable Spectrum can be read as a chatter frequency). In this research it wasn't created a notch filter but another approach has been used. Initially different notch filters and their combinations (comb filters) for different values of bandwidths have bene tested. But at the end, a more efficient strategy has been developed. It

separates each acquired spectra with a MATLAB® algorithm defined by the band amplitude and the position of the center of all these bands. This algorithm creates the Stable Spectrum keeping intact the values inside the bands centered around f_{tp} and rotational frequency and their harmonics and imposing zero the other values; it also creates Unstable Spectrum as the difference between the whole spectrum and the Stable one. This choice derived by observing that if the chatter frequency is near the cutting frequency of the notch filter, the amplitude of chatter is split between Unstable and Stable Spectrum, causing a bad response of the indices that can underestimate the chatter. For this reason, it has been decided to use a not conventional filter to have a clean identification of the chatter frequency. Anyway, if chatter frequency is so close to a supposed stable harmonics there is no way to detect chatter with this technique in any case. The choice of the amplitude of the band become a critical data because it affects the index threshold values and the capacity to recognize chatter frequency near f_{tp} and rotation. After some trial attempts, considering that the shape of the FFT peaks can be not perfectly narrow, for our test the band amplitude was fixed ±4 Hz: this bandwidth allows to obtain indices that match with the literature threshold (see chapter 4.5 for threshold values). This may be considered a general value for every type of machine, but not for every sensor, because it affect only the signal processing, not the physics of the system. Anyway. it's better to tune this value considering the chain of measurement and the parameters of signal processing.

4.4. Chatter indices definition

Four different indices have been used and compared to evaluate their efficiency in detecting chatter:

$$c_{i1} = \frac{PSD(t) - PSD_s(t)}{PSD(t)} \qquad \text{Equation 4.4}$$

$$c_{i2} = \frac{Y_{us-Max}}{Y_{s-Max}} \qquad \text{Equation 4.5}$$

$$c_{i3} = ln\left(\frac{C_{i1}(t) + 1}{C_{i1}(t - T_{shift}) + 1}\right) \qquad \text{Equation 4.6}$$

$$c_{i4} = ln\left(\frac{C_{i2}(t) + 1}{C_{i2}(t - T_{shift}) + 1}\right) \qquad \text{Equation 4.7}$$

Equation 4.4 and Equation 4.5 define two indices, computed internally to a single signal: these two are commonly found in literature [25]. In particular, Equation 4.4 is the ratio between the Unstable Spectrum $|X(j\omega)|^2$ and the whole signal $|X(j\omega)|^2$: if the operation is stable the value of this index must be around zero, as definition. Index introduced by Equation 4.5 is the ratio between the maximal value of amplitude peak of the Unstable Spectrum and the maximal one in the Stable Spectrum. Also this index must be zero for a stable operation. Equation 4.6 and Equation 4.7 use a recursive analysis of a time-dependent variable. In particular, both of them are referred to the values of index computed at the previous step, where T_{shift} refers to the time-shift used to obtain a higher number of index.

These indices could allow to detect the moment of arise of chatter (because they are defined in order to highlight the time variation of the behavior of the system) but, as long as the process reach a new equilibrium, the indices reach a new stable value. If the operation is stable, this indices value is around 0, as definition. These last two indices are proposed within this thesis.

The intent of the author isn't report four separate indices that can measure chatter, but It's to propose the simultaneous use of all them. Each index highlight a behavior or a trend of an unstable operation but it's not sufficient to describe all the cases: normally chatter indices have some week point and they may fail in operation transition or air cutting, giving false-positive feedbacks or false information. For this reason all indices are meant to be used together as reported in Table 10, in order to have a complete control over the complete milling task.

4.5. Experimental test and setup

Experimental activity has been executed to test the indices defined in chapter 4.4. These tests have been conducted on a Mori Seiki milling machine, a NMV 1500 DCG, available at our laboratory. Three tools have been used: OSAWA general purpose G2CS2 (diameter 8 mm) and a UOP 89155.0601KMX (diameter 6 mm). To measure the sound emitted in the milling task and the forces, to have a comparison between signals (forces are the best signal to monitoring chatter but it's not always possible to fix the workpiece to the dynamometric table) the following measure instruments have been used: a Kistler dynamometric table Type 9257A and a microphone Bruel & Kijer Type 4165. The signals have been acquired using a National Instrument© NI C-RIO 9215 and OROS25 PC-Pack and processed by a MATLAB© script. The tooltip FRF was measured through an impact hammer test performed by a Bruel & Kijer instrumented hammer and a SCADAS acquisition system. The material used, unalloyed C40 steel with 23 HRC, has been previously characterized in order to obtain its cutting coefficients. Starting from tooltip FRF and cutting coefficients, stability lobe diagram has been computed using Altintas and Budak [74] method described in chapter 2.2.1 in order to predict the critical axial depth of cut to predict chatter onset. Based on this chart, the cutting parameters for our test have been chosen, to design tests in which a transition to instability occurred. Forces were filtered using a Kalman filtering technique [113] in order to avoid distortions introduced by dynamometer dynamics. For each test the sampling frequency was chosen accordingly to Equation 4.1 in order to have T of 1 seconds and a sufficient f_{max}.

In this chapter a summary of test has been reported to explain how the four indices can be used for the purpose or obtaining an automated control logic.

Test 1 was a series of 6 slotting test with OSAWA end mill. Each test has a constant axial depth of cut from 3 mm (the first test) to 8 mm (the last test) with an incremental step of 1 mm. Test 1 features are showed in Table 7 and Figure 71.

Table 7: Test 1 parameters

Fs	Spindle Speed	Ft (feed per tooth)	Feed	D	Flutes
5120 Hz	1592 rpm	0.039 mm/tooth	124 mm/min	8 mm	2

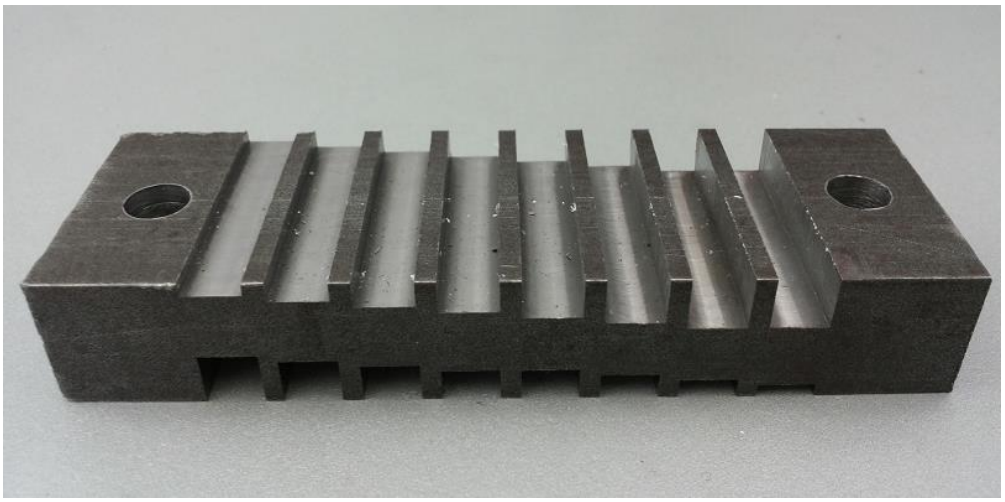

Figure 71: Specimen of Test 1

Test 2 was a series of flanking operation with constant radial depth of cut and a fixed axial depth of cut of 8 mm; the tool used was the OSAWA end mill. The radial depth of cut start from 3 mm (the first cut) to 8 mm (the last cut) with an increment of 1 mm. Two Spindle speed was used: 3000 rpm and 9000 rpm for all combinations of parameters. Test 2 features are showed in Table 8 and Figure 72.

Table 8: Test 2 parameters

Fs	Spindle Speed	Ft (feed per tooth)	Feed	D	Flutes
5120 Hz	3000 and 9000 rpm	0.03 mm/tooth	180 mm/min	8 mm	2

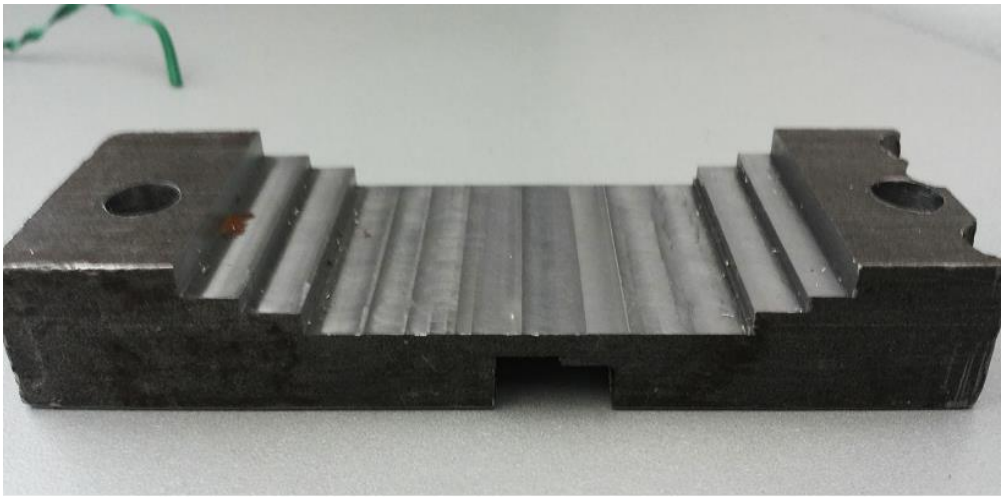

Figure 72: Specimen of Test 2

Test 3 was a series of ramp flank milling, using UOP end mill. The axial depth of cut wary from 1 mm to 6 mm linearly. The test was repeated for different spindle speeds, from 2124 rpm to 12744 rpm with an increment of 2124 rpm among the tests. Feed per tooth was kept constant. Test 3 features are showed in Table 9 and Figure 73 and Figure 74.

Table 9: Test 3 parameters

Fs	Ft (feed per tooth)	Radial depth of cut	D	Flutes
12800 Hz	0.03 mm/tooth	0.25 mm	6 mm	4

Figure 73: Specimen of Test 3 for S=2124rpm

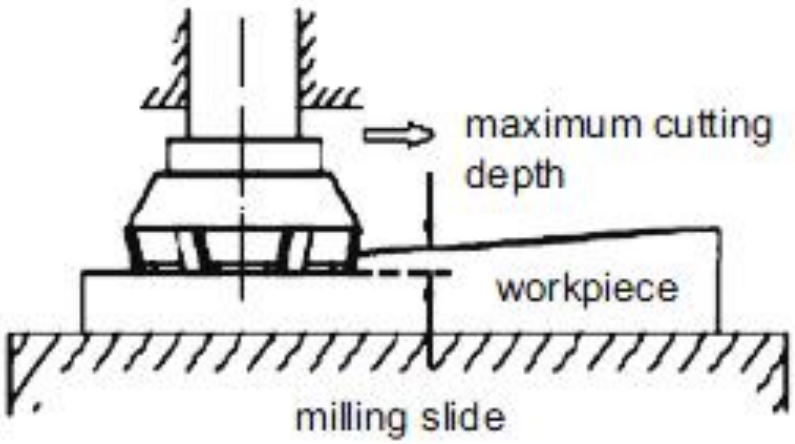

Figure 74: Test 3 procedure

4.6. Analysis of results

As it is possible to observe from Figure 75 and Figure 76, when the operation is stable (as experimentally verified in test 1 and 2 by analyzing surface finishing) chatter indices have a low value (under 0.5, that is the stable limit threshold fixed in literature for C_{i1} and 1 is the one for C_{i2}) that is more or less constant. The trend of indices is similar between forces and sound. However, acoustic indices are normally higher than forces ones; this is due to the fact that acoustic signal is noisier because it's measure comprehend also the acoustic response of the working chamber (this phenomenon can be observe for small engaged cuttings). In Tests 3 was experimentally observed (looking at surface marks, see Figure 73) a transition to an instability behavior around 3 mm of axial depth of cut (t=2.35s and S=2124rpm in Figure 73). That is visible from Figure 77 the trend of C_{i1} and C_{i2} in terms of time (each point correspond to a T_{shift} of 0.1s). It possible to see how works these indices are for chatter monitoring, in particular it's possible to see the same behavior between sound and forces; specifically microphone C_{i2} results higher than the corresponding force one, amplifying the instability effect. Theoretical values for C_{i3} are: 0 for air cutting and constant condition cutting (both stable and unstable), ln(2) for transition from stable to unstable, ln(1/2) for transition from unstable to stable. Theoretical values for C_{i4} are: 0 for air cutting and constant condition cutting (both stable and unstable), negative for decreasing of forces (including transition from unstable to stable), positive for increasing of forces. In Figure 78 the trend of C_{i3} and C_{i4} in Test 3 (with S=2124rpm) is reported.

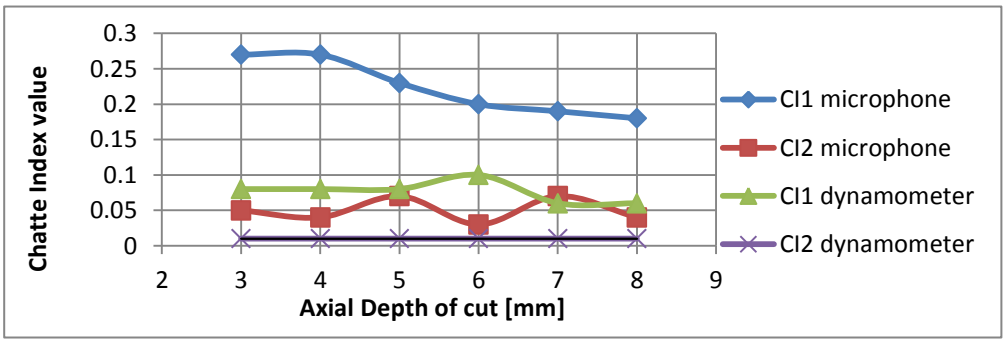

Figure 75: Trend of chatter index in Test 1

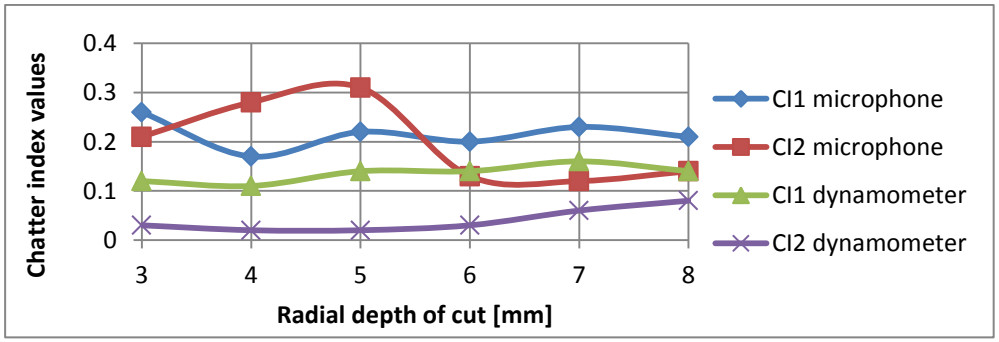

Figure 76: Trend of chatter index in Test 2

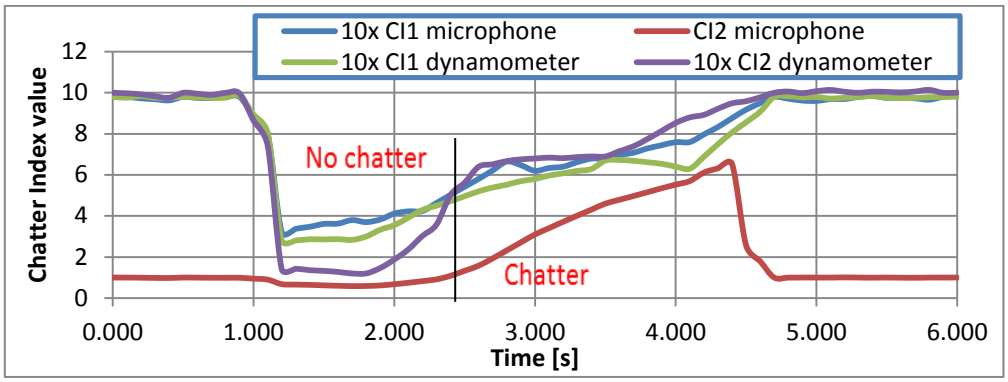

Figure 77: Temporal trend of chatter index C_{i1} and C_{i2} in test 4 with T_{shift}=0.1s. The engage of the tool is located at t=1.17s. Indices values are multiplied by 10, except for C_{i2} microphone

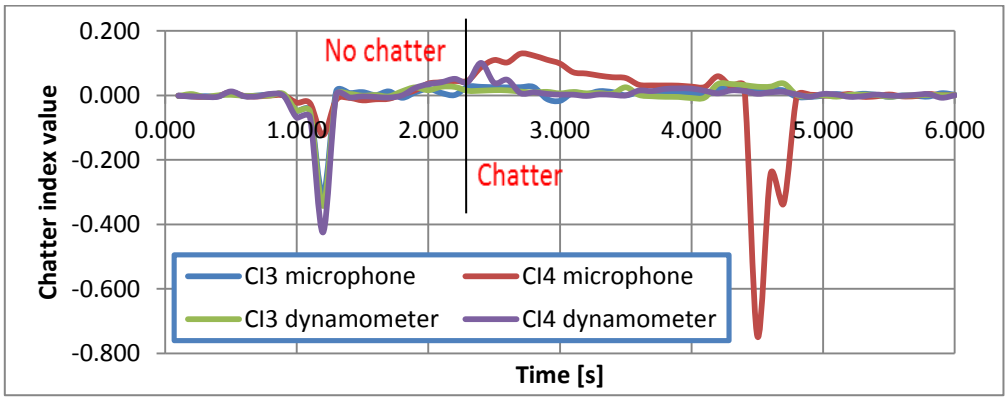

Figure 78: Temporal trend of chatter index C_{i3} and C_{i4} in Test 3 with T_{shift}=0.1s. Tool engage workpiece at t=1.17s

Looking at Figure 78 it's possible to notice a lot of sign changes around zero values. The thresholds of these indices are fixed as a narrow band around zero (they have been tuned by post-processing sound signals derived from other cutting tests, and chosen in order to point out the different phase of a known cutting task). C_{i3} chosen limits are from -0.05 to 0.022; C_{i4} chosen limits are from -0.1 to 0.1. To see how the combination of indices works see Figure 79 in which these transformation to indices values are applied: C_{i1}<0.5=0 and 1 elsewhere; C_{i2} <1=0, C_{i2}>1=2 and 1 in air cutting; C_{i3} and C_{i4}=0 between limits, 1 above and 0 under. Table 9 and Figure 79 point out how is possible to have a distinction among the phase of the cutting (with some error of shifting between values change around transition to chatter). C_{i3} and C_{i4} threshold values are affected by T_{shift}: the more indices you have and the less are the variations between two successive values, decreasing the needed threshold. A small T_{shift} makes C_{i1} and C_{i2} better in terms of monitoring, affects negatively C_{i3} and C_{i4} sensibility in particular in a band around zero, that can lead to misinterpretations; for these reason a tuning of C_{i3} and C_{i4} is required at least once after having fixed other parameters.

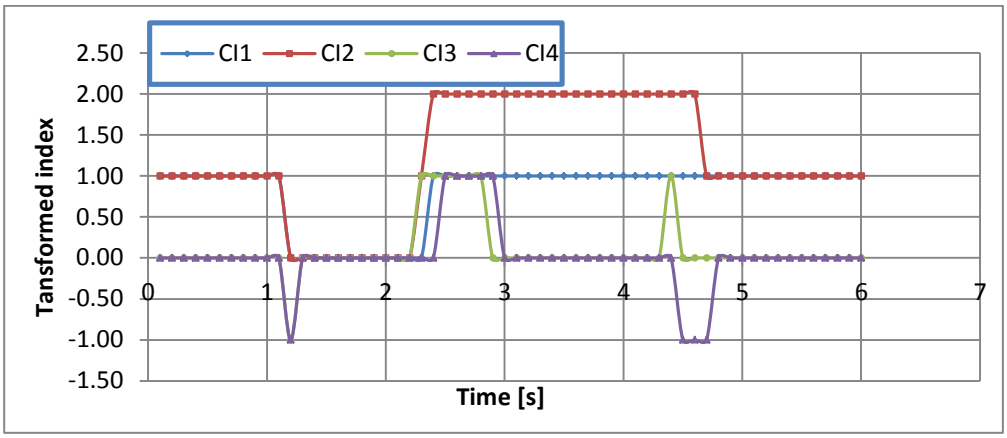

Figure 79: Temporal trend of transformed indices of Test 3 S=2124rpm

Table 10: Combination of indices in transition phase with theoretical indices values using threshold

Transition	$C_{i1}(t)$	$C_{i2}(t)$	sign($C_{i3}(t)$)	sign($C_{i4}(t)$)
air cutting to stable	<0.5	<1	-1	-1
air cutting to unstable	> 0.5	> 1	-1	1
stable to air cutting	1	1	1	1
stable to unstable	> 0.5	> 1	1	1
unstable to air cutting	1	1	1	-1
unstable to stable	<0.5	<1	-1	-1

Conclusions and final remarks

The activity presented in this thesis deals with the development of a plunge milling analytical chatter forecast model. A second part of thesis activity was to develop a control logic, able to perform a fully automation of chatter monitoring.

The work is originated by the increasing interest for plunge milling operations as a new approach to realize special features like impeller, die or mold, and in particular components of automotive or aerospace and energy industry.

Plunge milling guarantees more stiffness in federate direction, causing a redistribution of cutting force in the axial direction and, consequently, a growth of stability of the process respect to flank milling. Moreover, literature activity about plunge analytical models is very limited and comprehends few works. These have been used to farther develop the state of the art research about this process.

The basic principles derive from a work of Altintas presented in 2006, in particular he used his well-known Zeroth Order Solution, adapting it to cope with chip thickness along axial direction, instead of radial one.

To develop the proposed model, a lot of parts have been originally developed and validated using the traditional ZOA and Nyquist criterion to find the stability border:

- a methodology to measure cutting force coefficients in real plunge operations;
- an exhaustive geometrical description of the new configuration for subsequent plunging of vertical walls;
- an iterative cycle to obtain convergence between predicted results and input configuration because they are physically related.

The method to obtain plunge force coefficient, that are relative to frontal cutters (in plunge is the main one) is described in chapter 2.5.2. A summary of experimental activity and the validation of this model is reported in chapter 2.5.3. This method has been verified to be valid through a comparison between simulated and measured forces.

The new configuration description (chapter 2.6) allows to calculate the instantaneous radial chip thickness that is an important information to compute the average inclination of the flute respect to the horizontal plane XY. This value heavily affects the output of the model, taking into account the influence of lateral dynamics of the system into the prevision model. The geometry of the flute, from an axial-radial plane, is represented as a two segment, each of them characterizes by its own length and inclination. This approximation has given good results in terms of accuracy of stability limit.

The iteration algorithm (chapter 2.5.6) allows to maintain a physical coherence between input and output: the model need a geometrical configuration to compute the oriented FRF matrix, as usual in ZOA, and give an output that is equivalent to a new configuration, used as a new input for the following cycle. The algorithm stops when the input and the output difference is within a tolerance, imposed by the user.

The summary of the experimental activity has been reported in chapter 3.

The whole model has been tested in the laboratory of Department of Industrial Engineering of Florence (DIEF) and has been fully validated with a series of tests performed in the facility of an industrial partner, allowing to consider a large variety of process parameters. The results was accurate in terms of lobes position ad critical radial depth of cut.

The second part of this thesis describes a control logic, based on acoustic analysis of milling sound, able to recognize not only chatter but also to interpret the milling phase, as engagement and disengagement of the tool and transition of stability. This capability was not present in the literature common indices and it represent a limit if the control is demanded to a machine/software supervised control. The actual proposed control (chapter 4) use two classical indices and two novel indices. The experimental activity was used also to tune indices thresholds, compare acoustical information with others type of signals and validate this logic (just by post-processing data).

Acknowledgements

The present thesis work was carried out in the Department of Industrial Engineering of the University of Florence. Foremost, I would like to express my sincere gratitude to all the people working in this Department, starting from my Supervisors, Prof. Eng. Gianni Campatelli and Prof. Eng. Antonio Scippa. Then, I would like to express my gratitude to my PhD course colleague, to whom I wish success in life and in their researches.

I want also to thank industrial partners of DIEF for their human and technical support.

Finally, but not for importance, I would express my sincere gratitude to family and friends, whose support and encouragement was the best thrust and incentive to hold on my activity despite of all difficulties I found on my path.

Bibliography

[1] Yeon Hwang, Gyu Ha Kim, Young-Bok Kim, Jeong-Ho Kim, Sun-Kyu Lee, Suppression of the inflection pattern in ultraprecision grinding through the minimization of the hydrodynamic force using a toothed wheel, International Journal of Machine Tools and Manufacture, Volume 100, January 2016, Pages 105-115, ISSN 0890-6955, http://dx.doi.org/10.1016/j.ijmachtools.2015.10.009.

[2] Yanbin Zhang, Changhe Li, Dongzhou Jia, Dongkun Zhang, Xiaowei Zhang, Experimental evaluation of the lubrication performance of MoS2/CNT nanofluid for minimal quantity lubrication in Ni-based alloy grinding, International Journal of Machine Tools and Manufacture, Volume 99, December 2015, Pages 19-33, ISSN 0890-6955, http://dx.doi.org/10.1016/j.ijmachtools.2015.09.003.

[3] Pedro L. Guzzo, Alan A.A. Tino, Juliano B. Santos, The onset of particle agglomeration during the dry ultrafine grinding of limestone in a planetary ball mill, Powder Technology, Volume 284, November 2015, Pages 122-129, ISSN 0032-5910, http://dx.doi.org/10.1016/j.powtec.2015.06.050.

[4] Julong Yuan, Weifeng Yao, Ping Zhao, Binghai Lyu, Zhixiang Chen, Meipeng Zhong, Kinematics and trajectory of both-sides cylindrical lapping process in planetary motion type, International Journal of Machine Tools and Manufacture, Volume 92, May 2015, Pages 60-71, ISSN 0890-6955, http://dx.doi.org/10.1016/j.ijmachtools.2015.02.004.

[5] Tiberiu Dobrescu, Nicoleta-Elisabeta Pascu, Gabriel Jiga, Constantin Opran, Optimization Criteria of Plane Lapping Machines, Procedia Engineering, Volume 100, 2015, Pages 428-434, ISSN 1877-7058, http://dx.doi.org/10.1016/j.proeng.2015.01.387.

[6] Shi-jie GUO, Yi XU, Yi Han, Jin-yan LIU, Guan-xia XUE, Hiromi NAGAUMI, Near net shape casting process for producing high strength 6xxx aluminum alloy automobile suspension parts, Transactions of Nonferrous Metals Society of China, Volume 24, Issue 7, July 2014, Pages 2393-2400, ISSN 1003-6326, http://dx.doi.org/10.1016/S1003-6326(14)63362-8.

[7] V. Samarov, D. Seliverstov and Francis H. (Sam) Froes, 18 - Fabrication of near-net-shape cost-effective titanium components by use of prealloyed powders and hot isostatic pressing, In Titanium Powder Metallurgy, edited by Ma QianFrancis H. (Sam) Froes, Butterworth-Heinemann, Boston, 2015, Pages 313-336, ISBN 9780128000540, http://dx.doi.org/10.1016/B978-0-12-800054-0.00018-6.

[8] B.-A. Behrens, A. Bouguecha, I. Lüken, A. Klassen and D. Odening, 3.16 - Near-Net and Net Shape Forging, In Comprehensive Materials Processing, edited by Saleem HashmiGilmar Ferreira BatalhaChester J. Van TyneBekir Yilbas, Elsevier, Oxford, 2014, Pages 427-446, ISBN 9780080965338, http://dx.doi.org/10.1016/B978-0-08-096532-1.00323-X.

[9] F. W. Taylor, On the art of cutting metals, Transactions of ASME, 28 (1907), Pages 31–248404

[10] Xu Zhou, Dinghua Zhang, Ming Luo, Baohai Wu, Chatter stability prediction in four-axis milling of aero-engine casings with bull-nose end mill, Chinese Journal of Aeronautics, Available online 20 June 2015, ISSN 1000-9361, http://dx.doi.org/10.1016/j.cja.2015.06.001.

[11] Byoung K Choi, Dae H Kim, Robert B Jerard, C-space approach to tool-path generation for die and mould machining, Computer-Aided Design, Volume 29, Issue 9, September 1997, Pages 657-669, ISSN 0010-4485, http://dx.doi.org/10.1016/S0010-4485(97)00012-2.

[12] Elisa Vázquez, Alan Amaro, Joaquim Ciurana, Ciro A. Rodríguez, Process planning considerations for micromilling of mould cavities used in ultrasonic moulding technology, Precision Engineering, Volume 39, January 2015, Pages 252-260, ISSN 0141-6359, http://dx.doi.org/10.1016/j.precisioneng.2014.07.001.

[13] Salomon, C., Critical Machining Velocities. 1931: German Patent No. 523594.

[14] Guillem Quintana, Joaquim Ciurana, Chatter in machining processes: A review, International Journal of Machine Tools and Manufacture, Volume 51, Issue 5, May 2011, Pages 363-376, ISSN 0890-6955, http://dx.doi.org/10.1016/j.ijmachtools.2011.01.001.

[15] Wiercigroch, M., Krivtsov, A.M., Frictional chatter in orthogonal metal cutting, (2001) Philosophical Transactions of the Royal Society A: Mathematical, Physical and Engineering Sciences, 359 (1781), Pages 713-738.

[16] M. Wiercigroch, E. Budak, Sources of nonlinearities, chatter generation and suppression in metal cutting, Philosophical Transactions of the Royal Society London, 359 (2001), Pages 663–693264

[17] S.A. Tobias, Machine Tools Vibrations (Vibraciones en Máquinas-Herramientas), URMO, Spain (1961)

[18] J. Tlusty, M. Polacek, The stability of machine tools against self-excited vibrations in machining, International Research in Production Engineering (1963), Pages 465–474

[19] J. Tlusty, Upper saddle river, Prentice-Hall, NJ (2000)

[20] L.R. Foulds, K. Neumann ,A network flow model of group technology., Mathematical and Computer Modelling, 38 (5-6) (2003/9), Pages 623–635

[21] Y. Altintas, Manufacturing automation, metal cutting mechanics, Machine Tool Vibrations, and CNC Design, 2000Cambridge University Press, USA (2000)

[22] R.P.H. Faassen, N. van de Wouw, J.A.J. Oosterling, H. Nijmeijer, Prediction of regenerative chatter by modelling and analysis of high-speed milling, International Journal of Machine Tools and Manufacture, 43 (14) (2003/11), Pages 1437–1446

[23] R.P.H. Faassen, Chatter prediction and control for high-speed milling: modelling and experiments, Technische Universiteit Eindhoven; Thesis (2007)

[24] Y.S. Liao, Y.C. Young, A new on-line spindle speed regulation strategy for chatter control, International Journal of Machine Tools and Manufacture 36 (5) (1996/5), Pages 651–660.

[25] E. Kuljanic, G. Totis, M. Sortino, Development of an intelligent multisensor chatter detection system in milling, Mechanical Systems and Signal Processing, 23 (5) (2009), Pages 1704–1718

[26] T. Delio, J. Tlusty, S. Smith, Use of audio signals for chatter detection and control, Journal of Engineering for Industry, transactions of the ASME, 114 (2) (1992), Pages 146–157.

[27] T.L. Schmitz, K. Medicus, B. Dutterer, Exploring once-per-revolution audio signal variance as a chatter indi-cator, Machining Science and Technology 6 (2) (2002), Pages 215–233[28] T.L. Schmitz, Chatter recognition by a statistical evaluation of the synchronously sampled audio signal, Journal of Sound and Vibration 262 (3) (2003/5/1), Pages 721–730

[29] Guillem Quintana, Joaquim Ciurana, Daniel Teixidor, A new experimental methodology for identification of stability lobes diagram in milling operations, International Journal of Machine Tools and Manufacture, Volume 48, Issue 15, December 2008, Pages 1637-1645, ISSN 0890-6955, http://dx.doi.org/10.1016/j.ijmachtools.2008.07.006.

[30] T. Insperger, G. Stépán, Semi-discretization method for delayed systems, International Journal for Numerical Methods in Engineering, 55 (5) (2002),Pages 503–518

[31] T. Insperger, G. Stépán, Updated semi-discretization method for periodic delay-differential equations with discrete delay, International Journal for Numerical Methods in Engineering, 61 (1) (2004), Pages 117–141

[32] C. Henninger, P. Eberhard, Improving the computational efficiency and accuracy of the semi-discretization method for periodic delay-differential equations, European Journal of Mechanics, A/Solids, 27 (6) (2008), Pages 975–985

[33] Jeong Hoon Ko, Time domain prediction of milling stability according to cross edge radiuses and flank edge profiles, International Journal of Machine Tools and Manufacture, Volume 89, February 2015, Pages 74-85, ISSN 0890-6955, http://dx.doi.org/10.1016/j.ijmachtools.2014.11.004.

[34] Li Zhongqun, Liu Qiang, Solution and Analysis of Chatter Stability for End Milling in the Time-domain, Chinese Journal of Aeronautics, Volume 21, Issue 2, April 2008, Pages 169-178, ISSN 1000-9361, http://dx.doi.org/10.1016/S1000-9361(08)60022-9

[35] Y. Altintas, Philip K. Chan, In-process detection and suppression of chatter in milling, International Journal of Machine Tools and Manufacture, Volume 32, Issue 3, June 1992, Pages 329-347, ISSN 0890-6955, http://dx.doi.org/10.1016/0890-6955(92)90006-3.

[36] Ioannis Minis, Rafael Yanushevsky, Abel Tembo, Robert Hocken, Analysis of Linear and Nonlinear Chatter in Milling, CIRP Annals - Manufacturing Technology, Volume 39, Issue 1, 1990, Pages 459-462, ISSN 0007-8506, http://dx.doi.org/10.1016/S0007-8506(07)61096-8.

[37] Ioannis Minis, Rafael Yanushevsky, A new theoretical approach for the predictionof machine tool chatter in milling, Journal of Engineering for Industry, Transaction of the ASME, Volume 115, Issue 1, 1993, Pages 1-8,

[38] Y. Altintaş, E. Budak, Analytical Prediction of Stability Lobes in Milling, CIRP Annals - Manufacturing Technology, Volume 44, Issue 1, 1995, Pages 357-362, ISSN 0007-8506, http://dx.doi.org/10.1016/S0007-8506(07)62342-7.

[39] Mohammad Rezayi Khoshdarregi, Yusuf Altintas, Generalized modeling of chip geometry and cutting forces in multi-point thread turning, International Journal of Machine Tools and Manufacture, Volume 98, November 2015, Pages 21-32, ISSN 0890-6955, http://dx.doi.org/10.1016/j.ijmachtools.2015.08.005.

[40] Oguzhan Tuysuz, Yusuf Altintas, Hsi-Yung Feng, Prediction of cutting forces in three and five-axis ball-end milling with tool indentation effect, International Journal of Machine Tools and Manufacture, Volume 66, March 2013, Pages 66-81, ISSN 0890-6955, http://dx.doi.org/10.1016/j.ijmachtools.2012.12.002.

[41] Nicola Guglielmi, Ernst Hairer, Path-regularization of linear neutral delay differential equations with several delays, Journal of Computational and Applied

Mathematics, Volume 292, 15 January 2016, Pages 785-794, ISSN 0377-0427, http://dx.doi.org/10.1016/j.cam.2014.12.028.

[42] Qizhi Xie, Qichang Zhang, Jianxin Han, Hopf bifurcation for delay differential equation with application to machine tool chatter, Applied Mathematical Modelling, Volume 36, Issue 8, August 2012, Pages 3803-3812, ISSN 0307-904X, http://dx.doi.org/10.1016/j.apm.2011.11.011.

[43] Yung-Chou Kao, Nhu-Tung Nguyen, Mau-Sheng Chen, Shyh-Chour Huang, A combination method of the theory and experiment in determination of cutting force coefficients in ball-end mill processes, Journal of Computational Design and Engineering, Volume 2, Issue 4, October 2015, Pages 233-247, ISSN 2288-4300, http://dx.doi.org/10.1016/j.jcde.2015.06.005.

[44] Szymon Wojciechowski, The estimation of cutting forces and specific force coefficients during finishing ball end milling of inclined surfaces, International Journal of Machine Tools and Manufacture, Volume 89, February 2015, Pages 110-123, ISSN 0890-6955, http://dx.doi.org/10.1016/j.ijmachtools.2014.10.006.

[45] Kuanmin Mao, Ming Zhu, Weiwei Xiao, Bin Li, A method of using turning process excitation to determine dynamic cutting coefficients, International Journal of Machine Tools and Manufacture, Volume 87, December 2014, Pages 49-60, ISSN 0890-6955, http://dx.doi.org/10.1016/j.ijmachtools.2014.08.002

[46] N. Grossi, L. Sallese, A. Scippa, G. Campatelli, Chatter Stability Prediction in Milling Using Speed-varying Cutting Force Coefficients, Procedia CIRP, Volume 14, 2014, Pages 170-175, ISSN 2212-8271, http://dx.doi.org/10.1016/j.procir.2014.03.019.

[47] Yun Yang, Wei-Hong Zhang, Ying-Chao Ma, Min Wan, Generalized method for the analysis of bending, torsional and axial receptances of tool–holder–spindle assembly, International Journal of Machine Tools and Manufacture, Volume 99, December 2015, Pages 48-67, ISSN 0890-6955, http://dx.doi.org/10.1016/j.ijmachtools.2015.08.004.

[48] Mohammad Mahdi Rezaei, Mohammad R. Movahhedy, Hamed Moradi, Mohammad T. Ahmadian, Extending the inverse receptance coupling method for prediction of tool-holder joint dynamics in milling, Journal of Manufacturing Processes, Volume 14, Issue 3, August 2012, Pages 199-207, ISSN 1526-6125, http://dx.doi.org/10.1016/j.jmapro.2011.11.003.

[49] P. Albertelli, M. Goletti, M. Monno, A new receptance coupling substructure analysis methodology to improve chatter free cutting conditions prediction, International Journal of Machine Tools and Manufacture, Volume 72, September 2013, Pages 16-24, ISSN 0890-6955, http://dx.doi.org/10.1016/j.ijmachtools.2013.05.003.

[50] C. Chiou, M. Hong, K.F. Ehmann. The feasibility of eigenstructure assignment for machining chatter control, International Journal of Machine Tools and Manufacture, 43 (15) (2003/12), Pages. 1603–1620

[51] H. Moradi, F. Bakhtiari-Nejad, M.R. Movahhedi, Tunable vibration absorber design to suppress vibrations: an application in boring manufacturing process, Journal of Sound and Vibration 318 (2008), Pages 93–108.

[52] H. Moradi, F. Bakhtiari-Nejad, M.R. Movahhedy, Tuneable vibration absorber design to suppress vibrations: An application in boring manufacturing process, Journal of Sound and Vibration, 318 (1-2) (2008), pp. 93–108

[53] H. Moradi, F. Bakhtiari-Nejad, M.R. Movahhedy, Tuneable vibration absorber design to suppress vibrations: An application in boring manufacturing process, Journal of Sound and Vibration, 318 (1-2) (2008), pp. 93–108

[54] Y. Yang, J. Muñoa, Y. Altintas, Optimization of multiple tuned mass dampers to suppress machine tool chatter, International Journal of Machine Tools and Manufacture, Volume 50, Issue 9, September 2010, Pages 834-842, ISSN 0890-6955, http://dx.doi.org/10.1016/j.ijmachtools.2010.04.011.

[55] Hamed Moradi, Gholamreza Vossoughi, Mehdi Behzad, Mohammad R. Movahhedy, Vibration absorber design to suppress regenerative chatter in nonlinear milling process: Application for machining of cantilever plates, Applied Mathematical Modelling, Volume 39, Issue 2, 15 January 2015, Pages 600-620, ISSN 0307-904X, http://dx.doi.org/10.1016/j.apm.2014.06.010

[56] Yiqing Yang, Wei Dai, Qiang Liu, Design and implementation of two-degree-of-freedom tuned mass damper in milling vibration mitigation, Journal of Sound and Vibration, Volume 335, 20 January 2015, Pages 78-88, ISSN 0022-460X, http://dx.doi.org/10.1016/j.jsv.2014.09.032.

[57] Gianni Campatelli, Lorenzo Sallese, Antonio Scippa, Design of An Active Workpiece Holder, Procedia CIRP, Volume 34, 2015, Pages 217-222, ISSN 2212-8271, http://dx.doi.org/10.1016/j.procir.2015.07.041.

[58] I. Bediaga, J. Muñoa, J. Hernández, L.N. López de Lacalle, An automatic spindle speed selection strategy to obtain stability in high-speed milling, International Journal of Machine Tools and Manufacture, Volume 49, Issue 5, April 2009, Pages 384-394, ISSN 0890-6955, http://dx.doi.org/10.1016/j.ijmachtools.2008.12.003.

[59] Elio Chiappini, Stefano Tirelli, Paolo Albertelli, Matteo Strano, Michele Monno, On the mechanics of chip formation in Ti–6Al–4V turning with spindle speed variation, International Journal of Machine Tools and Manufacture, Volume 77, February 2014, Pages 16-26, ISSN 0890-6955, http://dx.doi.org/10.1016/j.ijmachtools.2013.10.006.

[60] Andreas Otto, Günter Radons, Application of spindle speed variation for chatter suppression in turning, CIRP Journal of Manufacturing Science and Technology, Volume 6, Issue 2, 2013, Pages 102-109, ISSN 1755-5817, http://dx.doi.org/10.1016/j.cirpj.2013.02.002.

[61] P. Albertelli, V. Mussi, C. Ravasio, M. Monno, An Experimental Investigation of the Effects of Spindle Speed Variation on Tool Wear in Turning, Procedia CIRP, Volume 4, 2012, Pages 29-34, ISSN 2212-8271, http://dx.doi.org/10.1016/j.procir.2012.10.006.

[62] J.H. Wang, K.N. Lee, Suppression of chatter vibration of a CNC machine centre an example, Mechanical Systems and Signal Processing, 10 (5) (1996/9), Pages 551–560

[63] E. Marui, S. Ema, M. Hashimoto, Y. Wakasawa, Plate insertion as a means to improve the damping capacity of a cutting tool system, International Journal of Machine Tools and Manufacture, 38 (10-11) (1998/10), Pages 1209–1220

[64] N.H. Kim, D. Won, J.C. Ziegert, Numerical analysis and parameter study of a mechanical damper for use in long slender endmills, International Journal of Machine Tools and Manufacture, 46 (5) (2006/4), Pages 500–507

[65] K. Shirase, Y. Altintas, Cutting force and dimensional surface error generation in peripheral milling with variable pitch helical end mills, International Journal of Machine Tools and Manufacture, 36 (5) (1996/5), Pages 567–5

[66] E. Budak, An analytical design method for milling cutters with nonconstant pitch to increase stability, part I: theory, Journal of Manufacturing Science and Engineering, Transactions of the ASME, 125 (1) (2003), Pages 29–34

[67] E. Budak, An analytical design method for milling cutters with nonconstant pitch to increase stability, part 2: application, Journal of Manufacturing Science and Engineering, Transactions of the ASME, 125 (1) (2003), Pages 35–38

[68] N.D. Sims, B. Mann, S. Huyanan, Analytical prediction of chatter stability for variable pitch and variable helix milling tools, Journal of Sound and Vibration 2008.

[69] S. Turner, D. Merdol, Y. Altintas, K. Ridgway, Modelling of the stability of variable helix end mills, International Journal of Machine Tools and Manufacture, 47 (9) (2007), pp. 1410–141

[70] Zoltan Dombovari, Yusuf Altintas, Gabor Stepan, The effect of serration on mechanics and stability of milling cutters, International Journal of Machine Tools and Manufacture, Volume 50, Issue 6, June 2010, Pages 511-520, ISSN 0890-6955, http://dx.doi.org/10.1016/j.ijmachtools.2010.03.006.

[71] Atabey, F., Lazoglu, I., and Altintas, Y., 2002, "Mechanics of Boring Processes: Part II-Multi-insert Boring Heads," Int. J. Mach. Tools Manuf., 43 Pages 477–484.

[72] Tobias, S.A., Fishwick, W., 1958, A Theory of Regenerative Chatter, The Engineer, London.

[73] Tlusty, J., Polacek, 1963, The Stability of Machine Tools Against Self Excited Vibrations in Machining, Int. Research in Production Engineering, 465-474.

[74] Y. Altintas, E. Budak, Analytical prediction of stability lobes in milling. CIRP Annals—Manufacturing Technology 1995, pp. 357–362

[75] Budak, E., Altintas, Y., 1998, Analytical Prediction of Chatter Stability Conditions for Multi-Degree of Systems in Milling. Part II: Applications, Transactions of ASME, Journal of Dynamic Systems, Measurement and Control, 120:31-36.

[76] Nouri M, Fussell BK, Ziniti BL, et al. Real-time tool wear monitoring in milling using a cutting condition independent method. Int J Mach Tool Manu, 2015, Volume 89, Pages 1–13.

[77] Sarhan A, Sayed R, Nassr AA, et al. Interrelationships between cutting force variation and tool wear in endmilling, J Mater Process Tech, 2001, Volume 109, Pages229–235.

[78] Merdol, A., Altintas, Y., 2004. Multi frequency solution of chatter stability for low immersion milling. ASME Journal of Manufacturing Science and Engineering 126, Pages 459–466.

[79] Y. Altintas, J.H. Ko, Chatter Stability of Plunge Milling, CIRP Annals - Manufacturing Technology, Volume 55, Issue 1, 2006, Pages 361-364, ISSN 0007-8506, http://dx.doi.org/10.1016/S0007-8506(07)60435-1.

[80] Wakaoka, S., Yamane, Y., Sekiya, K., and Narutaki, N., 2002, "High-Speed and High-Accuracy Plunge Cutting for Vertical Walls," J. Mater. Process. Technol., 127, Pages 246–250.

[81] Li, Y., Liang, S. Y., Petrof, R. C., and Seth, B. B., 2004, "Force Modelling for Cylindrical Plunge Cutting," Int. J. Adv. Manuf. Technol., 16, Pages 863–870.

[82] Tlusty, J., and Ismail, F., 1981, "Basic Nonlinearity in Machining Chatter", CIRP Ann., 30, Pages 21–25.

[83] Sutherland, J. W., and DeVor, R. E., 1986, "An Improved Method for Cutting Force and Surface Error Prediction in Flexible End Milling Systems," ASME J. Eng. Ind., 108, Pages 269–279.

[84] Altintas, Y., and Lee, P., 1998, "Mechanics and Dynamics of Ball End Milling," ASME J. Manuf. Sci. Eng., 120, Pages 684–692.

[85] Altintas, Y., and Engin, S., 2001, "Generalized Modeling of Mechanics and Dynamics of Milling Cutters," CIRP Ann., 50 1, Pages 25–30.

[86] Merdol, S. E., and Altintas, Y., 2004, "Mechanics and Dynamics of Serrated Cylindrical and Tapered End Mills," ASME J. Manuf. Sci. Eng., 126, Pages 318–326.

[87] Ko, J. H., and Cho, D.-W., 2005, "3D Ball-End Milling Force Model Using Instantaneous Cutting Force Coefficients," ASME J. Manuf. Sci. Eng., 127, Pages 1–12.

[88] Kejia Zhuang, Xiaoming Zhang, Dong Zhang, Han Ding, On cutting parameters selection for plunge milling of heat-resistant-super-alloys based on precise cutting geometry, Journal of Materials Processing Technology, Volume 213, Issue 8, August 2013, Pages 1378-1386, ISSN 0924-0136, http://dx.doi.org/10.1016

[89] Kline WA, DeVor RE and Lindberg JR. The prediction of cutting forces in end milling with application to cornering cuts. Int J Mach Tool D R 1982; 22: Pages 7–22.

[90] Altintas Y and Spence A. End milling force algorithms for CAD systems. CIRP Ann: Manuf Techn 1991; 40: Pages 31–34.

[91] Lazoglu I. Sculpture surface machining: a generalized model of ball-end milling force system. Int J Mach Tool Manu 2003; 43: Pages 453–462.

[92] Budak E, Altintas Y and Armarego EJA. Prediction of milling force coefficients from orthogonal cutting data. J Manuf Sci E: T ASME 1996; 118: Pages 216–224.

[93] Altintas Y and Lee P. A general mechanics and dynamics model for helical end mills. J Manuf Sci E: T ASME 1998; 120: Pages 684–692.

[94] Lee P and Altintas Y. Prediction of ball-end milling forces from orthogonal cutting data. Int J Mach Tool Manu 1996; 36: 1059–1072.

[95] Yucesan G and Altintas Y. Prediction of ball end milling force. J Eng Ind: T ASME 1996; 118: Pages 95–104.

[96] Engin S and Altintas Y. Mechanics and dynamics of general milling cutters. Part 1: helical end mills. Int J Mach Tool Manu 2001; 41: Pages 2195–2212.

[97] Wan M, Lu MS, Zhang WH, et al. A new method for identifying the cutter runout parameters in flat end milling process. Mater Sci Forum 2012; 697–698: Pages 71–74.

[98] Wan M and Zhang WH. Systematic study on cutting force modelling methods for peripheral milling. Int J Mach Tool Manu 2009; 49: Pages 424–432.

[99] Imani BM, Sadeghi MH and Elbestawi MA. An improved process simulation system for ball-end milling of sculptured surfaces. Int J Mach Tool Manu 1998; 38: Pages 1089–1107.

[100] Wan M, Lu MS, Zhang WH, et al. A new ternarymechanism model for the prediction of cutting forces in flat end milling. Int J Mach Tool Manu 2012; 57: Pages 34-45.

[101] Afazov SM, Ratchev SM and Segal J. Modelling and
simulation of micro-milling cutting forces. J Mater Process
Tech 2010; 210: 2154–2162.

[102] O¨ zel T, Sima M, Srivastava AK, et al. Investigations on
the effects of multi-layered coated inserts in machining Ti-6Al-4V alloy with experiments and finite element simulations. CIRP Ann: Manuf Techn 2010; 59: Pages 77-80.

[103] Gonzalo O, Jauregi H, Uriarte LG, et al. Prediction of specific force coefficients from a FEM cutting model. Int J Adv Manuf Tech 2009; 43: Pages 348–356.

[104] Altintas Y and Jin X. Mechanics of micro-milling with round edge tools. CIRP Ann: Manuf Techn 2011; 60: Pages77–80.

[105] Kaymakci M, Kilic ZM and Altintas Y. Unified cutting force model for turning, boring, drilling and milling operations. Int J Mach Tool Manu 2012; 54–55: Pages 34–45.

[106] Wan M and Altintas Y. Mechanics and dynamics of thread milling process. Int J Mach Tool Manu 2014; 87: Pages 16–26.

[107] Wan M, Pan WJ, Zhang WH, et al. A unified instantaneous cutting force model for flat end mills with variable geometries. J Mater Process Tech 2014; 214: Pages 641–650.

[108] Wan M, Kilic ZM and Altintas Y. Mechanics and dynamics of multifunctional tools. J Manuf Sci E: T ASME 2015; 137: 011019.

[109] Yussefian Z, Moetakef-Imani B and El-Mounayri H. The prediction of cutting force for boring process. Int J Mach Tool Manu 2008; 48: Pages 1387–1394.

[110] Wan M, Wang YT, Zhang WH, et al. Prediction of chatter stability for multiple-delay milling system under different cutting force models. Int J Mach Tool Manu 2011; 51: Pages 281–295.

[111] Grossi N, Sallese L, Scippa A, et al. Chatter stability prediction in milling using speed-varying cutting force coefficients. Proced CIRP 2014; 14: Pages 170–175.

[112] Grossi N, Sallese L, Scippa A, et al. Speed-varying cutting force coefficient identification in milling. Precis Eng. Epub ahead of print 20 April 2015. DOI: 10.1016/ j.precisioneng.2015.04.006.

[113] Scippa A, Sallese L, Grossi N, et al. Improved dynamic compensation for accurate cutting force measurements in milling applications. Mech Syst Signal Pr 2015; 54–55: Pages 314–324.

[114] Quintana G, Ciurana J, Ferrer I, et al. Sound mapping for identification of stability lobe diagrams in milling processes. Int J Mach Tool Manu 2009; 49: Pages 203-211.

[115] Rahman M and Ito Y. Detection of the onset of chatter vibration. J Sound Vib 1986; 109: Pages 193–205.

[116] Campatelli G and Scippa A. Prediction of milling cutting force coefficients for Aluminum 6082-T4. Proced CIRP 2012; 1: Pages 563–568 (In: 5th CIRP conference on high performance cutting, Zurich, 4–6 June 2012).

[117] Witty M, Bergs T, Scha¨ fer A, et al. Cutting tool geometry for plunge milling–process optimization for a stainless steel. Proced CIRP 2012; 1: Pages 506–511.

[118] Schmitz T, Duncan GS. Receptance coupling for dynamics prediction of assemblies with coincident neutral axes. Journal of Sound and Vibration

2006; 289(4–5): Pages 1045–1065

[119] Schmitz T, Duncan GS. Three-component receptance coupling substructure analysis for tool point dynamics prediction. Journal of Manufacturing Science and Engineering 2005;127(4): Pages 781–790.

[120] Duncan GS, Tummond M, Schmitz T. An investigation of the dynamic absorber effect in high-speed machining. International Journal of Machine Tools and

Manufacture 2005;45: Pages 497–507.

[121] Schmitz T, Davies M, Kennedy M. Tool point frequency response prediction for high-speed machining by RCSA. Journal of Manufacturing Science and Engineering 2001;123: Pages 700–707.

[122] Schmitz T, Donaldson RR. Predicting high-speed machining dynamics by substructure analysis. Annals of the CIRP 2000;49(1): Pages 303–308.

[123] Bishop RED, Johnson DC. The mechanics of vibration. London: Cambridge University Press; 1960

[124] Tlusty J, Zaton W, Ismail F. Stability lobes in milling. Annals of the CIRP 1983;32(1): Pages 309–313.

[125] Schmitz T, Mann B. Closed form solutions for surface location error in milling.

International Journal of Machine Tools and Manufacture 2006;46: Pages 1369–1377.

[126] Tony L. Schmitz, Torsional and axial frequency response prediction by RCSA, Precision Engineering, Volume 34, Issue 2, April 2010, Pages 345-356, ISSN 0141-6359, http://dx.doi.org/10.1016/j.precisioneng.2009.08.005.

[127] O. Özşahin, H.N. Özgüven, E. Budak, Analysis and compensation of mass loading effect of accelerometers on tool point FRF measurements for chatter stability predictions, International Journal of Machine Tools and Manufacture, Volume 50, Issue 6, June 2010, Pages 585-589, ISSN 0890-6955, http://dx.doi.org/10.1016/j.ijmachtools.2010.02.002.

[128] A. Ertürk, H.N. Özgüven, E. Budak, Effect analysis of bearing and interface dynamics on tool point FRF for chatter stability in machine tools by using a new analytical model for spindle–tool assemblies, International Journal of Machine Tools and Manufacture, Volume 47, Issue 1, January 2007, Pages 23-32, ISSN 0890-6955, http://dx.doi.org/10.1016/j.ijmachtools.2006.03.001.

[129] D. Biermann, P. Kersting, T. Surmann, A general approach to simulating workpiece vibrations during five-axis milling of turbine blades. CIRP Annals—Manufacturing Technology, Volume 59, Issue 1, 2010,Pages 125-128.

[130] S. Seguy, F.J. Campa, L.N.L. de Lacalla, L. Arnaud, G. Dessein, G. Aramendi, Toolpath dependent stability lobes for the milling of thin-walled parts, International Journal of Machining and Machinability of Materials 4 (4) (2008), pp. 377–392.

[131] F. Ismail, R. Ziaei, Chatter suppression in five-axis machining of flexible parts, International Journal of Ma-chine Tools and Manufacture, 42 (1) (2002/1), Pages 115–122.

[132] R.P.H. Faassen, E.J.J. Doppenberg, N. van de Wouw, J.A.J. Oosterling, H. Nijmeijer, CIRP (Eds.), Online de-tection of the onset and occurrence of machine tool chatter in the milling process, 12–13 June 2006, Vancou-ver, British Columbia, Canada, 2006.

[133] S.Y. Liao, Y.C. Young, A new On-line Spindle Speed Regulation Strategy for Chatter Control, International Journal of Machine Tools and Manufacture, 36/5 (1996) 651-660.

[134] Y. Liu, D. Zhang, B. Wu, An efficient full-discretization method for prediction of milling stability, International Journal of Machine Tools and Manufacture, 63 (2012) 44-48

[135] G. Totis, P. Albertelli, M. Sortino, M. Monno, Efficient evaluation of process stability in milling with Spindle Speed Variation by using the Chebyshev Collocation Method,Journal of Sound and Vibration, 333 (2014) 646-668